# Computational Analysis of Internal Coral Hydrodynamics

Md Monir Hossain

Dissertation submitted to the Faculty of the
Virginia Polytechnic Institute and State University
in partial fulfillment of the requirements for the degree of

Doctor of Philosophy
in
Engineering Mechanics

Anne E. Staples, Chair
Saad A. Ragab
Sunghwan Jung
Nina Stark
Hosein Foroutan

June 10, 2020
Blacksburg, Virginia

Keywords: Coral hydrodynamics, immersed boundary method , large eddy simulation,
mass transport, turbulent stress.

# Computational Analysis of Internal Coral Hydrodynamics

Md Monir Hossain

(ABSTRACT)

Knowledge of the detailed flow dynamics at the interior of branching corals is critical for a full understanding of nutrient uptake, mass transport, wave dissipation, and other essential processes. These physiological processes depend on the local velocity field, local concentration gradients of nutrients and waste, and the turbulent stresses developed on and above the coral surface. Though the large-scale hydrodynamics over coral reefs are well studied, the interior hydrodynamics, between the branches, remains uncharacterized due to limited optical and acoustic access to the interior. In the current thesis, a three-dimensional immersed boundary method in the large eddy simulation framework was used to compute the flow inside several branching coral colony geometries in order to study the effects of branch density and surface structure on the flow fields in the coral interiors. Two different *Pocillopora* colony species were studied at different Reynolds numbers. A ray-tracing algorithm was used for capturing the arbitrary branches of these complex geometries to obtain the three-dimensional flow fields within these colonies for the first time. The analysis showed the formation of vortices at the colony interior that stir the water column and thus passively enhance mass transport, compensating for the reduced mean velocity magnitude compared to the free stream value, within the densely branched *Pocillopora meandrina* colony. Further analysis showed that the mean streamwise velocity profile changes shape along the streamwise direction inside *P. meandrina*, whereas the mean velocity profile did not change shape from the front to the back for the loosely branched *Pocillopora* colony, *Pocillopora eydouxi*. Moreover, turbulent flow field quantities were computed for both these structures, and for two almost identical

*Montipora capitata* colony geometries, one with, and one without roughness elements called verrucae. The analyses demonstrated significant differences in the mean velocity profiles, Reynolds stress, and other flow quantities with changes in colony branch density and surface structure.

# Computational Analysis of Internal Coral Hydrodynamics

Md Monir Hossain

(GENERAL AUDIENCE ABSTRACT)

Coral reefs are the largest marine ecosystem, and play a critical role in protecting coastal areas against flooding and erosion. The majority of the world's corals are currently under threat from rising ocean temperatures, which disrupt the symbiotic relationship between the coral polyp and its symbiont algae causing coral bleaching. Bleaching involves processes mediated by the flow at the coral surface, but relatively little is known regarding the local flow dynamics between the branches of coral reefs. The current research seeks to characterize internal coral hydrodynamics, leading to insights about many critical physiological and other processes in corals, like drag formation, mixing, and mass or nutrient transport to and from the coral. In the current study, the influence of the coral branch density and surface structure on the resulting interbranch flow field were investigated by simulating the flow resulting from uniform oncoming ocean flow conditions using three-dimensional immersed boundary large eddy simulations. The detailed velocity and pressure fields were found throughout the interior of the colonies studied. A distinct mass transport mechanism was found inside one densely branched colony studied. For this coral, *Pocillopora meandrina*, the flow speed reduces substantially inside the coral because of the high branch density. But corals depends on the ocean flow to bring nutrients to the polyps on their surface. We found that *P. meandrina* sheds hundreds of small vortices from its branches, which stir the overlying water column, increasing the mass transport rate, and compensating almost exactly for the reduced flow in the interior. The study also included computing the flow through three other coral colony geometries, and comparisons of their mean velocity profiles and turbulent flow

statistics in order to examine the impact of the colony branch density and surface structures on the resulting hydrodynamic flow field. The current investigation of coral hydrodynamics may lead to an increased understanding of coral health and physiological activity, and may help in designing effective interventions for the challenges facing corals, which could have impacts in the fields of coral restoration, coastal protection, and public policy in the United States and abroad.

# Dedication

*Dedicated to my wife, Tanjila Shabnam.*

# Acknowledgments

I would like to express my sincere gratitude to my advisor Dr. Anne Staples, for her constant encouragement, generous support and motivation throughout this work. Dr. Staples has not only introduced me to the computational fluid dynamics but also guided me to understand the physical problems in nature.

I also want to acknowledge all other committee members, Dr. Jung, Dr. Ragab, Dr. Foroutan, and Dr. Stark, for their valuable comments and suggestions on my research. This manuscript has also benefited from their corrections.

My family has supported me through the ups and downs of my life. Their unconditional love and support have given me the strength to complete this journey. I am also much indebted to my wife Shabnam and my daughter Samarina for their love and patience. Without their support, I could not finish the writings in this COVID-19 pandemic.

# Contents

# List of Figures

# List of Tables

# Chapter 1

# Introduction

## 1.1 Motivation and Overview

Coral reefs are the largest marine ecosystem, containing almost 25% of all marine life even though they occupy only 1% of the ocean floor [1]. These reefs support the most biological diversity in comparison to any other ecosystem existing on earth. The diversity of living organisms and the health of the reef system itself are directly connected to the marine environment. In addition to hosting many species, coral reefs act as the first line of defense for the coastline against natural disasters and erosion. More than a half-billion people directly depend on the reefs for their livelihoods and these ecosystems contribute billions of dollars to the world economy [2]. Unfortunately, these reefs are in critical condition due to anthropological pollution and environmental degradation. Coral bleaching, which occurs due to the change in the thermal environment of the ocean, is one current phenomenon affecting the symbiotic relationship between algae and coral polyps [3]. Because of this combination of factors, frequently occurring natural disasters are putting tremendous pressure on coastal protection strategies. That is the reason engineers and scientists are currently more interested in natural solutions like coral reefs that will keep the natural environment intact.

Though coral reefs have been studied for decades, quantitative studies of corals and their interactions with their hydrodynamic environments are a more recent phenomenon. Numerous quantitative studies have been performed on many aspects of coral reefs and their

interactions with the surrounding ocean flow. The transport of nutrients, dissolved and particulate matter, is controlled by the hydrodynamic conditions both outside and inside the reef. However, previous studies were mainly focused on flow dynamics above the canopy [4, 5]. In most of those large reef scale hydrodynamics, the top of the reef was treated as a rough boundary and the velocity profile and turbulent stress, production, and dissipation rate were computed above the reef canopy without considering the diversity of the internal geometrical structures of the colony. In addition, the prediction of the drag force depends on detailed flow dynamics near the complex geometries of coral. Due to the lack of information concerning internal flow in the colony, empirical and semi-empirical models are used to predict the drag force developed inside the coral reef [6]. Now canopy flow theory can be an alternative for understanding the flow dynamics for simple and complicated geometries [7]. However, the spatial-temporal averaged flow field obtained from canopy theory lacks detailed flow information due to the heterogeneity of individual canopy elements. This double averaging approach also generates new terms in the Navier-Stokes equations, terms which require closure models, and the accuracy of these closure models within the canopy is still unknown.

Furthermore, the physiological processes of corals depend on the velocity profile and Reynolds stress near the surface. The mixing length, drag, kinetic energy budget, and thermal microenvironment are also inter-connected to the internal flow fields of coral. The turbulence generated in the colony impacts eggs and larvae. Additionally, the transport of dissolved metabolites ($O_2$, $CO_2$, $NH_4$, and $PO_4$) from the diffusion boundary layer to the surrounding water or the transfer of the nutrients and particulate from the overlying water column to the interior of the colony depends on the mass transport mechanism of branching corals. However, the transport mechanisms and detailed turbulent flow field within densely- or open-branching corals are still unresolved.

Examining the flow field directly inside the coral has proven difficult due to the limitation in instrumentation. Computational analysis might be an effective alternative for understanding these interactions. One of the big challenges for numerical simulation is capturing the arbitrary shape of the branching corals. Though there has been a tremendous increase in computational capability in recent years, performing three-dimensional large eddy simulation around such complex geometry is not straightforward. In the current study, an immersed boundary method was used in the large eddy simulation platform with the ray-tracing algorithm to investigate the effects of internal coral geometry and surface structure on the local flow field of colony and to understand the variation of mean flow profile with different branch density from the four different *Pocillopora* and *M. capitata* coral skeletons. The analysis also includes the magnitude of turbulent stress, quadrant analysis, and scalar transport from the surface of a coral colony under unidirectional oncoming flow conditions. The detailed microscopic flow field along with these critical parameters inside the colony can be used to develop critical parameterizations of subscale flow quantities like Reynolds stresses, dispersive stresses, and drag. The detailed hydrodynamics inside the colony may also help us to understand the transport mechanisms inside the branching corals for the first time.

## 1.2 Literature review

A new and important direction in understanding the coupled dynamics of corals and their hydrodynamic environments seeks to measure and model the flow inside coral reefs and individual colonies. Especially, the complex geometry of the coral makes for a challenging fluid dynamics problem and the scale of analysis may extend from a couple of millimeter to kilometer wide range for large scale reefs [8]. The details of these hydrodynamic analyses

also depend on these length scales. Over the past decades, numerous analyses have been performed on the reefs, but connecting the flow information between the large scale reef and a single coral was not possible due to tremendous variation in the geometrical structure of the individual colony. Therefore, the detailed flow field through the inter-connected polyps of a coral colony can play a key role in the comprehension of the physiological processes, nutrients, and mass transport mechanisms for coral.

To find out the interconnection between the flow and physiological parameters, Fabricius conducted an experimental study on the uptake rate of phytoplankton and growth rate of the coral and the results showed a positive relationship between these parameters and the flow magnitude [9]. Similarly, water movement affects the morphological plasticity of the coral [10]. In an early flume experiment, Chamberline *et al.* were able to visualize the flow characteristics around different morphologies of coral colonies and implied that the branching pattern might affect the suspended nutrient particles in the coral colony [11]. These suspended particles act as the supplement to whether the nourishment of nutrients is not sufficient from the symbiotic relationship between algae and coral polyp. In a flume study, Sebens *et al.* analyzed the influence of branch spacing and water motion on the particulate capturing capability through the corals [12]. The author showed maximum capturing of the particles at low and higher flow conditions for low and high aggregate corals respectively, and that the location of maximum consumption depends on the internal flow conditions. In some cases, corals change morphological structure to adapt to the surrounding flow condition and availability of nutrients. To examine the relation, Mass and Genin conducted a controlled study and developed an asymmetrical branching pattern due to the asymmetry in the flow conditions [13]. Kandorp and Kubler found a similar transformation and explained how the flow conditions can change internal morphology from densely branching to open structure based on the flow conditions [14].

Canopy flow theory is used to understand the macroscopic description of the flow. Due to the diversity of geometrical features, the actual flow field inside the canopy is never resolved. Instead, a double averaging i.e spatial-temporal averaging approach is generally used to obtain a macroscopic flow field [7]. A new dispersive stress term is generated at the momentum equation due to the averaging. In most of the analyses, this new term was neglected for dense canopies. However, the later studies showed that the magnitude of dispersive stresses may have significant contributions based on the sparsity of the branches [15]. The available closure models for this dispersive stress have been developed from the simplified array of canopy elements [16]. The accuracy of these models inside the canopy elements is not still clear. Though it is an excellent tool for large scale analysis, the detailed micro-environment flow information cannot be obtained through this analysis.

Physiological processes such as photosynthesis and respiration also depend on flow conditions. Pattersons and Seben exhibited that the production and respiration rate varies with flow conditions on the coral surface [17]. Mass *et al.* mentioned the positive response of the photosynthesis rate with an increase in flow [18]. Bruno *et al.* combined both the inter-branch distance and flow magnitude and found that respiration rates increase with an increase in branching distance and the oncoming flow speed. The authors suggested the increase in flow magnitude in the large branch spacing might decrease the diffusive boundary layer (DBL) thickness and enhance the transport rate [19]. The thickness of the DBL may vary from a couple of hundred microns to approximately 2 mm and the DBL is a strong function of flow profile over the coral surface [20, 21]. In a recent paper, Chan *et al.* suggested a negative correlation between tissue surface pH and water flow conditions, and the author predicted this relationship is also a function of micro-flow environment inside the colony geometry [22].

Extracting flow field from the complex internal structure of the colony is a challenging task

and different techniques were used to simplify the analysis. For example, Samuel *et al.* [23] used a hollow spherical ball to simulate the drag developed on the colony. Similarly, Lowe *et al.* [24] tried to capture the velocity profile and shear stress for coral canopies by modeling the coral as an array of cylinders for unidirectional and wavy flow conditions. The results showed a higher canopy flow for the wavy flow conditions than for the unidirectional flow. In the second part of this paper, the same canopy model was also used to estimate and compare mass transfer from the cylinder surface for both unidirectional and oscillatory flow. Here, the authors used the Sherwood (Sh) number to calculate the mass transfer coefficient for different flow conditions. Bilger and Atkinson were the pioneers in using similar engineering relationships to explain field-observed experimental data with the mass transport equations for rough boundaries [25] and used the Stanton number to predict the rates of phosphate uptake by coral colonies. But there, observed field values exhibited higher values than the predicted magnitude. In the consecutive paper, the author found that there exists a first-order relationship between phosphate uptake and velocity profile in the colony. They also provided a couple of explanations for the anomaly between the observed and estimated results, but no conclusion was drawn from the study. However, the author suggested that the geometry of the colony might somehow adapt to the flow conditions to enhance the mass transport, and that the roughness of the geometry might play a significant role by altering the thickness of the boundary layer [26].

Later, Reidenbach *et al.* performed experiments on the mass transport of rough coral beds and found that the mass transfer rate jumped for wavy flow compared to the unidirectional flow. The authors concluded that the increase in turbulent stress also increases the mass transfer rate. In the discussion, the authors mentioned the instability of the shear layer at the crest of the colony as the main mechanism of mass transport. For the densely-branched colony, the bursting and sweeping events dominate the transport mechanism and

the penetration depth is only 15% of the height of the colony [27]. In another analysis, the author estimated the friction velocity and indicated that existing turbulent boundary theory was also applicable over the bottom surface of the ocean covered by the rough coral reef. [28]. Friction velocity plays an important role in controlling the mass transfer rate. Hondzo *et al.* calculated the dissolved oxygen concentration near the sediment-water interface and the results show an increase in mass transfer rate with an increase in friction velocity [29]. Gardella *et al.* similarly calculated frictional velocities near the colonies of *D. stokesii* and *S. michilini*. The authors found the frictional velocities were a strong function of the flow regime but didn't find any dependence on the roughness.

The current discussions emphasize the impacts of coral geometry in generating the turbulence, but detailed flow dynamics and turbulent statistics through a single coral colony is not common. Stockings *et al.* performed such analysis above the healthy and algae-covered coral and showed that turbulent boundary layer theory can be applied to describe the formation of the boundary layer over the colony. In contrast, algae-covered coral showed the profile of the mixing layer and the author predicted less mass transport due to a reduction in Reynolds stress [30]. Jimenez *et al.* measured the thermal boundary layer (TBL) up to 3 mm at low flow conditions and found that TBL developed on the coral surface depends on flow magnitude [31]. In another paper, Jimenez *et al.* measured the thermal boundary layer and $O_2$ transfer on the coral surface and these two transfer processes were not analogous [32]. Asher *et al.* calculated drag force on a model reef of 81 *Pocillopora* colonies in a flume study and determined drag force as a function of colony height instead of a single value for the interior of the reef. The author also determined the mean velocity profile and Reynolds stress from the velocity measurement at a couple of points inside and outside the colony [33].

Many of these studies were performed using Particle Image Velocimetry (PIV) and Acoustic Doppler Velocimetry (ADV) to obtain velocity profiles at selected points within the colony,

but these few points are not sufficient for depicting the flow conditions inside a real skeleton. In recent years, visualization systems like magnetic resonance velocimetry (MRV) have been used for flow visualization of the flow field inside complex geometry. Chang *et al.* [34] has used the same MRV technique to reveal the turbulent flow field within the two different branch densities of *S. pistillata* coral. This is the first analysis where detailed velocity slices were obtained directly from different sections of the colony. Although the experiment provided a thorough visualization of flow fields inside coral, MRV is expensive and limited to a laboratory environment. Most importantly, conducting experiments repeatedly on such diverse coral structures with this technique is unrealistic. To solve this problem, numerical simulations can be an important tool.

For numerical simulations, complexity arises during the capture of the random geometrical shapes. Generating body-fitted curvilinear meshes, even for the simplest geometries, require very efficient meshing algorithms. In previous numerical experiments, simulations were performed by considering the geometries of coral as an isotropic, porous medium, but such porous analysis lacks the turbulent flow information inside the natural morphology of coral. [35]. Kaandorp et al used the Lattice Boltzmann method to understand the flow pattern inside the coral's skeletons of *Maracis mirabilis* [36, 37]. For the high flow morphology, the authors found a stagnation region inside the coral even at high Re number but these computations either lack the realistic coral morphology or were performed at low Re number (154 to 3840) due to stability issues. Similarly, Chindapol *et al.* [38] used the COMSOL Multiphysics tool to model the effect of flow on the growth of *Pocillopora verrucosa*. However, the simulation was performed on a laminar framework by suppressing the turbulence effects. Chang *et al.* [39] were the first to use the Immersed boundary method with a large eddy simulation to understand local shear and mass transfer on single corals. Here the author compared the simulation results through low and high flow morphologies *Stylophora* and

*Pocillopora* coral respectively for both unidirectional and wavy flow conditions and mentioned regarding the collapsing of the flow profile inside the same coral morphology even when the flow magnitude changed substantially at the exterior. The author also suggested that the corals adapt to natural flow conditions in such a way that the corals have similar mass transfer characteristics even when their morphological structure and hydrodynamic conditions are different.

Recently, Stockings *et al.* performed thermal and hydrodynamic analysis on brain corals with different thicknesses of rough surface on the colony. This turbulence analysis was performed on the external surface of the colony but did not provide information on the internal flow dynamics. Similarly, Cano *et al.* performed the drag force analysis on the open-branched colony of *Acropora palmata* by OpenFOAM toolbox [40]. In another analysis, the same authors computed the wave energy dissipation over the coral colony [41]. Ong *et al.* also used the OpenFOAM toolbox for finding the micro-thermal environment for hemispherical and branching corals. The study was limited to the thermal analysis [42, 43].

Most of the previous algorithm used for the complex geometries were developed for body-fitted meshes in Reynolds averaged Navier-stokes platforms. In comparison, the immersed boundary with arbitrary shape can be modeled on a fixed nonconforming grid by using an external force field. As the boundary may or may not coincide with the grid, the implementation of boundary conditions is more difficult. The method was first introduced by Peskin [44] and mostly used in low Reynolds number biological flows. In this analysis, the boundary was modeled as a set of elements linked by springs and a discrete delta function was used for spreading the forcing over a narrow band across the boundary. In this approach, the boundary is not sharply defined and the issue arises for a thin boundary layer near the boundary which causes relatively large errors for DNS and LES of turbulent flow analysis at moderate/high Reynolds numbers. In addition, for stationary solid boundaries, the case

becomes numerically stiff. Recently, Mohd-Yusof [45] and Fadlun *et al.*[46] introduced a non-boundary conforming formulation based on a direct forcing approach which successfully removes these deficiencies. In the direct forcing method, forcing is considered in the framework of the discretized equations and is explicitly defined in a way that the appropriate boundary conditions are enforced on the boundary itself. These methods put emphasis on local reconstruction of flow profiles near the boundary. Reconstruction of flow information near the boundary is not straightforward and in some cases, confusion arises regarding the direction of the reconstruction. Balaras *et al.* presented algorithms for such reconstruction which is suitable for both simple and complex geometries [47].

## 1.3 Research Overview

The present dissertation aims to address the hydrodynamics of branching coral colonies at different flow conditions and to analyze the impact of coral morphologies on the mass transport mechanism and turbulent statistics both interior and exterior to the colony.

The second chapter of this dissertation, "Passive vortical flows enhance mass transport in the interior of a coral colony," illustrates the effects of the morphological characteristics of corals on mass transfer. Detailed velocity slices and vortical profiles were obtained at different sections inside the colony to understand the interaction of densely branched *P. meandrina* with the surrounding fluid. The result shows the formation of large vortices at the outer periphery of the coral, which stirs the water column and assists in mass transport. At the interior of the colony, the flow field is highly vortical and the geometrical features of branching coral generate passive vortices that enhance the local mass transport. Mean velocity magnitude and advection time scale, calculated from the mean diameter of these local vortices, were plotted along the coral length. The results show almost constant advection

time scale along the length of the coral that compensates the drastic reduction of velocity at the interior of the densely branched colony. Additionally, a scalar transport equation was solved along with the Navier-Stokes equations for wavy flow conditions. When the mean scalar concentration was plotted as a function of radial distance, the plot shows a double peak behavior with maximum magnitude at the deep interior and exterior of the colony at the end of the wave cycle.

In the third chapter,"Effects of coral colony morphology on turbulent flow dynamics," the numerical experiments were extended further to depict the detailed flow field at the interior of two *Pocillopora* corals with different branching structures. The explicit vector profiles inside the colony were presented for the first time for a qualitative comparison of the flow field inside these geometries for unidirectional flow. These profiles exhibited a significant difference in the velocity magnitude between the front and rear half of the densely packed *P. meandrina* whereas relatively higher flow penetration was observed at the interior of *P.eydouxi* with the formation of wake regions behind each branch. For quantitative comparison, the mean velocity profile along the height of the colony was also obtained for the first time from front to back of the coral. The comparison shows distinct velocity profiles at different sections of *P. meandrina.* In contrast, *P. eydouxi* shows an almost uniform mean profile throughout its sparser branches. Quadrant analysis was performed on both these structures to understand the impact of injection and sweep on the Reynolds stress at the interior of the colony. In the second part of the paper, computational analysis was performed on another pair of geometries of *M. capitata* with and without verrucae to understand the effect of surface structure on surrounding fluids. The streamwise and vertical velocity components show maximum velocity magnitude close to the top of the coral surface which indicates comparatively better mass transport for *M. capitata* without verrucae. In addition, turbulent stress was also computed on the top of both the morphologies with maximum magnitude at the crest of the colony.

Higher turbulent stress near the top of the coral indicates higher friction velocity, better mass transport, and relatively larger drag force on *M. capitata* without verrucae for the same Reynolds number.

The fourth chapter, entitled "Mass transport and turbulent statistics within branching corals," presents the comparison of mass transport mechanisms between two different branching corals, *P. meandrina* and *P. eydouxi*. Detailed vector fields and streamlines showed the formation of passive vortices which enhance the mass transfer throughout the interior of densely-branched *P. meandrina*. In comparison, the size and number of vortices reduced substantially inside the open-branched *P. eydouxi* where the velocity magnitude was relatively higher across the colony. To compare the mass transfer rate, Stanton numbers were calculated based on the mean velocity magnitude and advection time scale from the front to the end of the colony. For the densely-branched *P. meandrina*, the results show up to 216% increase in Stanton number when the mean diameter of the vortices was used as a length scale in the calculation of the Stanton number instead of mean branch diameter. However, for *P. eydouxi*, the value of the Stanton number was more than twice the magnitude for *P. meandrina* and remained constant throughout the length for the same incoming flow. In addition, fluctuation velocity components were extracted from the instantaneous and mean velocity flow field. The fluctuating field shows a relatively higher concentration of velocity vectors near the top surface of the colony which contributes to a higher magnitude of turbulent stress on the top of the colony. The mean Reynolds stress and velocity variance calculated based on these fluctuating fields exhibit almost the same magnitude of Reynolds stress and velocity variance above the top of these both *Pocillopora* coral. However, within the colony, both these turbulent parameters were not dampened even for the densely branched morphology of *P. meandrina*.

In the fifth chapter, "Conclusions and future work", the work is summarized and recom-

mendations are made on possible future research on the flow and mass transport of coral colony.

# Bibliography


[1] NOAA. Rainforests of the Sea; 2020. Available from: https://www.fisheries.noaa.gov/national/habitat-conservation/shallow-coral-reef-habitat.

[2] NOAA. Coral reef ecosystems; 2019. Available from: https://www.noaa.gov/education/resource-collections/marine-life/coral-reef-ecosystems.

[3] Lesser MP, Farrell JH. Exposure to solar radiation increases damage to both host tissues and algal symbionts of corals during thermal stress. Coral reefs. 2004;23(3):367–377.

[4] Delandmeter P, Lambrechts J, Marmorino GO, Legat V, Wolanski E, Remacle JF, et al. Submesoscale tidal eddies in the wake of coral islands and reefs: satellite data and numerical modelling. Ocean Dynamics. 2017;67(7):897–913.

[5] Storlazzi C, Elias E, Field M, Presto M. Numerical modeling of the impact of sea-level rise on fringing coral reef hydrodynamics and sediment transport. Coral Reefs. 2011;30(1):83–96.

[6] Rosman JH, Hench JL. A framework for understanding drag parameterizations for coral reefs. Journal of Geophysical Research: Oceans. 2011;116(C8).

[7] Finnigan J. Turbulence in plant canopies. Annual review of fluid mechanics. 2000;32(1):519–571.

[8] Monismith SG. Hydrodynamics of coral reefs. Annu Rev Fluid Mech. 2007;39:37–55.

[9] Fabricius KE, Genin A, Benayahu Y. Flow-dependent herbivory and growth in zooxanthellae-free soft corals. Limnology and Oceanography. 1995;40(7):1290–1301.

[10] Todd PA. Morphological plasticity in scleractinian corals. Biological reviews. 2008;83(3):315–337.

[11] Chamberlain Jr JA, Graus RR. Water flow and hydromechanical adaptations of branched reef corals. Bulletin of Marine Science. 1975;25(1):112–125.

[12] Sebens KP, Witting J, Helmuth B. Effects of water flow and branch spacing on particle capture by the reef coral Madracis mirabilis (Duchassaing and Michelotti). Journal of experimental marine biology and ecology. 1997;211(1):1–28.

[13] Mass T, Genin A. Environmental versus intrinsic determination of colony symmetry in the coral Pocillopora verrucosa. Marine Ecology Progress Series. 2008;369:131–137.

[14] Kaandorp JA, Kübler JE. The algorithmic beauty of seaweeds, sponges and corals. Springer Science & Business Media; 2001.

[15] Poggi D, Katul G, Albertson J. A note on the contribution of dispersive fluxes to momentum transfer within canopies. Boundary-layer meteorology. 2004;111(3):615–621.

[16] Moltchanov S, Bohbot-Raviv Y, Shavit U. Dispersive stresses at the canopy upstream edge. Boundary-layer meteorology. 2011;139(2):333–351.

[17] Patterson MR, Sebens KP, Olson RR. In situ measurements of flow effects on primary production and dark respiration in reef corals. Limnology and Oceanography. 1991;36(5):936–948.

[18] Mass T, Genin A, Shavit U, Grinstein M, Tchernov D. Flow enhances photosynthesis in marine benthic autotrophs by increasing the efflux of oxygen from the organism to the water. Proceedings of the National Academy of Sciences. 2010;107(6):2527–2531.

[19] Bruno JF, Edmunds PJ. Metabolic consequences of phenotypic plasticity in the coral Madracis mirabilis (Duchassaing and Michelotti): the effect of morphology and water

flow on aggregate respiration. Journal of experimental marine biology and ecology. 1998;229(2):187–195.

[20] Shashar N, Kinane S, Jokiel P, Patterson M. Hydromechanical boundary layers over a coral reef. Journal of Experimental Marine Biology and Ecology. 1996;199(1):17–28.

[21] Larkum AW, Koch EM, Kühl M. Diffusive boundary layers and photosynthesis of the epilithic algal community of coral reefs. Marine Biology. 2003;142(6):1073–1082.

[22] Chan N, Wangpraseurt D, Kühl M, Connolly SR. Flow and coral morphology control coral surface pH: implications for the effects of ocean acidification. Frontiers in Marine Science. 2016;3:10.

[23] Samuel LC, Monismith SG. Drag coefficients for single coral colonies and related spherical objects. Limnology and Oceanography: Fluids and Environments. 2013;3(1):173–181.

[24] Lowe RJ, Koseff JR, Monismith SG, Falter JL. Oscillatory flow through submerged canopies: 2. Canopy mass transfer. Journal of Geophysical Research: Oceans. 2005;110(C10).

[25] Atkinson M, Bilger R. Effects of water velocity on phosphate uptake in coral reef-hat communities. Limnology and Oceanography. 1992;37(2):273–279.

[26] Bilger R, Atkinson M. Anomalous mass transfer of phosphate on coral reef flats. Limnology and Oceanography. 1992;37(2):261–272.

[27] Reidenbach MA, Koseff JR, Monismith SG. Laboratory experiments of fine-scale mixing and mass transport within a coral canopy. Physics of Fluids. 2007;19(7):075107.

[28] Reidenbach MA, Monismith SG, Koseff JR, Yahel G, Genin A. Boundary layer turbulence and flow structure over a fringing coral reef. Limnology and oceanography. 2006;51(5):1956–1968.

[29] Hondzo M. Dissolved oxygen transfer at the sediment-water interface in a turbulent flow. Water resources research. 1998;34(12):3525–3533.

[30] Stocking JB, Rippe JP, Reidenbach MA. Structure and dynamics of turbulent boundary layer flow over healthy and algae-covered corals. Coral Reefs. 2016;35(3):1047–1059.

[31] Jimenez IM, Kühl M, Larkum AW, Ralph PJ. Heat budget and thermal microenvironment of shallow-water corals: Do massive corals get warmer than branching corals? Limnology and Oceanography. 2008;53(4):1548–1561.

[32] Jimenez IM, Kühl M, Larkum AW, Ralph PJ. Effects of flow and colony morphology on the thermal boundary layer of corals. Journal of The Royal Society Interface. 2011;8(65):1785–1795.

[33] Asher S, Niewerth S, Koll K, Shavit U. Vertical variations of coral reef drag forces. Journal of Geophysical Research: Oceans. 2016;121(5):3549–3563.

[34] Chang S, Elkins C, Alley M, Eaton J, Monismitha S. Flow inside a coral colony measured using magnetic resonance velocimetry. Limnology and Oceanography. 2009;54(5):1819–1827.

[35] Ong RH, King AJ, Mullins BJ, Cooper TF, Caley MJ. Development and validation of computational fluid dynamics models for prediction of heat transfer and thermal microenvironments of corals. PloS one. 2012;7(6):e37842.

[36] Kaandorp JA, Sloot PM, Merks RM, Bak RP, Vermeij MJ, Maier C. Morphogenesis

of the branching reef coral Madracis mirabilis. Proceedings of the Royal Society B: Biological Sciences. 2005;272(1559):127–133.

[37] Kaandorp JA, Koopman EA, Sloot PM, Bak RP, Vermeij MJ, Lampmann LE. Simulation and analysis of flow patterns around the scleractinian coral Madracis mirabilis (Duchassaing and Michelotti). Philosophical Transactions of the Royal Society of London Series B: Biological Sciences. 2003;358(1437):1551–1557.

[38] Chindapol N, Kaandorp JA, Cronemberger C, Mass T, Genin A. Modelling growth and form of the scleractinian coral Pocillopora verrucosa and the influence of hydrodynamics. PLoS computational biology. 2013;9(1):e1002849.

[39] Chang S, Iaccarino G, Ham F, Elkins C, Monismith S. Local shear and mass transfer on individual coral colonies: Computations in unidirectional and wave-driven flows. Journal of Geophysical Research: Oceans. 2014;119(4):2599–2619.

[40] Osorio-Cano JD, Osorio AF, Alcérreca-Huerta JC, Oumeraci H. Drag and inertia forces on a branched coral colony of Acropora palmata. Journal of Fluids and Structures. 2019;88:31–47.

[41] Osorio-Cano JD, Alcérreca-Huerta JC, Osorio AF, Oumeraci H. CFD modelling of wave damping over a fringing reef in the Colombian Caribbean. Coral Reefs. 2018;37(4):1093–1108.

[42] Ong R, King A, Mullins B, Cooper T, Caley M. Computational fluid dynamics model of thermal microenvironments of corals. MODSIM 2011. 2011;.

[43] Ong RH, King AJ, Kaandorp JA, Mullins BJ, Caley MJ. The effect of allometric scaling in coral thermal microenvironments. PloS one. 2017;12(10).

[44] Peskin CS. The immersed boundary method. Acta numerica. 2002;11:479–517.

[45] Mohd-Yusof J. methods for complex geometries. Annual Research Briefs-1998. 1998; p. 325.

[46] Fadlun E, Verzicco R, Orlandi P, Mohd-Yusof J. Combined immersed-boundary finite-difference methods for three-dimensional complex flow simulations. Journal of computational physics. 2000;161(1):35–60.

[47] Balaras E. Modeling complex boundaries using an external force field on fixed Cartesian grids in large-eddy simulations. Computers & Fluids. 2004;33(3):375–404.

# Chapter 2

# Passive vortical flows enhance mass transport in the interior of a coral colony

**Publication information**

The contents of this chapter have been published:

Hossain, M., & Staples, A. (2019). Passive vortical flows enhance mass transport in the interior of a coral colony. *Phys. Fluids*, 31, 061701. https://doi.org/10.1063/1.5094076

This paper was selected as a *Featured Article* and an *Editor's Pick*

## 2.1 Abstract

Corals exchange nutrients and dissolved gases with the surrounding environment for metabolic purposes. A recent study demonstrated that corals can actively stir quiescent water columns and produce vortical flows that enhance mass transfer rates by up to 400%. Here, three-dimensional immersed-boundary simulations of the flow through a *Pocillopora meandrina* colony demonstrate that the passive geometric features of the branching colony produce highly vortical internal flows that enhance mass transfer at the interior of the colony, com-

pensating almost exactly for flows speed reductions there of up to 64% so that the advection time scale remains roughly constant throughout the colony.

## 2.2 Velocity field and mass transport inside *P. meandrina*

Benthic organism like corals depends on the surrounding flow dynamics to carry out their physiological activities. Numerous reef-scale studies have been performed to answer questions about how the surrounding ocean or laboratory hydrodynamics impacts things like nutrient availability, photosynthesis, and the morphological evolution of coral reefs[1, 2, 3, 4, 5, 6]. But the smaller scale flow dynamics within branching coral colonies has largely remained unexplored. Most considerations of coral hydrodynamics use the canopy flow theory approach, in which a coral reef is modeled as a rough porous medium[7, 8, 9]. A few studies have considered the intracolonial flow field and have concluded that the flow at the interior of an individual colony depends on the colony branching pattern and the flow Reynolds number and has strong effects on nutritional availability for the coral polyps located deep inside the colony[10, 11]. These studies have assumed that if the flow speed in the interior of the coral is reduced, the nutrient availability will suffer a proportional reduction[12, 13].

For corals situated in weak ambient flows, the exchange of nutrients, waste, and other materials between the reef and its environment was long assumed to be dominated by molecular diffusion, but a recent experimental and computational study demonstrated that the weak vortical flows produced by ciliary beating near a coral's surface can enhance the mass transport by up to 400% compared to molecular diffusion through an unstirred boundary layer alone[14]. For corals located in strong flow environments, the flow characteristics over the

reef and the mechanisms of mass transfer between the reef and the surrounding body of water are significantly different than for corals located in weak ambient flow conditions[15, 16]. However, branching corals in strong flow conditions suffer a similar deficit in their deep interiors. Crucially, the flow velocities at the interior of densely branched coral colonies can be reduced by up to 90% compared to the exterior, oncoming flow values[17, 18], placing the coral polyps deep in the interior of branching coral colonies that experience highly reduced flows into the same situation as corals situated in weak ambient flows. As for with corals in weak ambient flow conditions, though, in spite of this drastic reduction in flow speeds, the polyps at the interior of these densely branched coral are observed to continue their biological activities normally without apparent deficits, despite the drastic drop in velocity magnitude, pointing to an unknown mechanism by which mass transport is maintained in spite of the reduction in flow.

In this letter we seek to elucidate the mechanism behind the enhancement in mass transport at the interior of densely branched coral colonies that appears to compensate for the drastically reduced flows there. To address this question, we computed the flow through the interior of a single colony of the branching coral, *Pocillopora meandreanina*, a common reef building coral found in shallow reef environments in the Indian and Pacific oceans, for both unidirectional and oscillatory ambient flow conditions.

Quantifying the flow field and mass transport inside a complex coral colony geometry is a challenging task. Nutrient uptake correlations developed for model coral geometries are insufficient for capturing the actual flow conditions in densely branched corals [20]. And experimental measurements have displayed inconsistencies due to the lack of access to the coral interior and poor measurement resolution near the surface of the coral. In recent years, visualization methods like magnetic resonance velocimetry (MRV) and particle image velocimetry (PIV) have improved immensely and have been used for flow visualization within

complex geometries [21]. These techniques are expensive, however, and mostly restricted to laboratory conditions.

Computational approaches have been attempted as well. The Lattice Boltzmann method was used to simulate the flow through a computed tomography (CT) scan of a coral colony geometry for laminar flow conditions, but it failed at physiologically realistic Reynolds numbers due to numerical stability issues [22, 23]. Chang *et al.* recently performed the first successful computations of flow in the interior of a coral colony at realistic Reynolds numbers using the immersed boundary (IB) and large eddy simulation (LES) techniques [18]. In their investigation they quantified local shear and mass transport on individual *Stylophora pistillata* and *Pocillopora meandrina* coral colonies. But the analysis did not characterize the mass transport mechanism at the interior of the densely branched colonies where the flow was significantly reduced. This is what we aim to do in this work.

Three-dimensional simulations of the flow through a single *P. meandrina* colony were performed using the IB method implemented in the LES framework using a code developed by Balaras *et al.* The complete details of the code can be found in [24]. A ray tracing algorithm was implemented to identify the boundary between solid and fluid points, and a dynamic Smaogrinsky eddy viscosity model was used to model the contributions of the subgridscale motions.

Fig. 2.1 shows the rendered stereolithography (STL) file of the *P. meandrina* colony used in the present computations. The STL file, composed of 1.8 million triangles, was obtained from a computed tomography (CT) scan of a *P. meandrina* skeleton housed in the Laboratory for Environmental Fluid Dynamics at the Technion - Israel Institute of Technology in Haifa, Israel. *P. meandrina* is a common species of coral that generally grows in high flow conditions and is densely branched. The colony dimensions were $L = 0.172$ m, $W = 0.172$ m and $H = 0.1$ m, respectively, in the streamwise ($x$), lateral ($y$), and vertical ($z$) directions. The

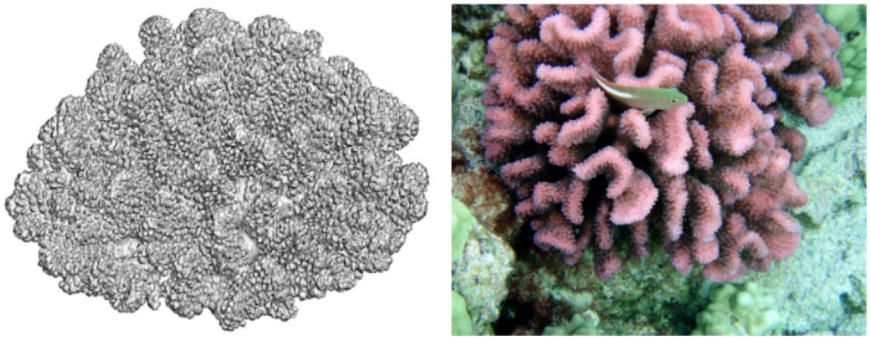

Figure 2.1: (left) Rendered stereolithography file of the *Pocillopora meandrina* colony used in the simulations. (right) A *P. meandrina* colony in its natural environment on the ocean floor. (Brocken Inaglory, Pocillopora meandrina with a resident fish, Wikimedia Commons, (2008); used in accordance with the Creative Commons Attribution (CC BY-SA 4.0) license[19].)

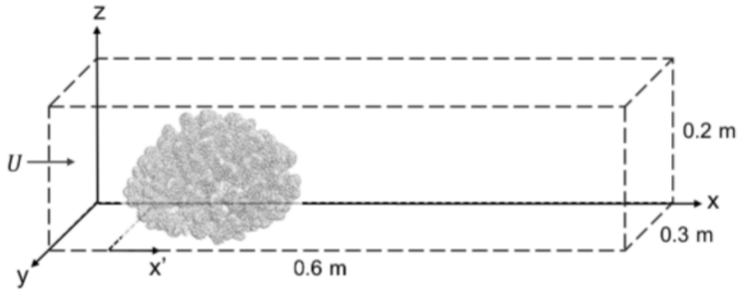


Figure 2.2: Schematic of the simulation flow domain (not to scale). $x' = 0$ at the beginning of the coral.

dimensions of simulation domain (Fig. 2.2) were 0.3 m in the lateral and vertical directions and 0.6 m in the streamwise direction. A second coordinate system ($x'$) was used in the streamwise direction, with $x'$ defined as zero at the start of the coral and $x' = L = 0.172$ m at the end of the coral. The center of coral was located at the center of the flow domain ($x = 0.3$ m, $y = 0.15$ m, $z = 0$ m. Dirichlet boundary conditions were applied at the inlet and convective boundary conditions were used at the outlet of domain. Slip boundary conditions were implemented on the side and top walls of the domain. A no-slip boundary condition was used on the bottom wall of the domain. The grid resolution was 1 mm in each direction. The total number of cells used in the simulation was 16 million. As the computations were not intended to resolve diffusion boundary layers less than 1 mm thick,

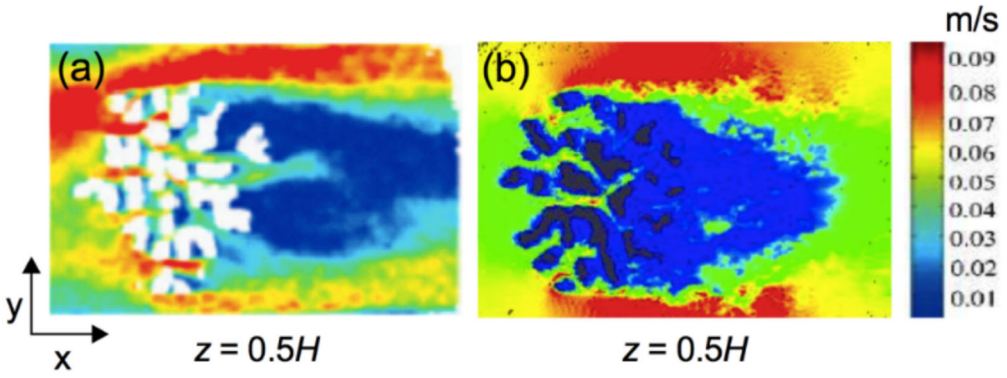


Figure 2.3: (a) Magnetic resonance velocimetry measurements of the velocity magnitude at colony mid-height ($z = 0.5H$) in a *P. meandrina* colony. Reproduced with permission from Limnol. and Oceanogr. **54**, 1819 (2009). Copyright 2009 John Wiley & Sons[17]. (b) Present LES simulations of the velocity magnitude at colony mid-height ($z = 0.5H$) in a similar *P. meandrina* colony.

the existing resolution of the grid is sufficient for the objectives of the current study[25]. We validated our computations to the extent possible with the experimental and computational results of Chang *et al.*, who performed magnetic resonance velocimetry measurements and LES simulations of the flow inside a nearly identical *P. meandrina* colony[17, 18]. We have replicated Chang *et al.*'s computational domain size, boundary conditions, and oncoming flow conditions in our simulations, in order to compare and validate our results against theirs. Fig 2.3 compares the velocity magnitude for the colony mid-height ($z = 0.5H$) cross section (top view) of Chang *et al.*'s experimental study[17] (Fig 2.3a) and the current simulation (Fig 2.3b). Although Chang *et al.*'s oncoming velocity profile is somewhat skewed owing to a curved, recirculating water channel, both velocity fields demonstrate the same characteristics: for these flow conditions, the colony largely acts as a baffle, diverting the majority of the flow around itself; and that in spite of this, however, high velocity regions, or "jets" whose speeds exceed the oncoming flow speed can be found deep in the coral interior in both cases.

Fig. 2.4 shows the instantaneous velocity field in a two-dimensional plane perpendicular to

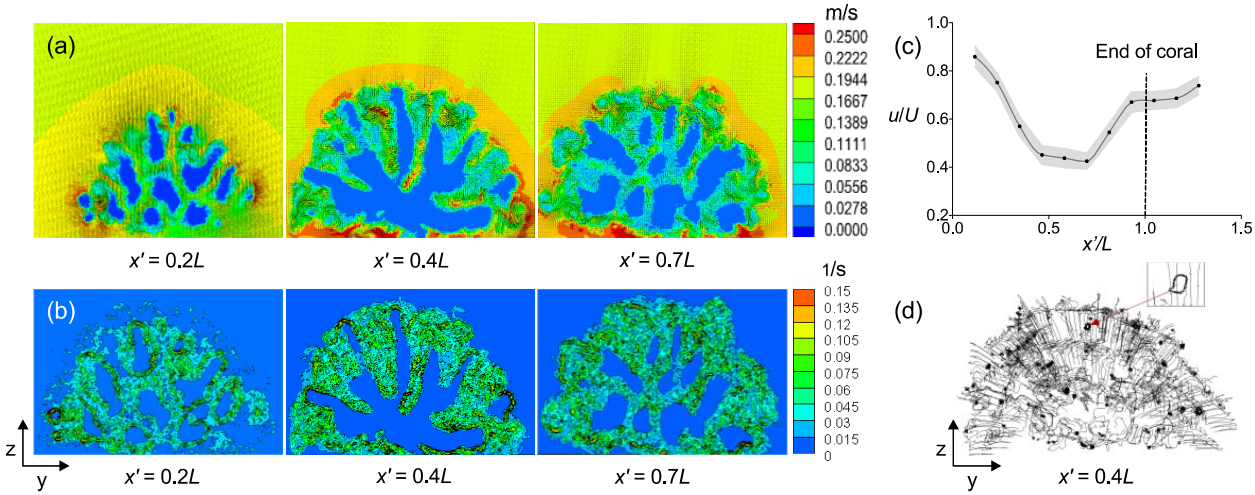


Figure 2.4: (a) Intracolonial velocity profile in a plane perpendicular to the flow direction at three streamwise ($x'$) locations. (b) Intracolonial vorticity profile in a plane perpendicular to the flow direction at the same three $x'$ locations as in (a). (c) Normalized intracolonial velocity values averaged over two-dimensional planes at eleven locations along the length of coral. The velocity deficit is greatest at $x' = 0.68L$, where the average velocity is just 43% of the oncoming value. Shading represents one standard deviation from the mean ($N = 6$). (d) Streamlines in a plane perpendicular to the flow direction at $x' = 0.4L$ clearly show the formation of vortices in the intracolonial velocity field. Inset: close-up of an individual in-plane vortex. All data displayed is for $t = 80.0$ s.

the oncoming flow direction at three different locations along the flow direction axis ($x$) for a Reynolds number of $20,000$ (based on the incoming flow speed, $U$, and the maximum height, $H$, of the colony) at time $t = 80.0$ s. Slices were chosen at upstream ($x' = 0.2L$ and $0.4L$) and downstream ($x' = 0.7L$) locations to highlight some major differences between anterior and posterior internal velocity profiles. In the figure, the maximum velocity zones, indicated by red shading, can be observed around the outer periphery of coral at both the upstream and downstream locations, and in the interior of the coral in the front half (upstream locations) only. Part of the reason for the high velocity values around the periphery of the colony is that the simulation domain constrains the flow around the coral and, at the same time, the coral acts as a baffle, providing hydrodynamic resistance to flow penetration under these flow conditions. *P. meandrina*, in particular, has a relatively high branch density, which

enhances the baffle effect. In their natural ocean flow environment, *P. meandrina* colonies exists both as solitary colonies, and as part of larger reef structures made up of several colonies. In fact, the flow conditions considered in this study may be rare for corals in their natural environment since the computational domain considered constrains the flow and may artificially impose mass conservation at unrealistically small scales. We are, however, limited by computational costs and by the need to validate the results against the two existing previous studies of the detailed flow field in a branching coral colony. Future studies of the detailed flow field in the interior of a branching coral colony with more realistic velocity boundary conditions will be an important step.

The high velocity regions in the interior of the upstream half of the colony are due to regions of energetic flow that do penetrate into the interior of the colony. Since the resistance to flow penetrations is not uniform across the colony, high speed jets form in the regions of low resistance.

In addition to the flow patterns described above, the formation of vortices can be observed at the periphery of the colony. The vortices facilitate mixing and mass transfer between the interior and exterior of the colony. These vortices form as the flow sheds from individual branches in the colony, and the number of vortices increase toward the posterior (downstream) end of the colony. The mean vorticity of the upstream flow field located at $x' = 0.4L$ is $9.62 \times 10^2\ s^{-1}$, while in the downstream velocity field ($x' = 0.7L$), it is $1.18 \times 10^3\ s^{-1}$: a roughly 23% increase while traversing 30% of the coral's length in the streamwise direction.

To quantify the change in the average velocity magnitude along the length of coral in the flow direction, the average velocity in lateral intracolonial velocity slices (like those in Fig. 2.4a) were computed at 20 mm intervals along the flow axis. The mean velocity value was then normalized by the incoming velocity magnitude and plotted versus $x'$ in Fig. 2.4c. The

vertical dotted line represents the downstream end of coral colony, and the mean velocity values past the dotted line are located in the wake. The plot shows a maximum reduction in velocity magnitude to 43% of the free stream value in the interior of the colony, about two-thirds of the way along the length of the coral at $x' = 0.68L$, which is comparable to results found in the experimental literature [17, 18]. Note that averaging a subportion of the colony interior that excluded the peripheral region would result in more significant reductions in the velocity magnitude. The average velocity then accelerates toward the end of the coral, as it enters the wake region, and continues to accelerate until it meets the unaffected free stream far behind the coral (not shown in Fig. 2.4c).

To assess the intracolonial flow structure more clearly, vorticity fields were calculated at several $x'$ locations. Fig. 2.4b shows anterior vorticity cross-sections at $x' = 0.2L$ and $x' = 0.4L$ and a posterior cross-section at $x' = 0.7L$. A highly vortical flow field was observed throughout most of the interior of the coral, and on the periphery of the colony. This highly vortical field will assist in the mixing of dissolved solutes with the bulk fluid more effectively and enhance mass transport rates from the interior of coral to the free stream and vice versa. At the entrance to the coral interior where the flow speed is not yet significantly reduced from the exterior value (approximately for $x' = 0\text{-}0.2L$), the vortices were less apparent. Here, the average colony branch diameter and oncoming flow speed are likely the appropriate length and velocity scales to use for characterizing the flow, as we do for the first entry in Table 2.1.

In order to characterize the rate of mass transport in the intracolonial flow field, we estimate the advection time scale as $\tau_{adv} \sim \ell/u$, and the diffusion time scale as $\tau_\nu \sim \ell^2/D_\nu$, where $\ell$ is a characteristic length scale of the flow, $u$ is a characteristic velocity, and $D_\nu$ is the molecular diffusion coefficient. The Péclet number can be defined in terms of the ratio of these two

time scales as follows

$$\frac{\tau_\nu}{\tau_{adv}} = \frac{u\ell}{D_\nu} = Pe \tag{2.1}$$

For the external flow at the periphery of the colony, and for the flow in the frontmost portion of the colony, the advection time scale can be calculated from the diameter of the colony branches and the bulk velocity, as discussed above. For the average branch diameter of 0.013 m and the bulk velocity of 0.2 m/s, the advection time scale was found to be 0.065 s at the exterior of the coral. The value of the diffusion coefficient for the small molecules important to coral physiological processes, such as oxygen, carbon dioxide, and bicarbonate, are on the order of $D_\nu \approx 10^{-9}\ m^2/\text{s}$ [25]. Using $10^{-9}\ m^2/\text{s}$ for $D_\nu$, the diffusion time scale at the coral's exterior is $1.69 \times 10^5$, leading to a value for the Péclet number of $Pe = 2.6 \times 10^6$.

But the length and velocity scales that characterize the flow change in the interior of coral. To calculate the advection time scale there, following Shapiro *et al.*[14], the vortex diameters and the interior flow velocities can be used as the appropriate length and velocity scales to calculate the advection and diffusion time scales at the interior of coral.

In Table 2.1 the mean vortex diameters ($\bar{\ell}$), with half of the maximum vorticity magnitude used as cutoff value) and mean velocity magnitudes ($\bar{u}$) are listed for two-dimensional, intracolonial flow fields at 5 different $x'$ locations along the length of the coral, along with the average advective time scale at those locations, calculated as the ratio of the mean vortex diameter to the mean velocity at that location. The final column of Table 2.1 contains the percent difference between the advective time scale calculated at an interior $x'$ location and the value of the advective time scale outside the colony. The intracolonial advective time scale is demonstrated to vary no more than 15.4% from the exterior value.

The interior characteristic length scale (the diameter of the vortices) was found to be significantly smaller than the exterior characteristic length scale (the average colony branch

Table 2.1: Advective time scale variation in the interior of the coral colony along the flow direction.

| $x'$ (m) | $\bar{u}$ (m/s) | $\bar{l}$ (m) | $\tau_{adv}$ (s) | % diff |
|---|---|---|---|---|
| $0.2L$ | 0.200[1] | 0.013[1] | 0.065 | 0.0% |
| $0.4L$ | 0.080 | 0.0050 | 0.063 | 3.1% |
| $0.6L$ | 0.076 | 0.0050 | 0.066 | 1.5% |
| $0.7L$ | 0.073 | 0.0055 | 0.075 | 15.4% |
| $0.8L$ | 0.100 | 0.0060 | 0.060 | 7.7% |

diameter). Similarly, the interior characteristic velocity scale (the average velocity magnitude) was smaller than the exterior scale (the mean flow velocity value outside the colony). Using these values, the mean advection time scale in the interior of coral in a two-dimensional plane located at $x' = 0.4L$, can be calculated to be 0.063 s, which differs from the value at the exterior of the colony by only 3.1%. Therefore, the loss of velocity magnitude does not appear to alter the transport mechanism in the interior of the colony and the advection time scale is almost identical to its exterior value throughout the interior of the colony.

In addition to the unidirectional oncoming flow conditions considered above, more realistic, oscillatory flow simulations were performed for *P. meandrina*. A sinusoidal wave with a period of $T = 7$ s and a maximum amplitude identical to that for the unidirectional flow case was used as the incoming flow condition. Similar to the unidirectional flow simulation case, most of the flow was diverted vertically and laterally. For the first half of the flow cycle, the frontal side of the coral experienced stronger incoming flow and the velocity reduced at the mid-colony with stagnation region behind the branches of the coral. The maximum velocity zones were found almost at the same locations in the interior of coral as for the unidirectional flow. Later in the flow cycle the stagnant region behind the branches became active and the wake switched sides with the change in flow direction.

To quantify the mass transfer, the transport of a scalar[26, 27], in this case, a stand-in for

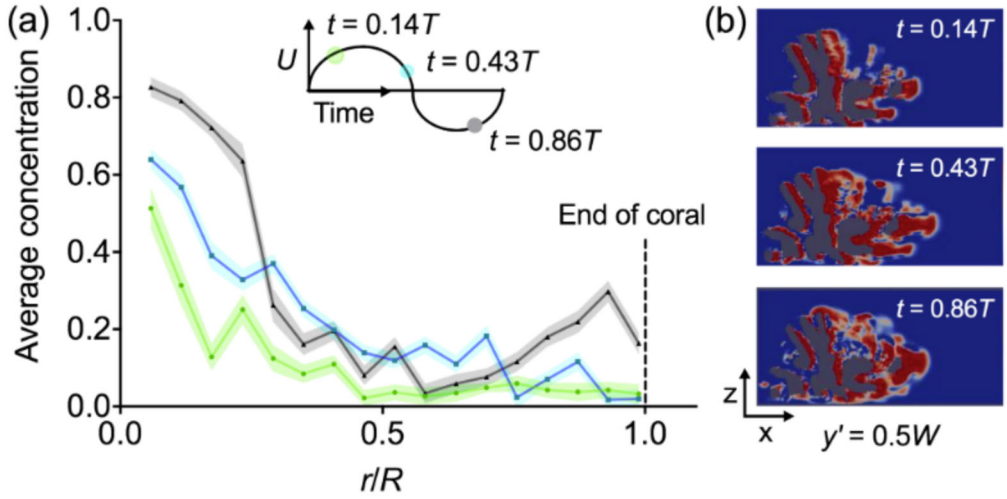


Figure 2.5: (a) Scalar concentration averaged over a spherical shell as a function of radial distance from the coral colony center under wave flow conditions at three times during the wave flow cycle (see schematic in inset for times). The dimensionless scalar concentration is set to unity at the coral surface. Shading represents one standard deviation from the mean. (b) Snapshots of the scalar concentration field in the mid-colony lateral plane ($y' = 0.5W$).

mass, was calculated from the surface of coral to the surrounding fluid as a function of radial distance from the geometric center of the colony, according to the following relations

$$\frac{\partial \phi}{\partial t} + \mathbf{u} \cdot \nabla \phi = D \nabla^2 \phi \tag{2.2}$$

$$D = \frac{\nu}{Sc} \tag{2.3}$$

where $\phi$ is the scalar (here, a proxy for the dissolved $O_2$, $CO_2$, or $CaCO_3$ (calcium carbonate) molecules mentioned above), $D$ is the diffusivity of the scalar and $Sc$ is the Schmidt number. A second order central differencing scheme was used for the spatial discretization of the advection diffusion equation, and a second order backward differentiation scheme was used for time discretization. The spatial resolution was identical to that used for the flow solver. We note that in this LES simulation framework, $\phi$ is the filtered scalar variable, $D$ is the turbulent diffusivity, $\nu$ is the turbulent eddy viscosity, calculated from the mo-

mentum equations, and $Sc$ is the turbulent Schmidt number. The transport was assumed to be steady state, with the concentration of the scalar at coral surface fixed at unity and initial concentration in surrounding fluid set to zero, representing mass transfer away from the coral, such as for the byproducts of photosynthesis. The gradient of the concentration was set equal to zero on the internal surfaces of the flow domain as a boundary condition. A turbulent Schmidt number of $Sc = 1,000$ was used, following Chang *et al.*[18]. The steady state transport assumption is an approximation. In the coral's natural environment the oxygen concentration at the coral surface varies continuously.

The average scalar concentration was calculated over a sequence of spherical shells at different radii from the center of coral by integrating the amount of scalar occupied in each shell to the shell void. Fig. 2.5a shows the averaged shell scalar concentration as a function of radial distance from the center of coral for the oscillatory oncoming flow. The figure plots the amount of the scalar in 17 adjacent spherical shells of increasing radius at three different times in a flow cycle, $t = 0.14T$, $t = 0.43T$, and $t = 0.86T$. At $t = 0$, the scalar starts to diffuse from coral surface. As time progresses, the magnitude of the velocity increases and diffused scalar moves from the center to the exterior portion of colony. Near the middle of the cycle, the flow starts to slow down and eventually freezes momentarily before reversing at mid-cycle. At this time of low flow, the concentration of the scalar increases at the center of colony.

After the brief stagnation part of the cycle, the flow reverses and some of the scalar that was advected away is transported back toward the center of the colony, as one can see in Fig. 2.5b. During the second half of the cycle, some concentration of the scalar builds up in the exterior portion of the colony, as is demonstrated by the second peak in the $t = 0.86T$ curve (near $x' = 0.9$) in Fig. 2.5a.

This study illustrates that the geometric features of branching coral colonies can passively

enhance mass transfer processes in the interior of the corals by producing highly vortical intracolonial flow fields under unidirectional and wave flow conditions, despite the reduction in flow velocity at the interior of the colony. The vortices, which are shed from the colony's branches, stir the flow, reducing the length and velocity scales in the intracolonial flow field, ensuring that the advection time scales throughout the interior remain essentially unchanged from the exterior values. Additionally, observing the mass transfer process over one oscillatory flow cycle reveals a double-peaked build-up of a passive scalar emanating from the surface of the *P. Meandrina* colony studied here. Validating this phenomenon in the laboratory or ocean flow setting would enhance our understanding of interior mass transport properties in corals.

# Bibliography

[1] Mass T, Genin A, Shavit U, Grinstein M, Tchernov D. Flow enhances photosynthesis in marine benthic autotrophs by increasing the efflux of oxygen from the organism to the water. Proceedings of the National Academy of Sciences. 2010;107(6):2527–2531.

[2] Finelli CM, Helmuth BS, Pentcheff ND, Wethey DS. Water flow influences oxygen transport and photosynthetic efficiency in corals. Coral Reefs. 2006;25(1):47–57.

[3] Sebens K, Done T. Water flow, growth form and distribution of scleractinian corals: Davies Reef (GBR), Australia. In: Proceedings of the 7th International Coral Reef Symposium. vol. 1; 1992. p. 557–568.

[4] Sebens KP, Witting J, Helmuth B. Effects of water flow and branch spacing on particle capture by the reef coral Madracis mirabilis (Duchassaing and Michelotti). Journal of experimental marine biology and ecology. 1997;211(1):1–28.

[5] Bruno JF, Edmunds PJ. Metabolic consequences of phenotypic plasticity in the coral Madracis mirabilis (Duchassaing and Michelotti): the effect of morphology and water flow on aggregate respiration. Journal of experimental marine biology and ecology. 1998;229(2):187–195.

[6] Dennison WC, Barnes DJ. Effect of water motion on coral photosynthesis and calcification. Journal of Experimental Marine Biology and Ecology. 1988;115(1):67–77.

[7] Monismith SG. Hydrodynamics of Coral Reefs. Annual Review of Fluid Mechanics. 2007;39(1):37–55. doi:10.1146/annurev.fluid.38.050304.092125.

[8] Antoniadis PD, Papalexandris MV. Dynamics of shear layers at the interface of a highly porous medium and a pure fluid. Physics of Fluids. 2015;27(1):014104. doi:10.1063/1.4905558.

[9] Wu Z, Mirbod P. Experimental analysis of the flow near the boundary of random porous media. Physics of Fluids. 2018;30(4):047103. doi:10.1063/1.5021903.

[10] Chamberlain Jr JA, Graus RR. Water flow and hydromechanical adaptations of branched reef corals. Bulletin of Marine Science. 1975;25(1):112–125.

[11] Mass T, Genin A. Environmental versus intrinsic determination of colony symmetry in the coral Pocillopora verrucosa. Marine Ecology Progress Series. 2008;369:131–137.

[12] Lesser MP, Weis VM, Patterson MR, Jokiel PL. Effects of morphology and water motion on carbon delivery and productivity in the reef coral, Pocillopora damicornis (Linnaeus): diffusion barriers, inorganic carbon limitation, and biochemical plasticity. Journal of Experimental Marine Biology and Ecology. 1994;178(2):153–179.

[13] Patterson MR. A chemical engineering view of cnidarian symbioses. American Zoologist. 1992;32(4):566–582.

[14] Shapiro OH, Fernandez VI, Garren M, Guasto JS, Debaillon-Vesque FP, Kramarsky-Winter E, et al. Vortical ciliary flows actively enhance mass transport in reef corals. Proceedings of the National Academy of Sciences. 2014;111(37):13391–13396.

[15] Reidenbach MA, Monismith SG, Koseff JR, Yahel G, Genin A. Boundary layer turbulence and flow structure over a fringing coral reef. Limnology and oceanography. 2006;51(5):1956–1968.

[16] Reidenbach MA, Koseff JR, Monismith SG. Laboratory experiments of fine-scale mixing and mass transport within a coral canopy. Physics of Fluids. 2007;19(7):075107.

[17] Chang S, Elkins C, Alley M, Eaton J, Monismitha S. Flow inside a coral colony measured using magnetic resonance velocimetry. Limnology and Oceanography. 2009;54(5):1819–1827.

[18] Chang S, Iaccarino G, Ham F, Elkins C, Monismith S. Local shear and mass transfer on individual coral colonies: Computations in unidirectional and wave-driven flows. Journal of Geophysical Research: Oceans. 2014;119(4):2599–2619.

[19] Inaglory B; 2008. https://en.wikipedia.org/wiki/Pocillopora_meandrina.

[20] Atkinson M, Bilger R. Effects of water velocity on phosphate uptake in coral reef-hat communities. Limnology and Oceanography. 1992;37(2):273–279.

[21] Elkins CJ, Alley MT. Magnetic resonance velocimetry: applications of magnetic resonance imaging in the measurement of fluid motion. Experiments in Fluids. 2007;43(6):823–858.

[22] Kaandorp JA, Koopman EA, Sloot PM, Bak RP, Vermeij MJ, Lampmann LE. Simulation and analysis of flow patterns around the scleractinian coral Madracis mirabilis (Duchassaing and Michelotti). Philosophical Transactions of the Royal Society of London B: Biological Sciences. 2003;358(1437):1551–1557.

[23] Kaandorp JA, Sloot PM, Merks RM, Bak RP, Vermeij MJ, Maier C. Morphogenesis of the branching reef coral Madracis mirabilis. Proceedings of the Royal Society of London B: Biological Sciences. 2005;272(1559):127–133.

[24] Balaras E. Modeling complex boundaries using an external force field on fixed Cartesian grids in large-eddy simulations. Computers & Fluids. 2004;33(3):375–404.

[25] Larkum AW, Koch EM, Kühl M. Diffusive boundary layers and photosynthesis of the epilithic algal community of coral reefs. Marine Biology. 2003;142(6):1073–1082.

[26] Tran-Duc T, Phan-Thien N, Khoo BC. A smoothed particle hydrodynamics (SPH) study of sediment dispersion on the seafloor. Physics of Fluids. 2017;29(8):083302. doi:10.1063/1.4993474.

[27] Tran-Duc T, Phan-Thien N, Khoo BC. A smoothed particle hydrodynamics (SPH) study on polydisperse sediment from technical activities on seabed. Physics of Fluids. 2018;30(2):023302. doi:10.1063/1.5019811.

[28] Merks R, Hoekstra A, Kaandorp J, Sloot P. Models of coral growth: spontaneous branching, compactification and the Laplacian growth assumption. Journal of Theoretical Biology. 2003;224(2):153–166.

[29] NOAA. How Do Stony Corals Grow? What Forms Do They Take?; 2017. Available from: https://oceanservice.noaa.gov/education/kits/corals/coral03_growth.html.

# Chapter 3

# Effects of coral colony morphology on turbulent flow dynamics

**Publication information**

The contents of this chapter have been submitted for publication:

Hossain, M., & Staples, A. (2019). Effects of coral colony morphology on turbulent flow dynamics. Preprint available at *bioRxiv*. https://doi.org/10.1101/839902

## 3.1 Abstract

Local flow dynamics play a central role in physiological processes like respiration and nutrient uptake in coral reefs. Despite the importance of corals as hosts to a quarter of all marine life, and the pervasive threats facing corals, characterizing the hydrodynamics between the branches of scleractinian corals has remained a significant challenge. Here, we investigate the effects of colony branch density and surface structure on the local flow field using three-dimensional immersed boundary, large-eddy simulations for four different colony geometries under unidirectional oncoming flow conditions. The first two colonies were from the *Pocillopora* genus, one with a densely branched geometry, and one with a comparatively loosely branched geometry. The second pair of geometries were derived from a scan of a single *Montipora capitata* colony, one with the roughness elements called verrucae covering

the surface intact, and one with the verrucae removed. For the *Pocillopora* corals, we found that the mean velocity profiles changed substantially in the center of the dense colony, becoming significantly reduced at middle heights where flow penetration was poor, while the mean velocity profiles in the loosely branched colony remained similar in character from the front to the back of the colony. For the *Montipora* corals, somewhat counterintuitively, the colony without verrucae produced almost double the maximum Reynolds stress magnitude above the colony compared to the colony without verrucae. This implies that the smooth colony will have enhanced mass transport and higher bed shear stress and friction velocity values relative to the colony with verrucae.

## 3.2 Introduction

A new and important direction in understanding the coupled dynamics of corals and their hydrodynamic environments seeks to measure and model the flow inside coral reefs and individual colonies. But the task is challenging due to the existence of a wide range of flow scales within different boundary layers around a coral reef [1, 2]. The transport of planktonic food in the reef is mainly governed by the large-scale flow motion, while diffusion [3, 4] takes place at the surface of the coral at a much smaller scale. Experimental studies performed at this smaller hydrodynamic scale [5, 6] show that the growth direction, dimensions, and sparsity of branches depend on the flow profile inside the coral[7, 8, 9]. Similarly, the velocity profile controls the nutrient distribution [7, 10, 11, 12, 13]. and physiological processes like photosynthesis and respiration [14, 15, 16, 17] near the coral surface. Flow motion also controls the thermal micro-environment [18, 19] at the coral surface, which is extremely important for phenomena like coral bleaching. Both the transfer of nutrients from the overlying water column to the colony and the transport of gases from the coral to the water column depend

on the detailed flow dynamics through and around the coral [20, 21]. All these physiological activities are directly related to the flow conditions in and around the coral geometry. To obtain a clearer understanding of these interdependent relationships, the authors tried to find answers to a few basic questions, including:

What are the impacts of the internal geometry of the colony on the surrounding fluid? How does the mean flow profile change within the coral with different branch density? What is the role of the surface structure of coral on the local hydrodynamics?

Though numerous studies have been performed earlier on coral reefs or above the canopy [22, 23], these analyses lack a detailed study of the flow field inside the coral. One of the reasons for the lack of such critical studies might be the complexity in measuring the flow parameters at the interior of colony due to a lack of optical and acoustic access. Though experimental flow field measurements have been performed on corals, data obtained at several points are not sufficient to measure the complete flow profile inside a coral. Canopy flow theory may be suitable to model the detailed flow dynamics inside a coral reef. In canopy flow studies on corals by Shavit *et al.*, the model reef geometries were composed of homogeneous, simplified elements and the double averaged Navier-Stokes equations [24] were used to simplify the analysis , which led to the modeling of a new unresolved dispersive stresses [25, 26].

To mimic the hydrodynamics at the interior of a coral reef, Lowe *et al.* [27] used an array of cylinders to capture the velocity profile and shear stress inside the reef. This model was also used to estimate the mass transfer from the surface of the coral. Bilger and Atkinson [28] used engineering mass transfer [29] correlations to predict rates of phosphate uptake by coral colonies and treated the top of the colonies as a rough boundary. Recently, Stocking *et al.* examined the impact of surface roughness on turbulent hydrodynamics and heat transfer above the grooved brain coral, which because of its convex spherical shape, provides excellent optical and acoustic access [30].

but the analysis did not provide sufficient information about the flow dynamics at the interior of branching corals Chang *et al.* [31] used magnetic resonance velocimetry [32] to reveal the internal flow profile of corals for two different branching patterns. Though the results provided an excellent visualization of the flow field inside the coral, the study did not provide sufficient information regarding the formation of mean velocity profile as a function of coral height. Additionally, repeating such experiments on diverse coral structures are expensive and unrealistic. To solve these problems, numerical simulations can be an important tool.

For numerical simulations, complexity arises during capturing the arbitrary boundaries of coral geometry. Specifically, meshing around the arbitrary branches of coral is a challenging task. For body-fitted mesh, even the simplest geometries require efficient meshing algorithms to reduce the computational cost. To overcome this issue, numerical experiments in previous studies were performed by considering coral as an isotropic, porous medium, but questions emerged due to non-consideration of coral's natural morphology [33]. In addition, Kaandorp *et al.* used the Lattice Boltzmann method to understand the effects of flow on coral structure and simulated flow patterns around the coral surface[34, 35] at low Reynolds numbers (154 to 3,840), due to stability issues. Similarly, Chindapol *et al.* [36] used COMSOL Multiphysics to analyze the effects of flow on coral growth only in a laminar framework. Recently Cano *et al.* have computed the drag co-efficient for open branched *Acropora palmata* but the study does not give sufficient information regarding the flow interaction and drag-coefficient for densely branched coral [37]. Chang *et al.* [38] were the first (according to the authors' knowledge) to introduce immersed boundary method with large-eddy simulation on real coral geometry while computing the velocity profile inside the densely branch coral like *Pocillopora meandrina*, but the analysis was mainly focused on local shear and mass transfer on the coral structure. In a recent paper, Hossain and Staples *et al.* [42] computed the flow profile on the inside of coral, and showed that the mass transfer remains almost constant throughout

the coral even when the velocity drops substantially inside it. However, the analysis lacks information regarding variation in the mean velocity profile through the coral height with the change in branching pattern, which will be discussed here in detail for two different *Pocillopora* branching structures.

In addition, it is important to understand the effects of natural flow conditions on coral morphology. To flourish in a changing environment, coral modifies its structure to adjust to the surrounding hydrodynamics. It has been found that under sheltered conditions, *Pocillopora damicornis* and *Seriatopora hystrix*, transformed from dense-branched to thin, larger-branched spacing coral due to the change in flow conditions [43]. Kaandorp and Kubler showed similar transformations for *Madracis mirabilis*[44]. Even a small modification can affect the boundary layer and turbulent stress developed at the coral surface and can change the mass transfer rate [45, 46]. These variations in turbulent flow profiles illustrate the effects of coral structure on hydrodynamics in different flow conditions. One such interaction can be observed in the hydrodynamics of loosely branched *Montipora capitata* in a strong flow environment. Normally, loosely branched coral grows in a quiet flow environment, but *Montipora capitata*, with verrucae on its surface, is found in turbulent flow conditions near Hawaii. Naturally, questions arise regarding the impact of the verrucae on the surrounding fluid. To understand these influences of surface structure on surrounding fluid , it is essential to comprehend and compare the formation of boundary layers and turbulent stresses on these altered coral structures of *Montipora capitata* with and without verrucae. Though there were numerous studies performed on coral reefs, capturing the morphological change with flow conditions is rare in the literature and is a challenging task. Here, a detailed comparative flow analysis was performed on *Montipora capitata* with and without verrucae to understand the impacts of the verrucae on hydrodynamics.

Based on the discussion above, the current manuscript can be divided into two different

sections. In the first segments, three-dimensional velocity components and mean velocity profile were computed at the interior of two *Pocillopora* corals with different branching patterns for the same incoming flow. In the second part of the manuscript, a comparative study was performed between velocity profiles and Reynolds stress developed on *Montipora capitata* with and without verrucae at two different Reynolds number. Then, the results of the computations were compared to understand the variation of velocity profiles and turbulent stress developed on the slightly altered coral structures for the same incoming flow.

## 3.3 Materials and Methods

### 3.3.1 Coral species and geometries

Stereolithography (STL) files of the coral geometries used in the current studies are shown in Fig 3.1. Between the two *Pocillopora* coral, the densely branched *P. meandrina* was obtained from computed tomography (CT) of a real coral skeleton from Professor Uri Shavit's laboratory in the Department of Civil and Environmental Engineering at the Technion - Israel Institute of Technology. *P. meandrina*, generally known as cauliflower coral, is common in the East Pacific and the Indo-West Pacific, and is mainly exposed to the reef front. The stream-wise length, width and height of *P. meandrina* used in the current simulation were 0.172 m, 0.172 m and 0.1 m respectively. In contrast, branches are distributed more sparsely in *P. eydouxi*. This coral is common throughout the Indo-West Pacific and occurs in most reef environments, especially at reef fronts where the currents are strong. The length, width and height of *P. eydouxi* used in the simulation were 0.12 m, 0.11 m and 0.1 m respectively. Though the genus was similar, there were substantial structural differences between these

two coral morphologies. The ratio of surface area of *P. meandrina* and *P. eydouxi* was 5:1 and the value of volume of bounding box ($L \times W \times H$) to surface area was approximately 2.61 times higher for *P. eydouxi* in comparison to *P. meandrina*, which indicates that the branches were more compact inside *P. meandrina* than *P. eydouxi*. The ratio of maximum projected area in flow direction to surface area were 0.0754 and 0.0556 for *P. meandrina* and *P. eydouxi* respectively, which represented a higher projected surface area for *P. meandrina*. To understand their structural differences, variations of the mean diameter of the individual branch inside the coral and cross-sectional area of the colony were plotted in Fig 3.1 with respect to height for both *Pocillopora* corals.

To comprehend the effects of verrucae on the surrounding fluid, two coral geometries with and without verrucae were used for computation. Both coral geometries originated from the same STL file of *Montipora capitata*. Fig 3.12 shows *M. capitata* without verrucae where the verrucae from the coral surface were completely removed while keeping the dimension of the geometry same. The length, width and height of the corals were 0.118 m, 0.114 m and 0.1 m respectively. The cone-shaped verrucae had a base diameter of approximately 3 mm and a length of 3–4 mm. *M. capitata* is usually found in highly turbulent flow conditions in the tropical north and central Pacific Ocean near Hawaii at approximately 20 m depth. All corals used in the current study had low living-tissue biomass, so using skeletons instead of coral with bio-tissue had a minimal effect on flow dynamics.

### 3.3.2 Numerical methodology

The authors were looking for a method that could be implemented easily for complex geometries while minimizing computational cost. Immersed boundary method (IBM) is suitable for such analysis where the computation is performed on a Cartesian grid and the interface

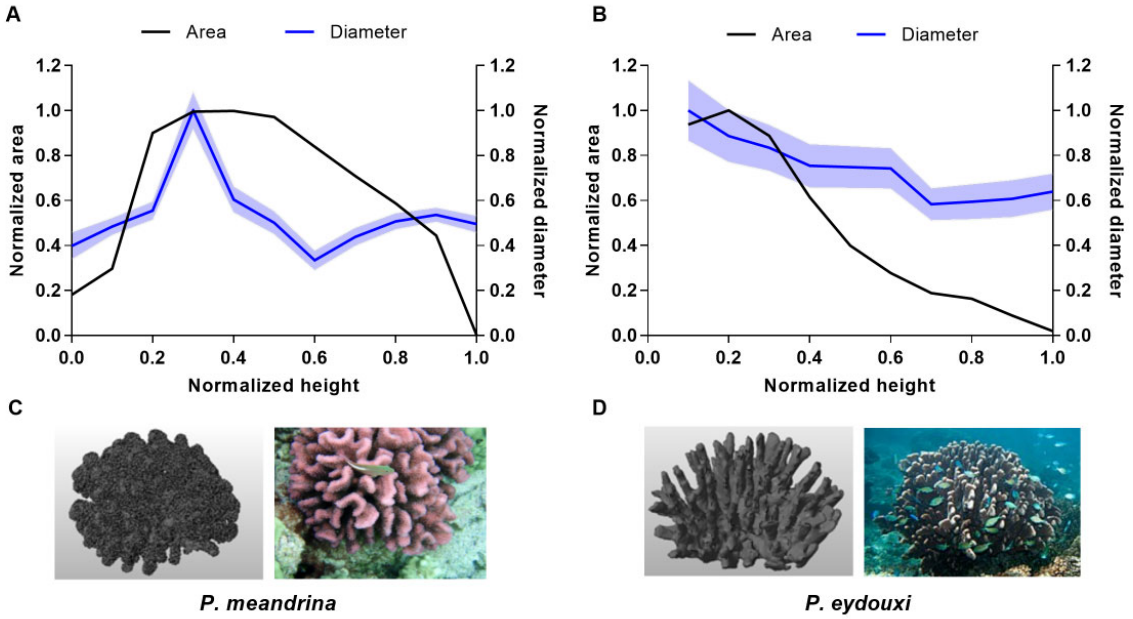


Figure 3.1: **STL files of *Pocillopora* coral geometries used in the current simulations.** (Left) Rendered stereolithography file of the *P. meandrina* colony used in the simulations and a *P. meandrina* colony in its natural environment on the ocean floor. [Brocken Inaglory, *P. meandrina* with a resident fish, Wikimedia Commons (2008); used in accordance with the Creative Commons Attribution (CC BY-SA 4.0) license [48]. (Right) STL file of the *P. eydouxi* colony and a *P. eydouxi* colony in its natural environment. [Paul Asman and Jill Lenoble, around antler coral *P. eydouxi*, Wikimedia Commons (2012); used in accordance with the Creative Commons Attribution (CC BY-SA 2.0) license [49]. (Top)Variation of cross-sectional area and branch diameter vs. height for *P. meandrina* and *P. eydouxi* respectively. The mean diameter was obtained by averaging the branch diameters at each height.

is tracked by identifying solid and fluid elements in the flow domain. For the current analysis, IBM was implemented in a large eddy simulation (LES) framework for a turbulent flow field where the largest scales of motion were calculated and the effects of the small scales were modeled. A top-hat filter was applied implicitly to the Navier-Stokes equations by the finite-difference operators and the resulting filtered equations are as follows:

$$\frac{\partial \bar{u}_i}{\partial t} + \frac{\partial \bar{u}_i \bar{u}_j}{\partial x_j} = -\frac{1}{\rho}\frac{\partial \bar{P}}{\partial x_i} + \nu \frac{\partial^2 \bar{u}_i}{\partial x_j x_j} - \frac{\partial \tau_{ij}}{\partial x_j} + f_i \tag{3.1}$$

$$\frac{\partial \bar{u_i}}{\partial x_i} = 0 \tag{3.2}$$

where $\bar{u_i}$ represents large-scale velocity vector, $P$ represents pressure, $\rho$ represents density, $\nu$ represents kinematic viscosity and $f_i$ represents the external body force used to implement boundary conditions for arbitrary objects with a non-conforming grid. Here, the overbar denotes a filtered variable.

The spatial filtering operation on the Navier-Stokes equations produces the subgrid scale stress term,$\tau_{ij} = \overline{u_i u_j} - \bar{u_i}\bar{u_j}$. Now if we use $u = \bar{u} + u'$ in the subgrid stress tensor, where $u'$ is the residual from the filter, new terms will be generated which cannot be evaluated directly. So the $\tau_{ij}$ needs a closure model to solve the system of equations (3.1) and (3.2). The dynamics eddy-viscosity model used in this study is of the following form:

$$\tau_{ij} - \frac{\delta_{ij}}{3}\tau_{kk} = -2C\bar{\Delta}^2 \mid \bar{S} \mid \bar{S_{ij}} \tag{3.3}$$

where $\mid \bar{S} \mid$ is the magnitude of the large-scale strain rate tensor, $\delta$ is Kronecker delta and $\bar{S_{ij}}$ is strain tensor and $\bar{\Delta}$ is the filter size, which can be defined as:

$$\bar{S_{ij}} = \frac{1}{2}(\frac{\partial \bar{u_i}}{\partial x_j} + \frac{\partial \bar{u_j}}{\partial x_i}) \tag{3.4}$$

$$\bar{\Delta} = (\Delta x \Delta y \Delta z)^{\frac{1}{3}} \tag{3.5}$$

Here, $\Delta x$, $\Delta y$ and $\Delta z$ are the local grid size, and C is the user-specified value for the Smagorinsky eddy viscosity model, where the usual value of C ranges from 0.1 to 0.2. However, the model does not behave properly near solid boundaries. So, in the computation analysis, the Lagrangian averaging procedure was used to compute the value of C from the

information of the resolved scale[50].

$$C = -\frac{1}{2}\frac{\langle L_{ij}M_{ij}\rangle}{\langle M_{ij}M_{ij}\rangle} \tag{3.6}$$

where

$$L_{ij} = \widehat{\bar{u}_i\bar{u}_j} - \hat{\bar{u}}_i\hat{\bar{u}}_i \tag{3.7}$$

$$M_{ij} = \hat{\bar{\Delta}}^2 \mid \hat{\bar{S}} \mid \hat{\bar{S}}_{ij} - \bar{\Delta}^2 \mid \bar{S} \mid \bar{S}_{ij} \tag{3.8}$$

An additional test filter, $\hat{\bar{\Delta}}$, which was twice the size of grid filter, $\bar{\Delta}$ was used to compute the value of $C$. All of the three-dimensional simulations on STL files of coral colonies were performed using the IB method implemented in the LES framework using a code developed by Balaras *et al.* The complete details of the numerical method can be found in Balaras *et al.* [51].

A standard second-order central-difference scheme on a staggered grid is used in the present study. The pressure and scalar variables are located at the center of the grid cell, and velocity components are located at the cell-face center. The solution of equations (1) and (2) is obtained by a second-order projection method. Here, time was advanced explicitly by using an Adams–Bashforth scheme. An explicit algorithm has been used to simplify the implementation of boundary conditions near a complex boundary. In a two-step time-splitting method, first a provisional value of the velocity field, which is not divergence free, can be obtained and used for updating the velocity. The intermediate velocity, $\hat{u}_i^n$ evaluated at n step can be written as follows:

$$\frac{\hat{u}_i^n - u_i^{n-1}}{\Delta t} = RHS_i^n + f_i^n \tag{3.9}$$

where RHS contains all of the terms in the right side of the momentum equation. After solving the Poisson equation, the final velocity, $u_i^n$, can be updated from the $\hat{u}_i^n$. The external force, $f_i^n$, needs to be calculated first to implement the desired boundary condition at the boundary point where the boundary may or may not coincide with the grid points. To do this, it is necessary to identify solid, fluid and forcing points near the boundary where forcing functions are implemented in the simulation domain. In the current study, accurate interface tracking methodologies were used for complex coral geometry. An immersed solid boundary of an arbitrary shape is represented by a series of markers shown in Fig. 3.2. After defining the immersed interface as a series of marker particles, the relationship between these particles and the underlying Eulerian grid can be established by ray-tracing algorithm. The procedures for identifying solid and fluid points in the computational adopted for the current study can be found in detail in [51]. The procedure includes Finding of the closest grid points near each marker particle. Then from each marker particle, a ray $\vec{r}$ is shot to the grid point and a normal, $\vec{n_b}$, is also calculated on the marker points. If $\vec{r}.\vec{n_b} < 0$, then this grid point is inside the solid ; otherwise, it is outside of the solid. The forcing points are the closest grid points near the marker points which have at least one solid point near the boundary. The procedure for finding solid, fluid and marker particles near the boundary are shown in Fig. 3.2.

As mentioned earlier, all of the simulations were performed on the STL files of coral geometries, which were composed of millions of triangles. A ray-tracing algorithm was implemented to establish a relationship between these triangles with a Eulerian grid.The coordinates of the vertices and normal of each triangle are stored in the STL file. The ray triangle intersection algorithm used in the reconstruction of the flow field consists of the following steps.

1. A ray is shot from a grid point to a triangle.

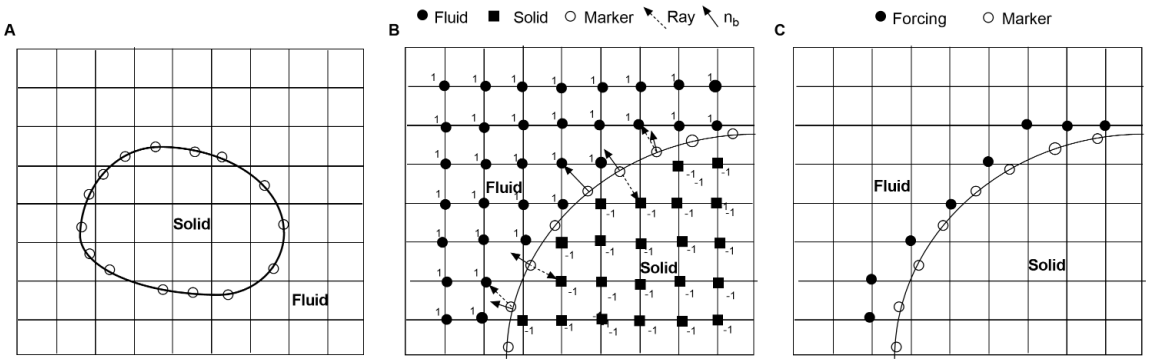


Figure 3.2: **Tracking of solid-fluid interface used in the immersed boundary method.** Fig. 3.2(A) An arbitrary shape solid in orthogonal computational domain. The marker particle at the boundary may or may not coincide with the Eulerian grid points. (B) Identification of solid and fluid points in the computational domain by ray tracing algorithm. (C) Identification of forcing points (where forcing will be applied) near the boundary after tagging solid and fluid grids in the computational domain.

2. Determine if the ray intersects the triangle or not.

3. Find the coordinates of the intersecting point.

In the solution procedure, the fluid points are the unknowns and the forcing points are boundary points, while the solid points do not influence the rest of the computation.

If the boundary coincides with the grid points, the forcing function can be calculated directly from the known $\hat{u}_i^n$ at the grid points. Otherwise, the value of velocity at the forcing points can be calculated from the interpolation of surrounding fluid points. The interpolation stencil in this method, however, involves a search procedure for suitable fluid points, and those points in the stencil may contain points that do not belong to the neighboring grid lines of the forcing point. The detailed procedure of identifying the immersed boundary, calculating the forcing function near the boundary, and the interpolation scheme can be found in Balaras *et al.* [51]. Here, the forcing function was calculated only at the boundary.

The simulation domain for the current study was not chosen randomly. Before performing

the current analysis, a near-as-possible validation simulation was performed to compare the current result with the experimental result of Chang *et al.*[31] for a high-flow morphology coral, *Stylophora pistillata*. For the current analysis, the domain of simulation was 0.6 m long in the stream-wise direction (x), 0.3 m wide (y) and 0.3 m in vertical direction (z), similar to the flow domain used in the experimental and numerical study of Chang *et al.*[31]. As in natural conditions, a single coral sits in the open flow domain or in a coral reef of multiple colonies and the natural flow always takes the path of least resistance. But, the flow domain chosen in the experiment and current simulation, which acts to constrain the flow field, will only be approximated in nature for a few rare coral colonies. If the simulation can be performed in an extremely large domain, that would represent the ideal flow scenario for a coral sitting in an open flow environment. At the same time, we have to be realistic regarding the computational expenses when performing a simulation around an extremely complex and arbitrary shape geometry. In addition, we want to stress the objectives and scale of the current study. We intended to analyze the detailed flow field through and around a single coral colony, where the length scale varies from an individual colony branch diameter to the length or diameter of a single colony, and the large-eddy simulation of the Navier-Stokes equations were used here to resolve the hydrodynamics of coral interior at these scales. These constraints have led us to limit the dimension of the simulation domain for a single coral. As the current analysis was not intended to resolve diffusion boundary layers less than 1 mm, which would be extremely difficult and computationally expensive for such arbitrary geometry, the current grid resolution of 1 mm in x, y and z directions was sufficient to meet the objectives of the current study. Similar to Chang *et al.*[38], Dirichlet boundary conditions were applied at the inlet, and an outflow boundary was used at the outlet of the domain. For the lateral direction, slip boundary conditions were implemented at both sides of the coral. Slip boundary conditions were also used at the top face of the domain, and the bottom of the domain was defined as a no-slip wall. In the current analysis, 54 million grid

cells were used for all of the simulations. All of the numerical experiments were performed on the Engineering Science and Mechanics (ESM) computing cluster at Virginia Tech. A schematic of the flow domain is shown in Fig 3.3.

In addition to the capability of the current Immersed boundary method to reveal the hydrodynamics process at the interior of the complex branching colony, few limitations exist in the current analysis. First, the hydrodynamic analysis preformed on the coral structure was only limited to unidirectional flow condition in the current study. But oscillatory flow significantly impacts the hydrodynamic conditions and biological activities of coral living in such flow condition. The literature review shows that the nutrient uptake and mass transport rate differ at the oscillatory flow [27, 39, 40]. In addition, the branching analysis was only performed on two *Pocillopora* coral structures. If a couple of more coral branching structures with different branching patterns were included in the current study, the detailed study of these structures can provide us valuable insight into the impact of branch thickness, inter-branch distance on the flow dynamics at the interior of coral. In the current study, it is not possible to resolve the diffusion boundary layer, which is in the order of several hundred micron to 1-2 mm thick on the coral surface [41]. To resolve this thin boundary layer on such complex geometry requires a large of grids on the surface which is extremely expensive and out of the scope of the current study. Besides, the current study requires more rigorous validation with the experimental results but unfortunately, detailed three-dimensional flow profile at the interior of coral is not common.

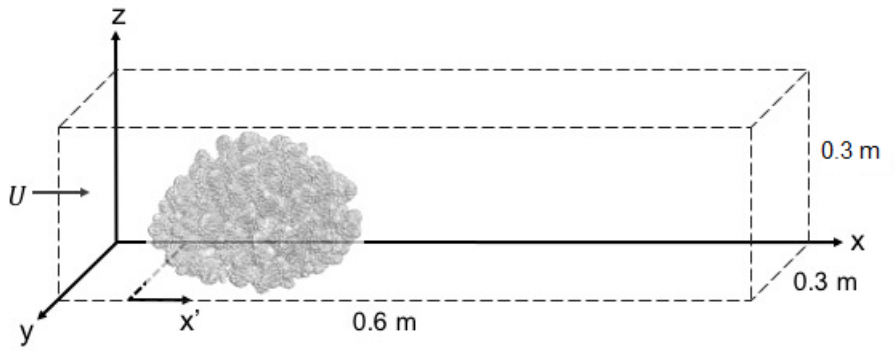


Figure 3.3: **Schematic of the simulation flow domain (not to scale).** $x = 0$ is the secondary axis used at the beginning of the coral. The center of the coral is located at the middle of the flow domain. Uniform grid spacing was used throughout the domain.

## 3.4 Results and discussion

### 3.4.1 Comparison of velocity and vector profiles between two *Pocillopora* geometries

Before comparing flow profiles between two *Pocillopora* structures, the results from the simulation were compared with the experimental results of Chang *et al.*[13] for the high-flow morphology of *Stylophora pistillata*. Although every coral is unique in nature, the dimensions of both the geometries used in the experiment and simulation were within the same order. In the experiment, the streamwise (x), cross-stream (y), and vertical (z) extents of the densely-branched coral were 0.128 m, 0.13 2 m and 0.1 m, respectively. In the simulation, the extents of the densely-branched coral were 0.172 m, 0.172 m and 0.1 m, respectively, in the stream-wise, lateral and vertical directions. Detailed physical and morphological properties of the two coral geometries are shown in Table 3.1. The channel dimensions for both the experiment and simulation domains were almost the same. In the experiment, the bulk velocity in the channel was 0.05 m/s and the Reynolds number, based on the diameter of the branch, was 580. Based on the height of the coral, it was approximately 5,000. A

similar Reynolds number was used in the simulation to keep the flow conditions close to the original experiment. For qualitative comparison, computational results were compared with the direct velocity slices obtained from the experiment. Fig 3.4 shows a comparison of the cross-sectional (top view) velocity profile obtained near the midsection of the coral between the current simulation (right) and the experimental results of Chang *et al.* (left) at the different heights inside the corals. For the experiment, the middle slice was obtained exactly at the mid-height of the coral and the slices were obtained at 5-mm intervals from the both sides. In the simulation, the slices were chosen exactly in the same manner and relatively high velocity magnitude was observed at both sides of the coral, and a distinct wake region formed behind the rare section. Because of the dense branch structure, the colony largely acts as a baffle and most of the flow was diverted outward and vertically upward. The branches located in the frontal section of the coral significantly reduced the velocity for the rare section. Although the oncoming velocity profile in Chang *et al.* is somewhat skewed owing to a curved, recirculating water channel, both velocity fields demonstrate the same characteristics for these flow conditions. The results also demonstrated a low velocity region behind the thick branches of the coral and the velocity magnitude was almost identical for both cases.

A comparative analysis was also performed to quantify the variation of average velocity between the experimental results of Chang *et al.*[31] for the high-flow morphology of *Stylophora pistillata* and current numerical simulation. In the experimental analysis, the variation of velocity at the interior of colony was plotted as a function of radial distance from the center of the coral. For comparison, similar approach was adopted for computational analysis. The center of the coral was selected by the midpoint of X,Y and Z extension of the colony and mean velocity was obtained at different radial distance from this point. Fig 3.5 shows comparison of mean velocity magnitude from exterior to interior of the colony for both the

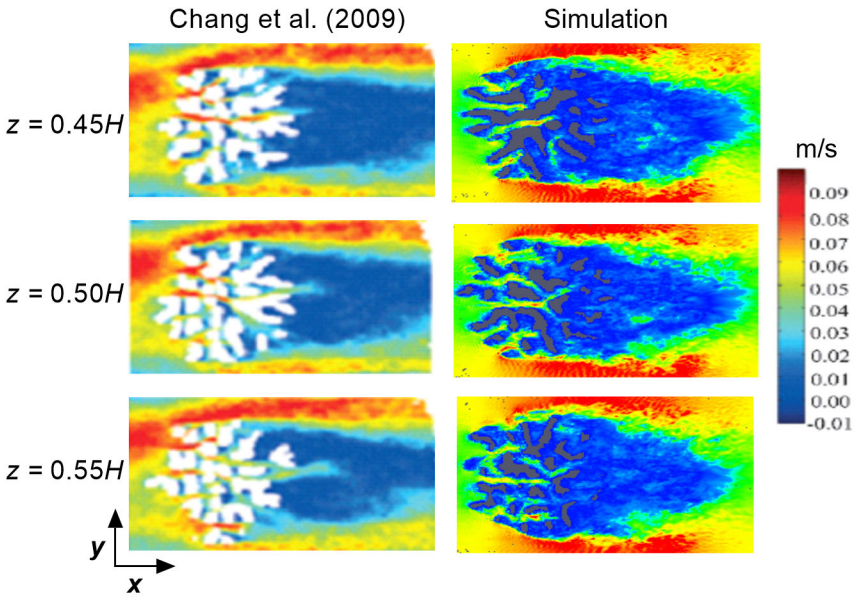


Figure 3.4: **Comparison of the top view of velocity slices between the experiment [31] and the simulation at different heights inside of the corals.** (Left) Top view of velocity slices inside *S. pistillata* obtained by magnetic resonance velocimetry at mid-height, z= 0.5 H of the coral (middle slice) and the other slices were obtained at 5-mm intervals from both sides. Reproduced with permission from *Limnology and Oceanography* 54, 1819 (2009). Copyright 2009 by John Wiley and Sons, Inc. (Right) Present LES simulations of the velocity magnitude obtained inside *P. meandrina* at the same height described in the experiment. The size of coral and the domain used for both studies had almost the same dimensions.

studies. In general, the two profiles show similar velocity trend from exterior to the deep at the interior of colony. Except at the mid point of the colony, computational profile shows lower velocity magnitude than the experimental analysis though the overall trend remains same. One reason behind such discrepancy might be the difference of the compactness of the branch density between these two geometries. In terms of inter-branch distance to branch diameter ratio, the geometry used in the computational analysis has a lower ratio than the experiential geometry which results in more resistance to the flow at the interior of colony.

Flow inside the coral is a function of inter-branch distance, branch diameter, coral height,

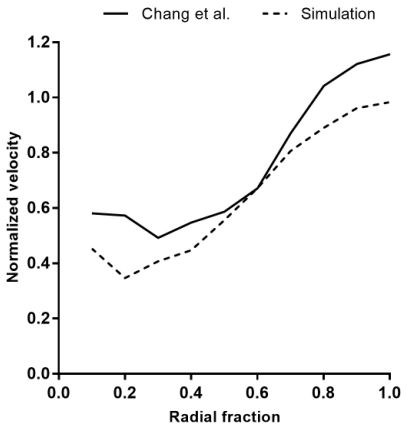


Figure 3.5: Comparison of normalized averaged velocity plotted as a function of radial distance from the center to the exterior of coral between the experiment [31] and the simulation. The difference in velocity magnitude between these two structures might be due to the difference in branch distance to branch diameter ratio shown in table 1. The experimental data is obtained from flow profile of high flow morphology inside *S. pistillata* obtained by magnetic resonance velocimetry. Reproduced with permission from *Limnology and Oceanography* 54, 1819 (2009). Copyright 2009 by John Wiley and Sons, Inc.

Table 3.1: Physical properties of coral geometry in Chang *et al.* and current simulation.

| Coral geometry | Chang *et al.* | Current simulation |
|---|---|---|
| Ratio of volume to surface area | 2.0 | 2.0 |
| Ratio of frontal to surface area | 0.078 | 0.0754 |
| Ratio of branch distance to diameter | 4.5 | 3.0 to 4.0 |

and incoming velocity. To understand the branching effect of coral on the surrounding fluid, flow through two different branching patterns of the same *Pocillopora* coral was evaluated and compared for the same incoming flow. The simulation parameters for these the two coral geometries are shown in Table 3.2. Top views of flow through these two *P. meadrina* corals were shown in Fig 3.6 for an incoming flow of 0.15 m/s. The incoming velocity was selected based on the natural flow condition near the *Pocillopora* coral habitat. The middle velocity slice was obtained at approximately the midsection of the coral and the rest of the slices were obtained at 20-mm intervals on both sides. For both the coral geometry, a stagnation

region formed near the front section, and the effect was higher for *P. meandrina* due to high branch density. For *P. meandrina*, higher velocity was observed at the top and both sides of the coral and the velocity reduced substantially and became almost uniform in the latter half of the coral. As most of the flow is diverted to the top and both sides of the coral, the restriction of flow due to the high compactness of the interior branches was more visible for *P. meandrina*. During interaction with internal branches, mixing and transportation takes place at the coral surface. At the downstream end of the coral, a distinct wake region containing a large circulating eddy formed behind the coral. In contrast, the flow penetration at the interior of *P. eydouxi* was easier than in *P. meandrina*. As the geometry became more open, the interior received more flow, which was apparent from the flow slices exhibiting higher velocity zones at the interior of the coral. Though a large portion of the flow was diverted outward, the penetration was much better in *P. eydouxi* than *P. meandrina*.

Table 3.2: Simulation parameters for *Pocillopora*. Here Reynolds number was calculated based on coral height.

| Coral species | Flow | $U_{incoming}$ (m/s) | Re |
|---|---|---|---|
| *P. meandrina* | Unidirectional | 0.15 | 15,000 |
| *P. eydouxi* | Unidirectional | 0.15 | 15,000 |

For qualitative measurements of the variation of velocity profiles along the lateral direction, a velocity slice (perpendicular to flow) was taken at $x' = 0.5L$ for both of the corals. Fig 3.6(B) shows a comparison of velocity slices obtained at the middle of the coral, perpendicular to the flow direction. For both of the corals, the outer periphery shows higher velocity magnitudes due to the constraints of the flow domain. For the same incoming flow conditions, *P. meandrina* shows relatively low velocity magnitude at the coral interior and the incoming flow loses most of its momentum due to high branch density. In comparison, *P. eydouxi* shows relatively higher velocity magnitudes between the branches, especially at the narrow corner between the branches, where the flow accelerates.

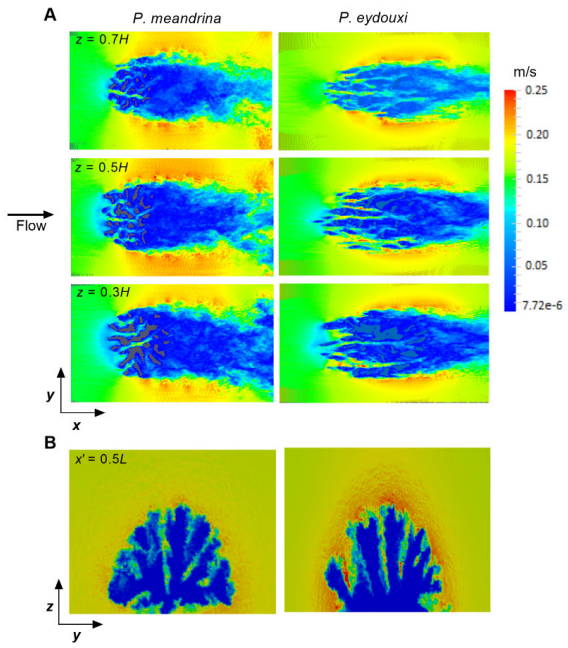


Figure 3.6: **Comparison of top view velocity slices between two *Pocillopora* colonies with different branching structures.** (A) Top view of velocity slices inside *P. meandrina* (left) and *P. eydouxi* (right) at $z = 0.3H$, $0.5H$, and $0.7H$ above the base of the coral for the same oncoming velocity of 0.15 m/s, where $H$ is the height of the colony. (B) Comparison of front view velocity slices between *P. meandrina* (left) and *P. eydouxi* (right). These slices were obtained at the middle of the coral ($x' = 0.5L$) along the flow direction, where $L$ is the length of the colony.

To have a clear understanding of the interaction of incoming flow with the branches, vector profiles at the interior of colony were captured from the velocity slices. Fig 3.7 shows top view of velocity vector inside *P. meadrina* at different height from the base of the colony. From the vector profiles at z=0.3 & 0.5H it can be clearly observed that the frontal section has higher velocity magnitude than the rear half. This is an interesting feature for the densely branched colony. The difference in flow magnitude between the front and rare section will impact the mass transfer rate which has been discussed in detail in literature section. In addition, two vector profiles perpendicular to stream wise flow direction were also captured at the frontal and rare section of *P. meadrina* (Fig 3.8). It is interesting to notice the formation of vorticies at the outer periphery of the colony. These external vorticies stir the water column

and enhance the transport process at the exterior of colony. To compare the variation of flow profile through the branches of *P.eydouxi*, velocity vector were similarly captured at the different height from the base of the colony (Fig 3.9). These vector profiles demonstrate substantial difference between the flow profile of inside the two structures. Because of the more open spaces between the branches, formation of wake zones can be observed behind the each branches in addition to wake region behind the rare section of colony. The formation of the recirculating zones actually helps the *P.eydouxi* by keeping the crossing solute in this zones which enhances the transport process.

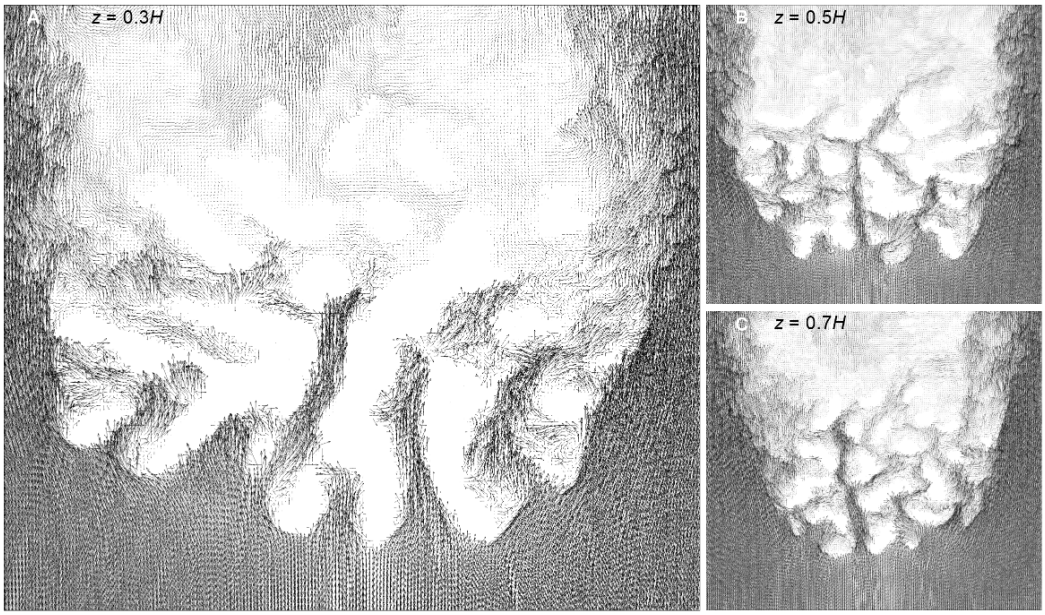


Figure 3.7: **Top view of velocity vector at the interior of colony at three different heights inside *P. meandrina*.** These vectors profiles were obtained inside *Pocillopora* at z= 0.3 H (left), 0.5 H and 0.7 H (right) from the base of the coral. The figure reveals relatively higher vector magnitude at the at the frontal section and relatively lower vector magnitude indicating low velocity profiles at the rare section of the colony.

Up to now, we have provided qualitative comparisons of flow structure between these *Pocillopora* colonies. But for better comparison, we require quantitative measurements of flow variation between these two corals. To attain this objective, mean velocity profiles were

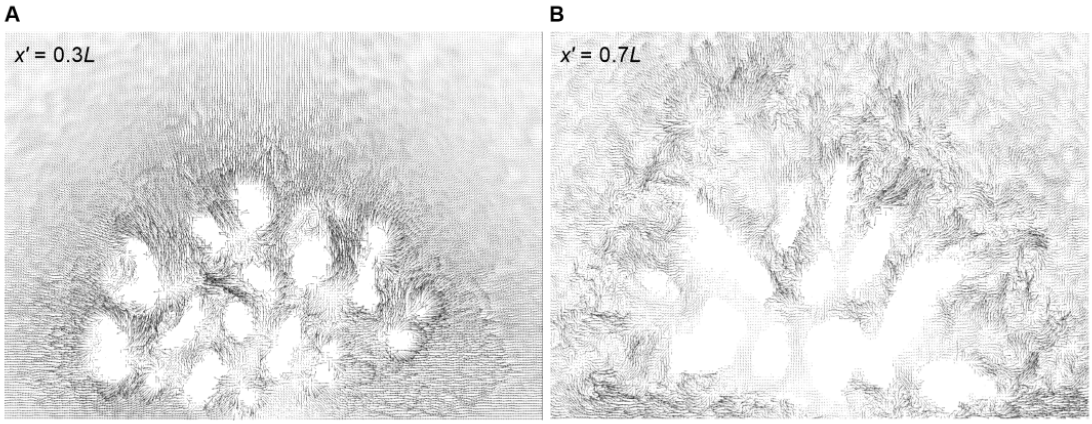


Figure 3.8: **Front view of velocity vector at the front and rare section of *P. meandrina* perpendicular to stream direction.** These vectors profiles were obtained at $x'$= 0.3 L (left)and 0.7 L (right) from the frontal section of the coral. At $x'$= 0.7 L, The vector profile shows the formation of vorticity at the exterior of coral.

obtained as a function of coral height inside both of the corals at 20-mm intervals along their length. As the branches are extended randomly, it is difficult to obtain mean velocity profiles at different sections inside the coral. To overcome this issue, these velocity profiles were calculated by the averaging the velocity magnitudes of the closest 10 neighbor grids at each location in the $X-Z$ planes, and then a second average was performed along the lateral direction ($y$ axis) within the coral. These velocity profiles not only depicted the progression of flow inside the coral, but also indicated the amount of mixing and transportation that takes place along the length of the coral. The mean velocity profiles obtained for both the *Pocilloppra* corals are shown in Fig 3.10(A) and (C). For *P. meandrina*, the mean velocity profiles were almost similar up to 40 mm. This was the frontal portion of the coral, where the flow penetration was easy and the maximum velocity dropped approximately 33% of incoming velocity at the interior. For 60 to 80 mm, the flow started to slow down and dropped to a maximum 50 % of the incoming flow. At this section, the velocity profiles changed substantially. Interestingly, at 80 mm, the profile displayed an increase in velocity magnitude, where we expected further decline in incoming velocity. From 100 mm up to the

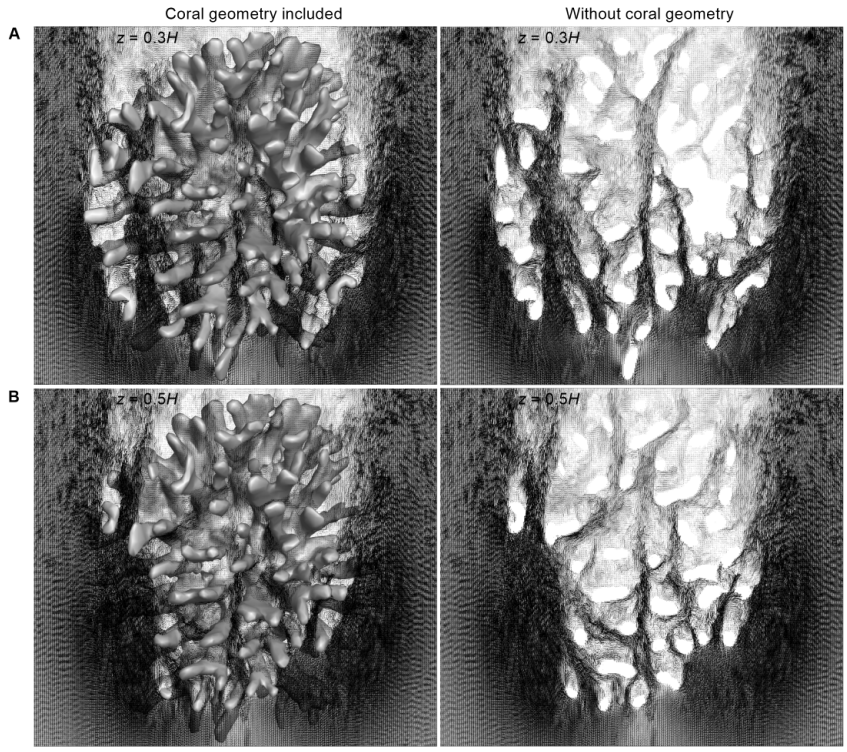


Figure 3.9: **Top view of velocity vector at the interior of colony at two different heights inside *P. eydouxi* with and without the STL geometry.** These vectors profiles were obtained inside *Pocillopora* at (A) z = 0.3 H and (B) z=0.5 H from the base of the coral. The figure shows formation of wake behind the individual branches of colony and relatively better penetration of flow at the interior of colony than *P. meandrina*.

end of coral, the velocity profiles were almost identical and displayed a reduction in velocity magnitude at mid-height of the coral. In general, the velocity profiles showed low velocity at the middle of the coral and comparatively higher velocity at the top and bottom sections of the coral.

In contrast, the velocity profiles within *P. eydouxi* remained almost the same from front to the back of the colony even though the velocity dropped substantially at the rare section of coral. Due to the openness of the structure, the flow did not vary much within the top half of the coral, where the flow magnitude was comparatively higher than the lower half of the coral. Inside *P. eydouxi*, the velocity reduced abruptly at this lower section due to the

solid hemispherical structure. At z=0.5 H, the mean velocity profile shows increased velocity magnitude due to the accelerated flow in the reduced area between the branches at lower section of the coral. At the rare section of coral (between 80 and 120 mm) the maximum velocity dropped to almost 50% of the incoming flow.

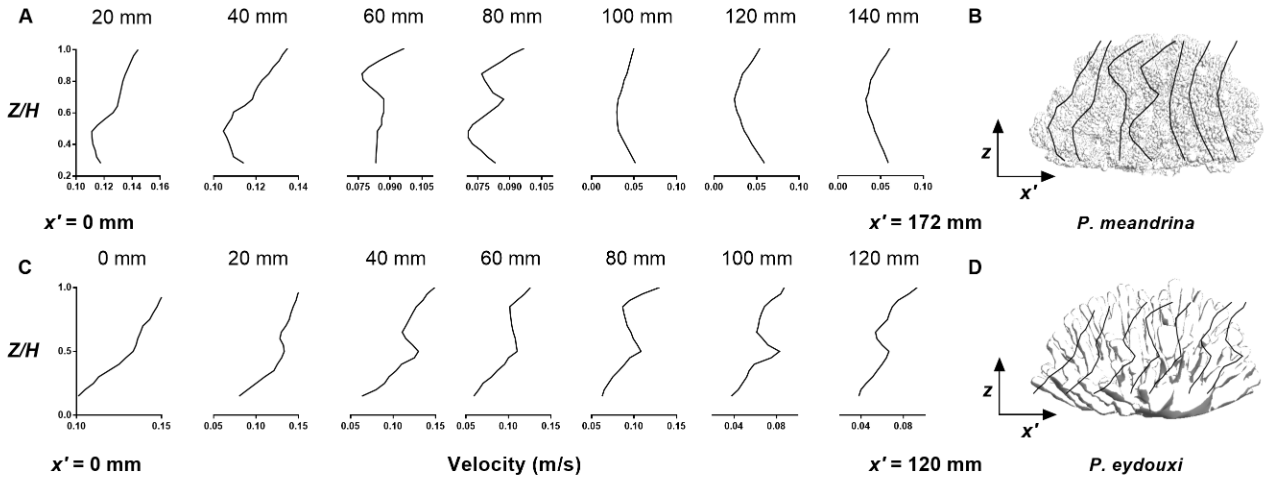


Figure 3.10: **Variation of mean vertical velocity profiles inside *Pocillopora*.** (A & C) Mean velocity profiles inside *Pocillopora* were obtained at 20-mm intervals along the length of the coral by averaging velocity magnitudes of the closest 10 neighbor grids at each location in the $X - Z$ planes, and then averaging velocity magnitudes over the lateral direction (y-axis) within the coral. (B & D) Location of these mean velocity profiles within the coral (not to scale).

In addition to mean velocity profile, we also computed the fluctuating component for all the velocity components and performed quadrant analysis to quantify the interactions of ejections (Q2) and sweep (Q4) and their relative contribution to the Reynolds stresses at the interior of colony. Here stream-wise and vertical velocity fluctuation were grouped into quadrants. Fig 3.11 shows comparison of Q2 ($u' < 0$ & $w' > 0$) and Q4 ($u' > 0$ & $w' < 0$) as a function of coral height for both these coral structures. For densely branched *P.meandrina*, the dominance of Q2 over Q4 was observed at the exterior of colony and mixed zones were observed at the interior of colony. Similar profile for Q2 and Q4 has been mentioned by Asher *et al.* for the exact *P.meandrina* coral in a flume study preformed on multiple coral

colonies. In contrast, the contributions of Q2 and Q4 to the Reynolds stress is quite different *P.eydouxi* within the branches of colony. Here, the ejection contributes more than the sweep after z=0.4H from the height of the colony.

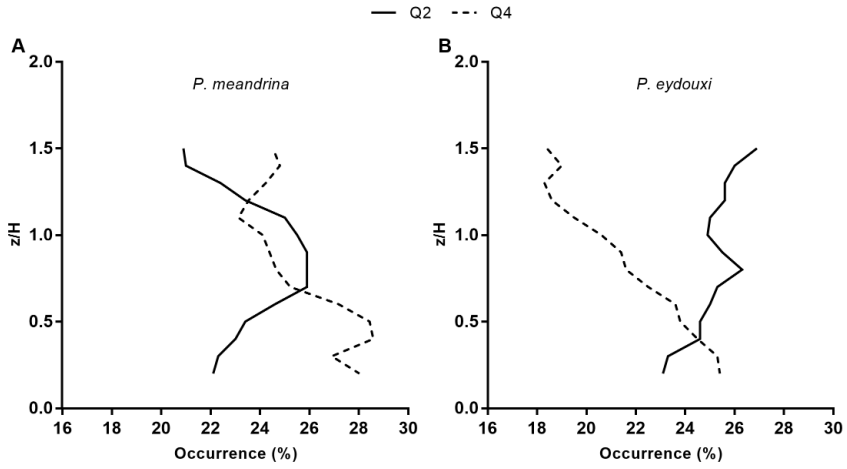


Figure 3.11: **Quadrant analysis performed as a function of coral height inside both the *Pocillopora*.** Comparison of ejections (Q2) and sweep (Q4) and their relative contribution to the Reynolds stresses between (A ) *P.meandrina* and (B) *P.eydouxi*.

### 3.4.2 Comparison of flow dynamics over *M. capitata*

For coral, nutrient transfer to the colony and transport of gas from the coral surface depends on shear, turbulent mixing and the concentration gradient near the surface. Quantifying the turbulent stress is essential for explaining mixing, stress and drag developed on the coral surface. Even small changes in flow conditions can change these turbulent statistics over the boundary layer. As mentioned earlier, *M. capitata* with verrucae scattered on the coral surface grows near Kanehoe Bay in Hawaii. To ascertain the impact of verrucae in natural flow conditions, computational analysis was performed on two different coral morphologies of loosely-branched *M. capitata* as described in the coral geometry section (Fig 3.12). To characterize the boundary layers and the turbulent stress developed on both

of these structures, velocity profiles were computed over the coral surface at two different Reynolds number. Based on the low-to-high water velocity near Kanehoe Bay and the height of the coral, Reynolds numbers 5,000 and 15,000 were used to simulate the flow conditions for *M. capitata*. For ease of discussion, we have used CV and CWOV for the abbreviation of *M. capitata* with and without verrucae, respectively, hereafter. Fig 3.12 shows slices of the flow field around *M. capitata* with and without verrucae at Reynolds number 15,000. After capturing flow fields for both the structures, velocity and stress were calculated at $x' = 0.7L$ above the surface of the corals at two different Reynolds numbers. Then, the velocity and stress profiles obtained were averaged along the lateral (y) direction within coral to obtain a mean of the profiles on top of the coral's surface. The mean profiles were compared for CV and CWOV at the same flow conditions to capture the effects of verrucae on the flow field clearly.

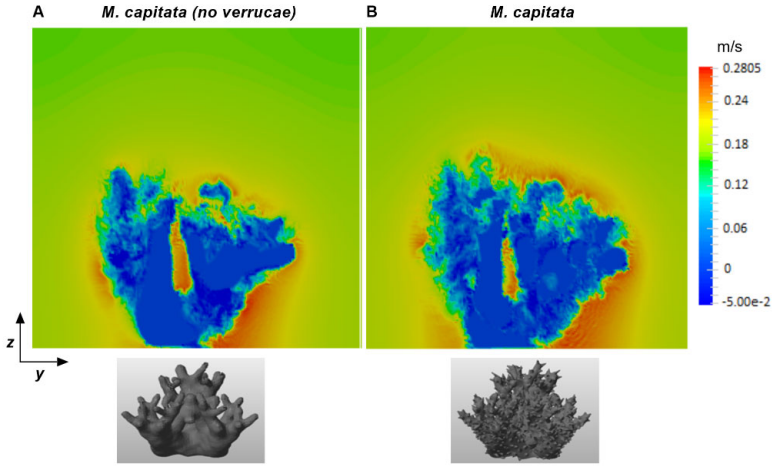


Figure 3.12: **shows two *M. capitata* with and without verrucae and velocity slice perpendicular to flow direction at $x' = 0.7L$ at Reynolds number 15,000.** The structure of coral without verrucae was obtained by removing verrucae from the coral surface while keeping the other features same.

Fig 3.13 (A & B) shows a comparison of stream wise velocity profiles at the top of *M. capitata* with and without verrucae at Reynolds numbers 5,000 and 15,000 respectively. Here, the

mean velocity profile was normalized by the incoming velocity magnitude. At both these Reynolds number, the location of maximum velocity for CV was almost twice the height for that of CWOV from the top of the coral surface. A comparison of the two stream wise velocity profiles at Reynolds number 5,000 reveals that the two profiles were almost identical up to 75% of the normalized velocity. In contrast, there were significant difference in stream wise velocity profiles at Reynolds number 15,000 for both thses geometries. At this Reynolds number, the stream wise velocity reached 50 % of its maximum magnitude at about 2 and 5 mm above the surface of CWOV and CV respectively. Recently, Reidenbach and Stocking *et al.* [46, 52] measured stream wise velocity components at the top of a single coral for unidirectional flow and their results show similar velocity profiles at the top of colony and the location of inflection points were almost identical.

As the coral depends on natural flow conditions for the transfer of nutrient uptake, removal of waste and mass transport, the high velocity magnitude near the coral surface indicates fast mass and momentum transfer from the coral surface [27, 39]. This is very important for biological processes like photosynthesis and respiration which depends the thickness of the diffusion boundary layer (DBL) on the surface of coral. Experimental studies show that the thickness of the DBL decreases with the increase in flow magnitude [41]. If comparison is made between CWOV and CV, the mixing and transport should be better for CWOV at both of the Reynolds numbers, due to higher stream wise velocity magnitude near the coral's surface.

Fig 3.13(C & D) show the comparison of vertical velocity profiles above the coral surface at Reynolds numbers 5,000 and 15,000 respectively. At both these Reynolds number, the vertical velocity magnitude was relatively small in comparison to streamwise velocity component. At Reynolds number 5,000, the vertical velocity profiles were almost similar for both the cases. As the Reynolds number increased, the velocity profile demonstrated a rela-

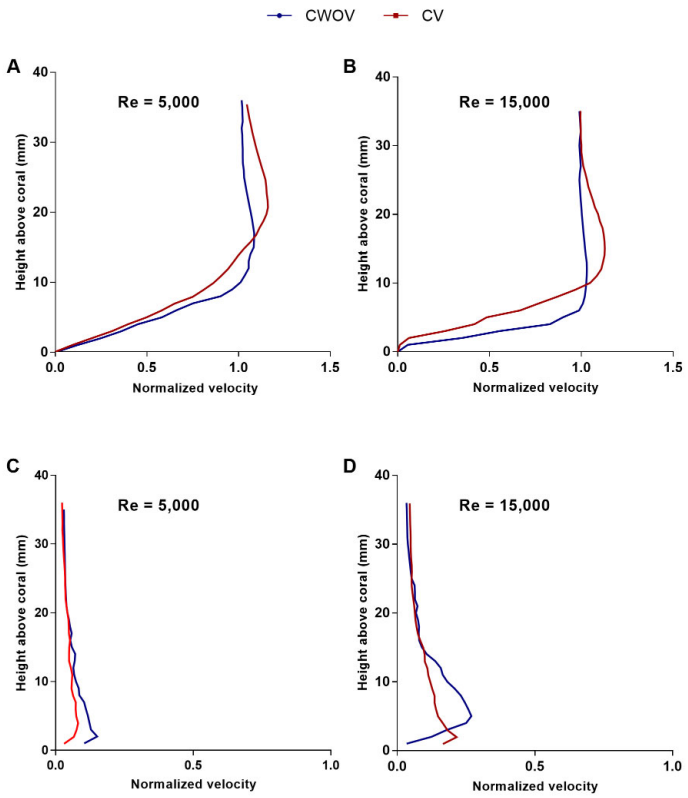


Figure 3.13: **Comparison of velocity profiles at the top of *M. capitata* with and without verrucae at Reynolds numbers 5,000 and 15,000** The streamwise (A & B) and vertical (C & D) velocity profiles were obtained at the top of the coral at $x' = 0.7L$ and averaged over the lateral (y) direction. The Reynolds number was selected based on natural flow conditions and the height of *M. capitata*.

tively higher magnitude near the top of CWOV. For both cases, the vertical velocity profiles reached a constant magnitude at approximately 15 mm above the coral surface. If we compare the stream wise velocity to the vertical profile, the mass and momentum transport is mainly dominant in the horizontal direction at both these Reynolds numbers. If the vertical flow profiles for these two coral structures are compared, CWOV should have better mixing and transportation along the vertical direction than CV. Also, the nutrient gradient above the canopy will be more uniform for CWOV due to comparatively higher vertical flow.

### 3.4.3 Turbulent stress over coral surface

In addition to velocity profile, the transfer of nutrients and mass between coral and the overlying water column depends upon turbulent stress developed on the coral surface. To calculate these values, time-and-space averaged turbulent stress component $<u'u'>$, $<w'w'>$ and $<u'w'>$, were computed at the top of *M. capitata* with and without verrucae for unidirectional flow at two different Reynolds number, where the Reynolds stress, $<u'w'>$, is mainly responsible for mixing near the coral surface. To capture the fluctuating quantities, mean values were subtracted from instantaneous values of velocity components and the computation was given enough time for the stability of mean flow. Fig 3.14 (A & C) shows turbulent stress developed at the top of *M. capitata* without verrucae at Reynolds numbers 5,000 and 15,000 respectively.

At Reynolds number 5,000, the $<u'u'>$ turbulent stress showed relatively higher magnitude than $<w'w'>$ and $<u'w'>$ and reached maximum value at approximately 9 mm above the top of coral surface, indicating maximum stream wise momentum near the coral polyps. All these turbulent stress components approached zero magnitude at approximately 20 mm above the coral surface and the maximum magnitude of Reynolds stress was almost 50% of the maximum value of $<u'u'>$ stress. In contrast, when the Reynolds number increased to 15,000, the maximum magnitude of $<u'u'>$ stress increased to almost four times that for Re 5000, with the maximum value of all the stress components raised to approximately 15 mm above the top of the coral. At the higher Reynolds number, the maximum magnitude of Reynolds stress, $<u'w'>$ increased significantly and contribute to better mixing and vertical transport due to maximum shear at the top of the coral.

Fig 3.14 (D) shows the components of turbulent stress developed on top of *M. capitata* with verrucae (CV) at Reynolds number 15,000. Here, the value and location of maximum magni-

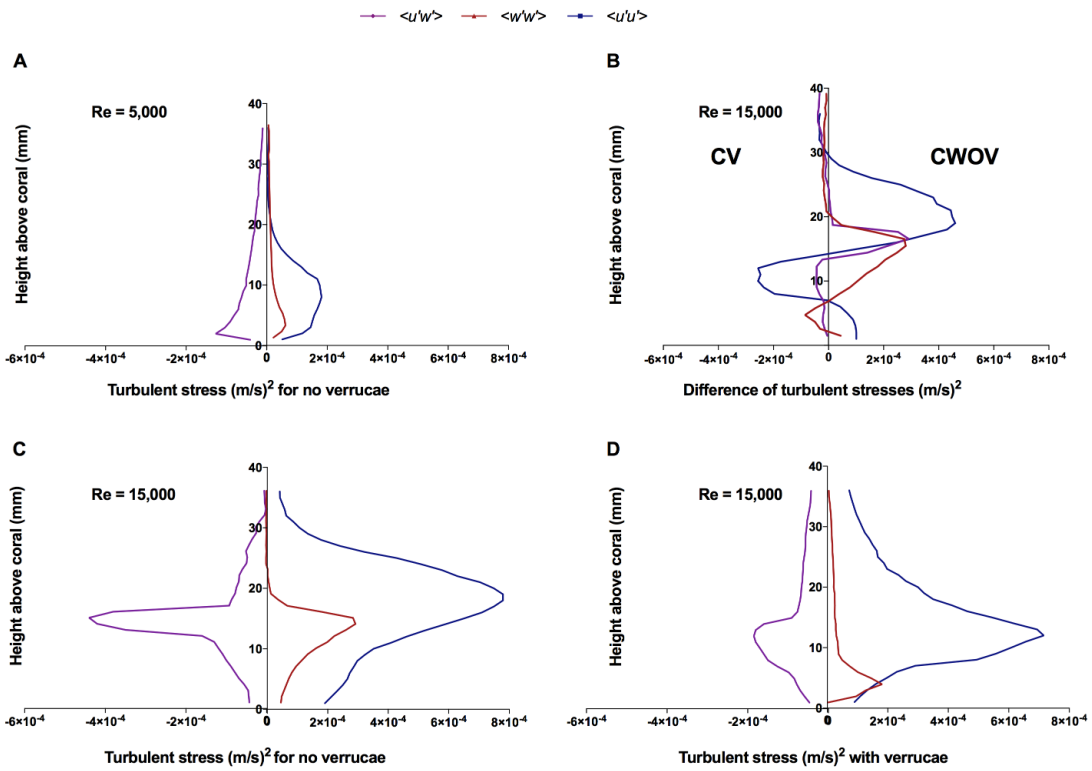


Figure 3.14: **Turbulent stress over *M. capitata* at different flow conditions.** Fig 3.14(A,C & D) shows turbulent stress over *M. capitata* with and without verrucae at Reynolds numbers 5,000 and 15,000. (B) Difference between turbulent stress over *M. capitata* with and without verrucae at Reynolds number 15,000. All of the profiles were obtained at the top of the coral at $x' = 0.7L$ and averaged over the lateral (y) direction.

tude of <u′u′> stress was similar to stream wise stress component developed on CWOV. For the vertical stress component, <w′w′>, CWOV shows greater magnitude than CV. Similarly for Reynolds stress, the maximum magnitude of <u′w′> for CWOV was almost twice that of CV. To validate these results, these turbulent profiles were compared with the turbulent stress measured on top of a single coral from the experimental study by Stocking *et al.*[52]. In the experimental study, the maximum magnitude of turbulent stress takes place within 20 mm above the top of the coral. In case of simulation, the locations of maximum turbulent stress components were found within 20 mm above the coral surface, and the magnitude of the stress components are within the same order of magnitude as those found in the ex-

periment. In the experiment, the vertical stress, <w′w′>, was almost half of the stream wise turbulent stress, <u′u′>, but in the simulation comparatively lower vertical stress was observed except for the CWOV at Reynolds number 15,000. For better understanding of the impact of verrucae on turbulent stress, the difference of their magnitude were plotted as a function of height at the top of *M. capitata* at Reynolds number 15,000 in Fig 3.14 (B).

In general, the maximum magnitude of the Reynolds stress can be found just at the top of colony for both the structures and these values decreased with the height. Similarly, maximum magnitude for <u′u′> and <w′w′> were located close to the top of the both those structures. In addition, we were also able to capture some distinct features of the turbulent stress which have direct implication on hydrodynamics and biological activities of coral. For example, the bed shear stress computed through $t_b = -\rho$ <u′w′> [53] indicates that magnitude of the bed stress will be higher at the top of the coral for CWOV than CV in the unidirectional flow because of relatively higher Reynolds stress. The Reynolds stress can be also used to calculate friction velocity at top of coral surface. Friction velocity is an important parameter for turbulent analysis to characterize the stress of the overlying water column on top of the coral surface. In the canopy flow analysis, the friction velocity is calculated from $u_* = \sqrt{<}$u′w′ > [25] where the Reynolds stress is the maximum magnitude within the canopy. From the comparison of Reynolds stress profiles for both the colony, it can be concluded that CWOV has higher friction at the top of the colony than CV. Now the drag co-efficient also depends on frictional velocity, $u_*$ and is defined by $C_d = \frac{u_*^2}{U_0^2}$ [45] where $U_0$ is the reference velocity. As both the analysis was preformed on *M. capitata* for the same incoming flow condition, the co-efficient of drag will be higher for CWOV as $u_*$ is higher on the top of this structure. Similarly the transport mechanism from the coral surface can be expressed as $m = k(C_f - C_s)$ [54] where K is the mass transfer co-efficient. Now there is a linear relationship between K and $u_*$ which suggests that for the same concentration gradient

between the coral surface and surrounding fluid, CWOV will have better mass transfer rate than CV.

# Conclusion

Computational studies were performed in order to understand the differences in mean flow profile characteristics inside two *Pocillopora* coral colony geometries with different branching patterns, one comparatively loosely branched (*P. eydouxi*), and one densely branched (*P. meandrina*). Velocity magnitude and vector fields were presented at different cross sections of the colonies to depict flow around the coral branches. Horizontal velocity slices showed higher velocity magnitudes at the anterior end of both colonies compared to the posterior end. To quantify the differences in mean flow characteristics between the two colony geometries, mean velocity profiles were plotted as a function of coral height from the front to back of the colonies. For the dense geometry, *P. meandrina*, the mean velocity profile shows distinct changes through the interior of coral. The anterior part of the colony, which faces the oncoming flow, shows higher velocity magnitudes at the top and base of the colony, with a velocity deficit at mid-colony heights. The dense branching pattern presents higher resistance to flow in the middle part of the colony, resulting in a peak in the mean velocity profile at the colony mid height which may represent jetting. Finally, the mean velocity profile loses the mid height peak in the posterior third of the colony, and the profile recovers the overall shape it had in the anterior third of the colony. The mean normalized velocity along the length of the coral drops to approximately 38% of the freestream value in the middle of the coral, but recovers to 65% at the rear of the coral. In contrast, the mean velocity profiles remain largely uniform throughout the loosely branched geometry, *P. eydouxi*. These profiles have their maximum magnitude at the top of the colony and decrease in value approximately

linearly with a decrease in height. Additionally, quadrant analyses was preformed on both these structures to understand the impact of injection and sweep on the Reynolds stresses at the interior of colony.

Simulations were also performed on a *M. capitata* colony geometry with and without verrucae at two different Reynolds numbers to understand the impact of verrucae on the local hydrodynamics. The results displayed distinct inflection points and differences in the mean streamwise velocity profiles for the colonies with and without verrucae. At both Reynolds numbers, the maximum magnitude of the mean streamwise velocity can be observed closer to the top surface of the CWOV colony than the CV colony. Similarly, the mean vertical velocity shows a relatively higher magnitude nearer to the top of the CWOV structure. Higher velocity magnitudes near the surface of the colony ensure better mass transport, so we expect to see higher rates of mass transport from the surface of the colony without verrucae. In addition to velocity profiles, the turbulent stresses were also calculated for both colony morphologies. The profiles of all the turbulent stress components displayed maximum magnitudes just above the top surface of the colonies. For both structures, the streamwise stress, $\langle u'u' \rangle$ showed similar magnitudes for the same oncoming flow conditions. But significant differences were found between the Reynolds stresses, $\langle u'w' \rangle$, developed on the top surface of the colonies. For the CWOV structure, the maximum magnitude of $\langle u'w' \rangle$ was almost twice than for the CV structure. The difference in the turbulent stresses was plotted at the top of *M. capitata* with and without verrucae. This showed higher turbulent stresses for the CWOV structure than the CV structure. From the comparisons of the mean velocity profiles and turbulent stresses it can be concluded that the CWOV structure will experience higher bed stress and friction velocities above the colony than will the CV structure. The higher friction velocity values for the structure without verrucae means it will have a larger drag coefficient and better mass transport for the same oncoming flow condition compared

to the structure with verrucae. This is not paradoxical. *M. capitata* develops verrucae in high flow conditions where high rates of mass transport naturally occur. It is the colony without verrucae that is found in low flow conditions in nature, and hence needs to have enhanced mass transport rates.

# Bibliography

[1] Monismith SG. Hydrodynamics of coral reefs. Annu Rev Fluid Mech. 2007;39:37–55.

[2] Shashar N, Kinane S, Jokiel P, Patterson M. Hydromechanical boundary layers over a coral reef. Journal of Experimental Marine Biology and Ecology. 1996;199(1):17–28.

[3] Shick JM. Diffusion limitation and hyperoxic enhancement of oxygen consumption in zooxanthellate sea anemones, zoanthids, and corals. The Biological Bulletin. 1990;179(1):148–158.

[4] Shashar N, Cohen Y, Loya Y. Extreme diel fluctuations of oxygen in diffusive boundary layers surrounding stony corals. The Biological Bulletin. 1993;185(3):455–461.

[5] Fabricius KE, Genin A, Benayahu Y. Flow-dependent herbivory and growth in zooxanthellae-free soft corals. Limnology and Oceanography. 1995;40(7):1290–1301.

[6] Todd PA. Morphological plasticity in scleractinian corals. Biological Reviews. 2008;83(3):315–337.

[7] Sebens K, Done T. Water flow, growth form and distribution of scleractinian corals: Davies Reef (GBR), Australia. In: Proceedings of the 7th International Coral Reef Symposium. vol. 1; 1992. p. 557–568.

[8] Chamberlain Jr JA, Graus RR. Water flow and hydromechanical adaptations of branched reef corals. Bulletin of Marine Science. 1975;25(1):112–125.

[9] Sebens KP, Witting J, Helmuth B. Effects of water flow and branch spacing on particle capture by the reef coral Madracis mirabilis (Duchassaing and Michelotti). Journal of experimental marine biology and ecology. 1997;211(1):1–28.

[10] Graus RR, Macintyre IG. The zonation patterns of Caribbean coral reefs as controlled by wave and light energy input, bathymetric setting and reef morphology: computer simulation experiments. Coral Reefs. 1989;8(1):9–18.

[11] Falter JL, Atkinson MJ, Coimbra CF. Effects of surface roughness and oscillatory flow on the dissolution of plaster forms: Evidence for nutrient mass transfer to coral reef communities. Limnology and oceanography. 2005;50(1):246–254.

[12] Sebens K, Vandersall K, Savina L, Graham K. Zooplankton capture by two scleractinian corals, Madracis mirabilis andMontastrea cavernosa, in a field enclosure. Marine Biology. 1996;127(2):303–317.

[13] Thomas FIM, Atkinson MJ. Ammonium uptake by coral reefs: effects of water velocity and surface roughness on mass transfer. Limnology and Oceanography. 1997;42(1):81–88.

[14] Lesser MP, Weis VM, Patterson MR, Jokiel PL. Effects of morphology and water motion on carbon delivery and productivity in the reef coral, Pocillopora damicornis (Linnaeus): diffusion barriers, inorganic carbon limitation, and biochemical plasticity. Journal of Experimental Marine Biology and Ecology. 1994;178(2):153–179.

[15] Bruno JF, Edmunds PJ. Metabolic consequences of phenotypic plasticity in the coral Madracis mirabilis (Duchassaing and Michelotti): the effect of morphology and water flow on aggregate respiration. Journal of experimental marine biology and ecology. 1998;229(2):187–195.

[16] Dennison WC, Barnes DJ. Effect of water motion on coral photosynthesis and calcification. Journal of Experimental Marine Biology and Ecology. 1988;115(1):67–77.

[17] Finelli CM, Helmuth BS, Pentcheff ND, Wethey DS. Water flow influences oxygen transport and photosynthetic efficiency in corals. Coral Reefs. 2006;25(1):47–57.

[18] Jimenez IM, Kühl M, Larkum AW, Ralph PJ. Effects of flow and colony morphology on the thermal boundary layer of corals. Journal of The Royal Society Interface. 2011; p. rsif20110144.

[19] Nakamura T, Van Woesik R. Water-flow rates and passive diffusion partially explain differential survival of corals during the 1998 bleaching event. Marine Ecology Progress Series. 2001;212:301–304.

[20] Reidenbach MA, Koseff JR, Monismith SG, Steinbuckc JV, Genin A. The effects of waves and morphology on mass transfer within branched reef corals. Limnology and Oceanography. 2006;51(2):1134–1141.

[21] Baird M, Atkinson M. Measurement and prediction of mass transfer to experimental coral reef communities. Limnology and Oceanography. 1997;42(8):1685–1693.

[22] Delandmeter P, Lambrechts J, Marmorino GO, Legat V, Wolanski E, Remacle JF, et al. Submesoscale tidal eddies in the wake of coral islands and reefs: satellite data and numerical modelling. Ocean Dynamics. 2017;67(7):897–913.

[23] Storlazzi C, Elias E, Field M, Presto M. Numerical modeling of the impact of sea-level rise on fringing coral reef hydrodynamics and sediment transport. Coral Reefs. 2011;30(1):83–96.

[24] Finnigan J. Turbulence in plant canopies. Annual review of fluid mechanics. 2000;32(1):519–571.

[25] Moltchanov S, Bohbot-Raviv Y, Shavit U. Dispersive stresses at the canopy upstream edge. Boundary-layer meteorology. 2011;139(2):333–351.

[26] Moltchanov S, Shavit U. A phenomenological closure model of the normal dispersive stresses. Water Resources Research. 2013;49(12):8222–8233.

[27] Lowe RJ, Koseff JR, Monismith SG. Oscillatory flow through submerged canopies: 1. Velocity structure. Journal of Geophysical Research: Oceans. 2005;110(C10).

[28] Atkinson M, Bilger R. Effects of water velocity on phosphate uptake in coral reef-hat communities. Limnology and Oceanography. 1992;37(2):273–279.

[29] Dipprey DF, Sabersky RH. Heat and momentum transfer in smooth and rough tubes at various Prandtl numbers. International Journal of Heat and Mass Transfer. 1963;6(5):329–353.

[30] Stocking JB, Laforsch C, Sigl R, Reidenbach MA. The role of turbulent hydrodynamics and surface morphology on heat and mass transfer in corals. Journal of the Royal Society Interface. 2018;15(149):20180448.

[31] Chang S, Elkins C, Alley M, Eaton J, Monismitha S. Flow inside a coral colony measured using magnetic resonance velocimetry. Limnology and Oceanography. 2009;54(5):1819–1827.

[32] Markl M, Chan FP, Alley MT, Wedding KL, Draney MT, Elkins CJ, et al. Time-resolved three-dimensional phase-contrast MRI. Journal of Magnetic Resonance Imaging: An Official Journal of the International Society for Magnetic Resonance in Medicine. 2003;17(4):499–506.

[33] Ong RH, King AJ, Mullins BJ, Cooper TF, Caley MJ. Development and validation of computational fluid dynamics models for prediction of heat transfer and thermal microenvironments of corals. PloS one. 2012;7(6):e37842.

[34] Kaandorp JA, Koopman EA, Sloot PM, Bak RP, Vermeij MJ, Lampmann LE. Simulation and analysis of flow patterns around the scleractinian coral Madracis mirabilis

(Duchassaing and Michelotti). Philosophical Transactions of the Royal Society B: Biological Sciences. 2003;358(1437):1551–1557.

[35] Kaandorp JA, Sloot PM, Merks RM, Bak RP, Vermeij MJ, Maier C. Morphogenesis of the branching reef coral Madracis mirabilis. Proceedings of the Royal Society of London B: Biological Sciences. 2005;272(1559):127–133.

[36] Chindapol N, Kaandorp JA, Cronemberger C, Mass T, Genin A. Modelling growth and form of the scleractinian coral Pocillopora verrucosa and the influence of hydrodynamics. PLoS computational biology. 2013;9(1):e1002849.

[37] Osorio-Cano JD, Osorio AF, Alcérreca-Huerta JC, Oumeraci H. Drag and inertia forces on a branched coral colony of Acropora palmata. Journal of Fluids and Structures. 2019;88:31–47.

[38] Chang S, Iaccarino G, Ham F, Elkins C, Monismith S. Local shear and mass transfer on individual coral colonies: Computations in unidirectional and wave-driven flows. Journal of Geophysical Research: Oceans. 2014;119(4):2599–2619.

[39] Lowe RJ, Koseff JR, Monismith SG, Falter JL. Oscillatory flow through submerged canopies: 2. Canopy mass transfer. Journal of Geophysical Research: Oceans. 2005;110(C10).

[40] Thomas FI, Cornelisen CD. Ammonium uptake by seagrass communities: effects of oscillatory versus unidirectional flow. Marine Ecology Progress Series. 2003;247:51–57.

[41] Larkum AW, Koch EM, Kühl M. Diffusive boundary layers and photosynthesis of the epilithic algal community of coral reefs. Marine Biology. 2003;142(6):1073–1082.

[42] Hossain MM, Staples AE. Passive vortical flows enhance mass transport in the interior of a coral colony. Physics of Fluids. 2019;31(6):061701.

[43] Veron JJ, Pichon MM, et al. Scleractinia of Eastern Australia. Part I: Families Thamnasteriidae, Astrocoeniidae, Pocilloporidae. Australian Government Publishing Service; 1976.

[44] Kaandorp JA, Kübler JE. The algorithmic beauty of seaweeds, sponges and corals. Springer Science & Business Media; 2001.

[45] Reidenbach MA, Monismith SG, Koseff JR, Yahel G, Genin A. Boundary layer turbulence and flow structure over a fringing coral reef. Limnology and oceanography. 2006;51(5):1956–1968.

[46] Reidenbach MA, Koseff JR, Monismith SG. Laboratory experiments of fine-scale mixing and mass transport within a coral canopy. Physics of Fluids. 2007;19(7):075107.

[47] Mass T, Genin A. Environmental versus intrinsic determination of colony symmetry in the coral Pocillopora verrucosa. Marine Ecology Progress Series. 2008;369:131–137.

[48] Inaglory B. Pocillopora meandrina with a resident fish; 2008. Available from: https://en.wikipedia.org/wiki/Pocillopora_meandrina.

[49] Asman P, Lenoble J. Around antler coral Pocillopora eydouxi; 2012. Available from: https://species.wikimedia.org/wiki/Pocillopora_eydouxi.

[50] Meneveau C, Lund TS, Cabot WH. A Lagrangian dynamic subgrid-scale model of turbulence. Journal of fluid mechanics. 1996;319:353–385.

[51] Balaras E. Modeling complex boundaries using an external force field on fixed Cartesian grids in large-eddy simulations. Computers & Fluids. 2004;33(3):375–404.

[52] Stocking JB, Rippe JP, Reidenbach MA. Structure and dynamics of turbulent boundary layer flow over healthy and algae-covered corals. Coral Reefs. 2016;35(3):1047–1059.

[53] Kastner-Klein P, Rotach MW. Mean flow and turbulence characteristics in an urban roughness sublayer. Boundary-Layer Meteorology. 2004;111(1):55–84.

[54] Hondzo M. Dissolved oxygen transfer at the sediment-water interface in a turbulent flow. Water resources research. 1998;34(12):3525–3533.

# Chapter 4

# Mass transport and turbulent statistics within branching corals

**Publication information**

The contents of this chapter have been submitted for publication:

Hossain, M., & Staples, A. (2020). Mass transport and turbulent statistics within branching corals. *Invited* submission to *Fluids*.

## 4.1 Abstract

Large eddy simulations were performed to characterize the flow and mass transport mechanisms in the interior of two *Pocillopora* corals with different branching patterns, one with a relatively loosely branched morphology (*P. eydouxi*), and the other with a relatively densely branched morphology (*P. meandrina*). Detailed velocity vector and streamline fields were obtained inside the colonies for the same unidirectional oncoming flow conditions, and significant differences were found between the flow profiles and transport mechanisms in the interior of the two colonies. For the densely branched colony, the formation of vortices shedding from individual branches was observed in the interior of the colony. The vortices passively stirred the water column and enhanced the mass transport inside the colony. The vortices were absent within the more loosely branched structure. To further understand the

impact of the branch density on the internal transport process, the Stanton (St) number was calculated based on the local flow timescale and compared between the colonies. The results showed up to a 216% increase in St due to the local vortices inside *P. meandrina* in comparison to St calculated based on the mean branch diameter as the length scale, and the St number almost doubled for the loosely branched *P. eydouxi*. Turbulent flow statistics were also calculated, including the fluctuating components of the velocity, the mean Reynolds stress. The variance of the velocity components along the height of the flow domain was also computed for both structures. The results showed similar Reynolds stress profiles, but higher velocity variations, in the interior of *P. meandrina*.

## 4.2 Introduction

Determining hydrodynamic properties at the interior of coral are essential for the growth and mass transport for branched coral colonies [1, 2]. During the interaction with the coral morphologies, distinct flow fields evolve both at the interior and exterior of the colony. This internal flow field depends upon the morphological parameters such as porosity, diameter, and inter-branch distance, and the Reynolds number. Flow profiles inside the colony influence the exchange of solute across the interface of coral tissue and control the transport of nutrients at the interior of the colony, removes sediment, and determine the dissolved oxygen concentration near the coral surface [3]. Physiological processes like Photosynthesis and respiration depends on the thickness of this boundary layer [4]. Experimental studies show that the growth of the coral and reef development is influenced by theses metabolic responses, which directly depend on flow dynamics at the interior of coral [2, 5].

In open flow conditions, coral changes its internal branch structure to adapt to the flow environment to perform all these physiological activities [6]. Besides, reef corals depend

on surrounding water for their nourishment and their morphology affects food availability. For example, loosely branched colonies have a relatively higher probability of obtaining suspended food inside the colony. In contrast, tightly branched colonies must contend with the low availability of food inside the coral due to complex branching structure [7]. The presence of an arbitrary structure of branches strongly affects the transport of momentum and concentration gradient near the colony. In one of the studies, Chamberlain *et al.* [7] introduced the effect of colony orientation on flow and discussed the hydrodynamic adaptation of branched reef corals. Sebens *et al.* [8] analyzed the impact of branch spacing on particulate capture within the colony. Similarly, Hunter *et al.* have shown the effect of colony bushiness on the feeding effectiveness in unidirectional and wavy flow [9]. Thus, the hydrodynamics changed significantly with the change in a branching pattern, which needs to be resolved in detail to understand the subtle difference in their transport process.

All these parameters described earlier are critical for corals and depend on their internal hydrodynamics but the question arises why didn't we have detailed turbulent statistics and flow profile at the interior of the colony. One of the reason might be a large number of study has been performed on the flow profiles and momentum transport above the reef [10, 11, 12]. In most of these cases, the canopy elements were homogeneous in nature with a uniform branching pattern. But these simplified structure does not represent the natural colony in open flow condition. Another reason for the lack of such detailed flow data may be the inability to obtain optical and acoustic access at the interior of coral. Sampling hydrodynamics at several points over a large area at the interior of the colony is not sufficient to describe the actual hydrodynamics experienced by the coral. Although non-intrusive test like particle image velocimetry (PIV) and Acoustic Doppler velocimetry (ADP) has been used extensively for flow visualization but these method has been found ineffective in the visualization of the flow field at the interior of branching colony in natural flow condition.

Chang *et al.* [13] used the magnetic resonance velocimetry (MRV) to visualize the first detailed flow profile at the interior of the colony and compared the mean velocity profile between the low and high flow coral geometries with different inter-branch distance. This is the first of this kind of study where detailed velocity slices were used for flow analysis and the authors emphasized the intra-colonial variability as an important parameter for mass transfer. In another study, Chang *et al.* [14] computed the flow profile inside *Pocillopora* and *Stylophora* and derived a correlation between local shear stress and scalar transport from the surface of coral. The authors also suggested the similarity in the mass transfer characteristics despite differences in their physical shapes and hydrodynamic conditions. Recently, Shapiro *et al.* [15] have shown that the ciliary on coral can stir the water column and creates the vortices that can enhance the mass transport by 400% near the coral surface However, these studies do not answer an important question if the internal geometry can play an important role in the mass transfer at the interior of coral. In one of the recent papers, Hossain and Staples *et al.* [16] studied the detailed flow profile inside *P. meandrina* and found the formation of passive vortices within the densely branched colony which assist the transport process interior of this complex geometry. In the current study, we want to extend this analysis for the two different branching corals and want to evaluate if the same mass transport characteristics hold for densely and open branched colony. To explain the internal transport mechanism, the first part of the paper will discuss how does the internal hydrodynamics control the transport process for the branching corals. Now, Engineering co-relation, used for the heat and mass transfer, might be another important tool for quantifying the mass transfer rate for these colonies. Atkinson and Bilger *et al.* [17, 18] were pioneers in such analysis and used the Stanton number to compute the uptake of phosphate of coral and compared the experimental flume study data with the engineering correlation from heat and mass transfer. Similarly, Sherwood number has been used to calculate mass transfer rates from submerged canopies of arrays of cylinders for both unidirectional and oscillatory flow

[19]. Similar approach was adopted in the current study and a Stanton number was used for the calculation of mass transfer rate along the length of both these colonies.

The mass transport between the overlying water columns to the interior of the coral reef also depends on the turbulent flow profile developed both at the exterior and interior of the reef [20, 21]. For example, the transport of eggs and sperms from the surface of *Acropora* to the overlying water and the transport of nutrients from the water to the interior of the colony depends on turbulent stress developed at the topology of the coral reef. The turbulent flow statistics is also important for the calculation of Reynolds stress, bed shear stress and controls the momentum transport and sedimentation rate on the bottom layer of the reef or over a colony [22, 23, 24]. Though numerous studies performed earlier to study the effects of these parameters over the coral reef, computation of the local turbulent flow properties inside the reef is still a challenging task.

Now canopy flow theory can be used to compute the turbulent flow dynamics through these complex structures to understand macroscopic turbulent flow field around the colony. Generally, double-averaged Navier-Stokes equations are used to solve the spatial-temporal averaged velocity components and turbulent statistics from the flow field [25]. The averaging procedure creates a new term such as dispersive stress, which needs closure models to solve these equations [26]. These closure models were developed for homogeneous structure and the accuracy of these models inside the complex geometry of the reef is still not clear. Though it is an excellent tool for large scale flow analysis, the detailed micro-environment flow information can not be achieved through this method. In addition, we still depend on empirical and semi-empirical data for the calculation drag force inside the reef [27]. If we can resolve the flow field inside the coral, the drag forces or the models used for the calculation of dispersive stress can be evaluated more accurately. To achieve this objective, we will continue our analysis of the turbulent stress, momentum transfer, and mixing through both

the structures in the second part of the paper.

To achieve both these objectives, we want to implement a numerical approach, which will assist us to solve the flow dynamics inside the coral. Capturing the arbitrary boundary of coral is really a challenging task. Now different numerical approach has been impalement earlier to solve this issue but the problem arises due to non-consideration of the natural morphology of coral or the turbulent flow. Therefore, a new interest has grown in the direction of numerical simulation of hydrodynamics of the real coral colony. In a recent paper, Stocking *et al.* [28] numerically investigated heat and mass transport for flow over the exterior of natural and modeled coral structure and discussed the effect of roughness on heat and mass transport. Similarly, Cano *et al.* [29] performed the drag force analysis on real open-branched structure coral. These analyses provide an excellent overview of the flow dynamics for real corals but turbulent flow structure such as fluctuation components of velocity, detailed velocity vector, and development of local shear stress inside the morphology of the coral is still unresolved. Now, Kaandorp *et al.*[30, 31] used the Lattice Boltzman method to understand the flow pattern inside the coral's skeletons of *Maracis mirabilis* and Similarly, Chindapol *et al.* [32] used COMSOL Multiphysics tool to model the effect of flow on the growth of *Pocillopora verrucosa*. However, these simulations were performed on a laminar framework. Now Immersed Boundary Method (IBM) is suitable for handling such arbitrary shape in the turbulent flow and the governing equations are discretized on fixed Cartesian grids with an external force. Chang *et al.* [14] were the first to use the immersed boundary (IB) method to simulate the flow inside the arbitrary branches of colonies. In the current analysis, we have used the similar IB algorithm to perform all these simulations in Large-Eddy Simulation (LES) framework.

## 4.3 Materials and Methods

### 4.3.1 Immersed boundary method with large eddy simulation

IB method was first introduced by Peskin *et al.* [33] and used mainly for low Reynolds number biological flows by modeling the boundary as a set of interconnected spring elements. But this approach causes stiffness for the stationary boundary. Later Mohd-Yusof *et al.* [34]and Fadlun *et al.* [35] have solved this issue by introducing a direct forcing approach in this algorithm. In the direct forcing method, forcing is implemented in such a way that the appropriate boundary conditions are enforced on the boundary itself. The IB method used in the current study has been developed by Balaras *et al.* [36] and the details of the implementation and accuracy of the method can be found in the referenced papers. Here a brief description is introduced to describe the main features of the algorithm. The filtered Navier- Stokes equations used in the current analysis is shown below:

$$\frac{\partial \bar{u}_i}{\partial t} + \frac{\partial \bar{u}_i \bar{u}_j}{\partial x_j} = -\frac{1}{\rho}\frac{\partial \bar{P}}{\partial x_i} + \nu \frac{\partial^2 \bar{u}_i}{\partial x_j x_j} - \frac{\partial \tau_{ij}}{\partial x_j} + f_i \tag{4.1}$$

$$\frac{\partial \bar{u}_i}{\partial x_i} = 0 \tag{4.2}$$

where the bar represents the filtering operations. In the LES, the large scale of the flow is resolved whereas the small scale is modeled. The velocity components are defined by $\bar{u}_i$ and P represents the dynamic pressure. The term $f_i$ is used for the external forcing used in the immersed boundary method. Here the subgrid stress tensor is defined by $\tau_{ij} = \overline{u_i u_j} - \bar{u}_i \bar{u}_j$ and must be modeled to solve the velocity field. There are different techniques to parameterize the subgrid stress. In the current study, a Lagrangian dynamic Smaogrorinsky [37] model has been used for the complex structure. A uniform grid spacing of 1mm has been used in the X, Y and Z co-orientates with a domain dimension shown in Fig 2. A finite difference

algorithm with the second order accuracy in space and time has been used to discretize the N-S equations. Here the time step was advanced explicitly with a second-order Adams-Bashforth time marching algorithm. A uniform incoming velocity boundary condition at the inlet and a convective boundary condition have been used at the outlet of the domain. Slip boundary condition assumed in the lateral direction and at the top of the flow domain.

In the current IB method, a ray-tracing algorithm has been implemented to capture the interface of solid and fluid in the Cartesian grid. To provide a short description, different stages used in the IB method is shown in Fig 4.1.

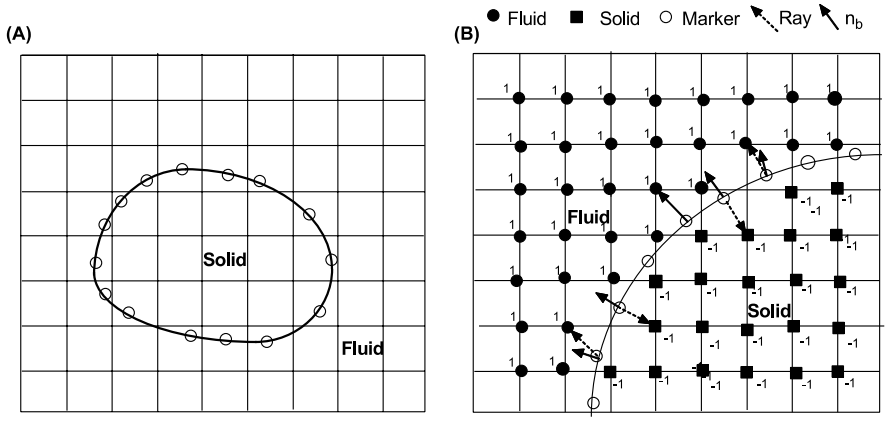


Figure 4.1: (A) An arbitrary object immersed in Cartesian co-ordinates. (B) Identification of solid and fluid points in computational domain by ray tracing algorithm in the immersed boundary algorithm [36, 38]

Fig 4.1 shows a solid object submerged in the Cartesian grids and the boundary is marked by a series of marker particles. In the case of the STL file, the boundary of the solid object is composed of millions of triangles. A searching algorithm is used to identify the nearest grids around the marker particles. Then a ray is sent from these markers to the nearest grid and a normal is calculated on the marker particle. Then the dot product of the normal and ray determines if the location of the grid point is inside the solid or not. In the case of the stationary boundary, this process is performed at the beginning of the simulation. Then

the closest grid points near the boundary in the fluid are chosen for the implementation of the forcing function. The velocity of the forcing points is interpolated from the surrounding fluid. There are different techniques available for interpolation to reconstruct the velocity field near the solid boundary. The reconstruction procedure and the implementation of the immersed boundary method can be found in detail in the referenced paper of Balaras & Young et al [38].

In addition to the main features of the current algorithm, we also want to discuss the limitations of the current study. The experimental studies show that mass and flow dynamics change significantly in the case of oscillatory flow conditions [39]. In the current analysis, only the uniform flow was considered to study the impact of coral structures on the hydrodynamics. In addition, coral grows in a natural reef environment and the colony sitting in the wake region of another coral will have different flow dynamics than the frontal one. Besides, a single coral sitting in an open flow condition does not represent a typical condition. However, resolving the flow field with a fine-scale resolution at the interior of the reef is extremely expensive. Even for the single coral, 54 million grids were needed for all the simulation performed in the current study. This gives an idea of how expensive the simulation will be in case the computation performed on multiple corals. In addition, the sidewall of the domain may constrain the flow but this effect can be neglected due to the presence of the neighboring corals, which may have similar effects on the flow domain. Overall, the objective of the current study is to find the detailed hydrodynamics inside a colony and the maximum length scale of the analysis is the height of the coral. Besides, the current analysis was also not intended for resolving the diffusive boundary layer, which is approximately a few hundred microns near the coral surface. Therefore, we believe the current setup of the flow domain and the resolution of the simulation will be sufficient to provide the required information to meet the objectives of the study mentioned earlier.

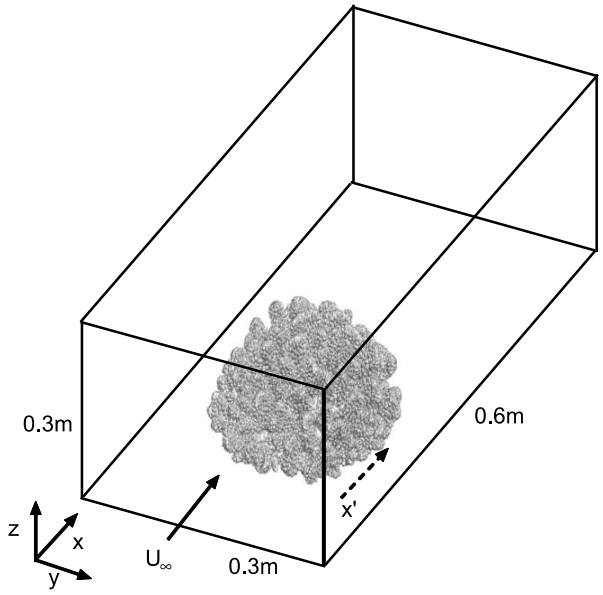


Figure 4.2: Schematic of flow domain used in the simulation (not in scale). x'=0 represents the beginning of the coral in the flow domain.

### 4.3.2 Coral geometries

From the previous discussion, it is clear that the current analysis needs to be performed on the real coral geometries with different branching patterns. To attain this objective, stereolithography (STL) files of two *Pocillopora* colonies were used for all the simulations. The densely branched *P. meandrina* also known as Cauliflower coral generally found in indo and eastern pacific and grows in strong flow condition. Whereas relatively more open space can be observed among the branches of *P. eydouxi*, which is found in the frontal reef area. The STL file was obtained from the computed tomography (CT) scan of the real coral skeleton and shared by Dr. Uri Shavit from the Israel Institute of technologies (Technion). The dimension and the geometric features of both these colonies can be found in Table 1. In addition to the geometrical dimensions, the mean branch diameter was plotted as a function of colony height for both the structures in Fig 4.3. It is to be noted these are the stony corals, where the tissue poses little contribution to the body mass index. Therefore, using

the coral skeleton instead of real coral geometries will have a little impact on the current computational results.

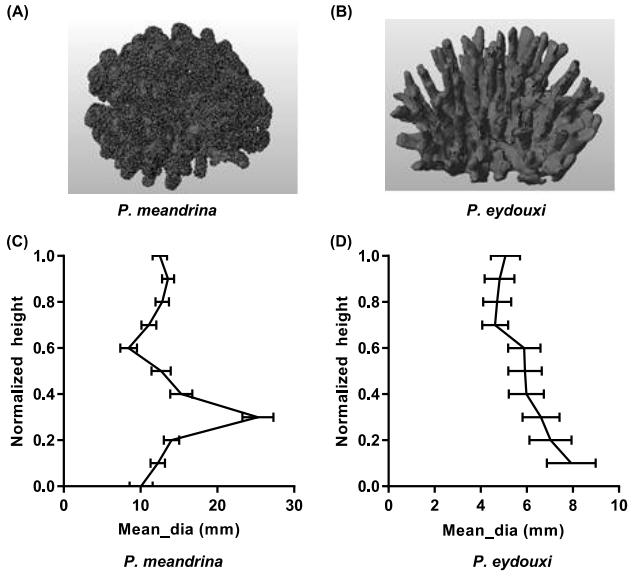


Figure 4.3: (A & B) Rendered stereolithography file of the *P. meandrina* and *P. eydouxi* used in the simulations. (C & D) Mean branch diameter at normalized height from the base of both these *Pocillopora* corals.

Table 4.1: Geometrical features of *Pocillopora* colonies.

| Coral | Length (m) | Width (m) | Height (m) | Vol./surface area (mm) | Branch dist./dia |
|---|---|---|---|---|---|
| P. meandrina | 0.172 | 0.172 | 0.10 | 2.06 | 2.8 to 4.0 |
| P. eydouxi | 0.12 | 0.11 | 0.10 | 2.09 | 8 |

## 4.4 Results

### 4.4.1 Validation of the simulation results

The current simulation has been validated with two experimental results from Chang *et al.* [13] and Asher *et al.* [40] respectively. The detail validation of the simulation with the

experiment of Chang *et al.* can be found in reference paper of Hossain and Staples *et al.* [41]. Only a brief description of the main features of the comparison will be discussed here. Chang *et al.* used magnetic resonance velcoitymetry to detect the flow field at the interior of the densely branched coral (high flow morphology) of *Styolophora*. In the experiment, the value of Reynolds number was 5000 based on the height of the colony . For the numerical simulation, the computation was performed on *P. meandrina* with the same Re number based on the height and incoming uniform flow. The geometrical features of both these colonies and the flow domain were almost similar in dimensions. For qualitative comparison, velocity slices, from the same normalized height were extracted and compared between the experimental and simulation results. In addition, quantitative comparison was also perform by measuring the mean velocity magnitude as a function of radial distance from the center to the exterior of the colony and the result shows similar velocity trend for both these structures.

The second comparison was performed with the flume study carried out on the *P. menadrina* by Asher *et al.* [40] who used the same coral colony, used in the current simulation, for the measurement of the vertical variation of drag forces. In the experimental study, eighty-one *P. menadrina* coral skeletons were used for the calculation of mean stream-wise velocity profile and the Reynolds stress developed over the colony. These velocity profiles were obtained by the Laser Doppler Anemometry over 19 (X, Y) position inside and around the *P. menadrina*. In this flume study, the ratio of the height of the water column to the colony was three, which represents the optimum depth after which the flow structure does not alter with the increase in the depth to coral height ratio [42] and the magnitude of the Reynolds number was 23,513 based on the uniform incoming flow and height of the colony. The mean velocity and Reynolds stress profile were obtained through double averaging in the stream-wise and lateral direction and normalized by the friction velocity, which was calculated from the equation of Pokrajac *et al.* [43]. For the simulation, the same water depth to coral height ratio and

Reynolds number was used in the flow domain. Here the Reynolds number was calculated based on the height and uniform flow at the inlet of 0.21 m/s. To match the dimension of the experiment, only the height of the colony, used in the simulation, was extended up to 0.111m. Similar to the experimental study, a double averaging was also implemented here in the stream-wise and lateral direction up to the extension of the *P. menadrina* to obtain the mean streamwise velocity and Reynolds stress profiles developed through these colonies. Both these mean profiles were normalized by the friction velocity calculated from the square root of the maximum values of Reynolds stress found at the top of the colony [26]. Fig 4.4 shows the comparison of mean stream-wise velocity and Reynolds stress profiles between the flume study and current simulation through the *P. menadrina*. In general, the comparison shows a close match between the experiment and current simulation results for both these profiles. For the stream-wise velocity, both the results showed an inflection point located near the z/h $\approx$ 0.5 at the interior of the colony, and the profiles matched well up to the z/h $\approx$ 1.5 above the coral. Now above z/h $\approx$ 1.5, the experimental result displayed a relatively higher velocity magnitude in comparison to the simulation. To capture the turbulent mixing and shear, Reynolds stress was also plotted along with the height of the colony and averaged, in the same manner, discussed earlier. The Reynolds stress exhibited the maximum magnitude at the top of the colony for both the cases, which indicates higher mixing and momentum transport at the top of the coral and these results corroborate the exiting experimental results over a single coral colony. For the Reynolds stress, the results show the close match from the base up to z/h $\approx$ 1.5 in the flow domain, and beyond this height, the simulation result reached the zero magnitudes quickly than the experiment. One reason for these discrepancies between the experimental and simulation might be the number of corals used for these two cases. The slip boundary condition used similar to Chang *et al.*[14] at the top of the colony might also have some effects on the overlying water column. The third reason might be the length of the flow domain where the averaging was computed.

In the case of experiment, the averaging was performed on the 81 *P. menadrina* colonies whereas only one single coral were used for the simulation. Therefore, some discrepancies can be observed between the experimental and simulation results. It is interesting to note that both the velocity and Reynolds stress profiles matched well within the colony up to the chest height. This might be interesting for future analysis if the simulation results on a couple of colonies can be used for the representation of large-scale reef? Though the results show a good match between the experiment and numerical studies, the comparison between only one set of geometry is not sufficient to come at such a conclusion from the current study.

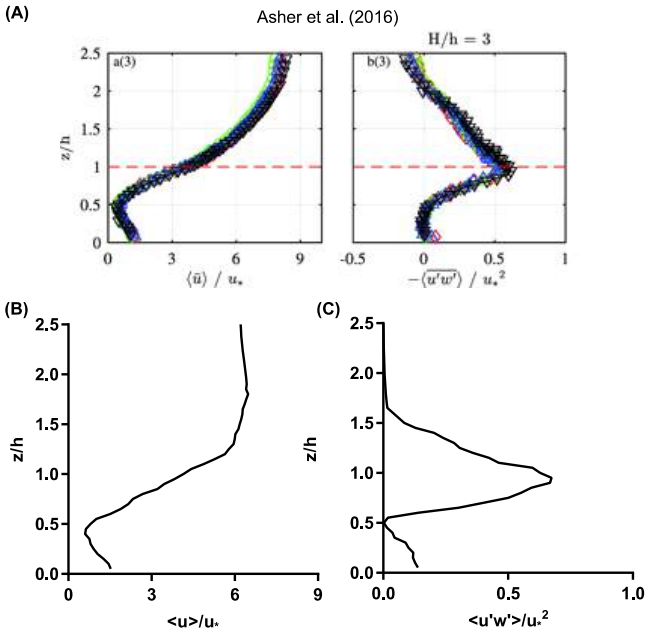


Figure 4.4: (A) Mean normalized velocity and Reynolds stress profiles over *P. meandrina* obtained from the flume study of 81 geometries at Re 23,513 by Asher *et al.* [40]. Reproduced with permission from Asher *et al.*[40]. Comparison of (B) mean velocity profile and (C) Reynolds stress along the height of the coral at Re 23,513. Here both the profiles were normalized by the friction velocity.

### 4.4.2 Comparison of flow profiles and transport mechanism between *Pocillopra* geometries

In the current study, a comparison of flow profiles was performed between the two *Pocillopora* geometries at Reynolds 15,000. The Reynolds number was determined from the uniform flow magnitude and the height of the colony. For the internal flow comparison between these two branching corals, detailed vector profiles were obtained inside the different sections of coral. Fig 4.5 & 4.6 shows a comparison of the top view of vector profile at the interior of both the colonies obtained at the same normalized height from the base of the coral and a side view in the middle of the colony. For the *P. menadrina*, the flow profile shows a relatively higher velocity magnitude at the frontal half of the coral, which indicates the difference in flow magnitude and the probability of the nutrient availability between the front and rare section of the coral. Here most of the flow was diverted outside because of the dense branch structure of the colony. In contrast, the vector profiles inside *P.eydouxi* better penetration at the deep interior of the colony due to the openness of the structure. One of the interesting features of the flow profile of *P.eydouxi* was the formation of the wake region behind the individual branches in addition to a large wake region behind the coral. Though these vectors profiles highlight the qualitative comparison of the distinct flow features for the two different branching patterns, the transport mechanism at the interior of the colony was not clear. To understand the transport mechanism, streamlines were plotted at the X-Z planes perpendicular to the flow direction from the front to the back of the colony. Fig 4.7(a) shows the formation of local vortices at the interior of *P. meanndrina* plotted at $x' = 0.5L$ perpendicular to the flow direction. For this densely branched colony, the highly vortical flow was observed from the $x' = 0.2L$ to the back of the colony, specifically in the middle where the mean flow magnitude started to drop at the interior. These passively formed vortices stir the water near the coral surface and enhance the mass transport rate. Similar formation

of vortices at the exterior of the colony due to the ciliary beating was cited by Shapiro *et al.* In one of the recent papers, Hossain *et al.* mentioned the formation of these vortices for the same *P. menadrina* colony and the authors calculated the advective time scale along the length of the coral. The authors also suggested that these passive vortices compensate the reduction of the flow speed at the interior of coral. In the current study, we want to extend this analysis for relatively open uniform branching coral-like *P. eydouxi* and want to check if these local vortices formed at a large number like *P. meandrina*. To achieve this objective, streamlines were also plotted at the same normalized location at the interior of *P. eydouxi* (Fig 4.7 b). In this case, the formation of these local vortices reduced substantially among its branches. Similar slices were obtained at the different sections from the front to the back of the coral and most of the slices did not show these vortices, except for a couple of small ones. This corroborates our previous assumptions [16] that passive geometric features create high vertical flow at the interior of coral. When the branching pattern becomes relatively open and uniform, coral does not need to compensate for the drop in velocity magnitude by generating vortical fields inside the colony.

We want to further investigate the transport rate for both these branching structures. Atkinson and Bilger *et al.* [17] previously used the Stanton number to compute the phosphate uptake in the reef environment. The Stanton number is the ratio of mass transfer rate to the advection rate on the surface. Here we will use the same simple mathematical formulation introduced by Atkinson and Bilger to calculate the Stanton number along the length of the both of these geometries. The Stanton number can be defined as:

$$St = \frac{m}{u_b(C_b - C_w)} \tag{4.3}$$

Where m is the mass transfer rate and $C_b$ and $C_w$ are concentration at the surface and water

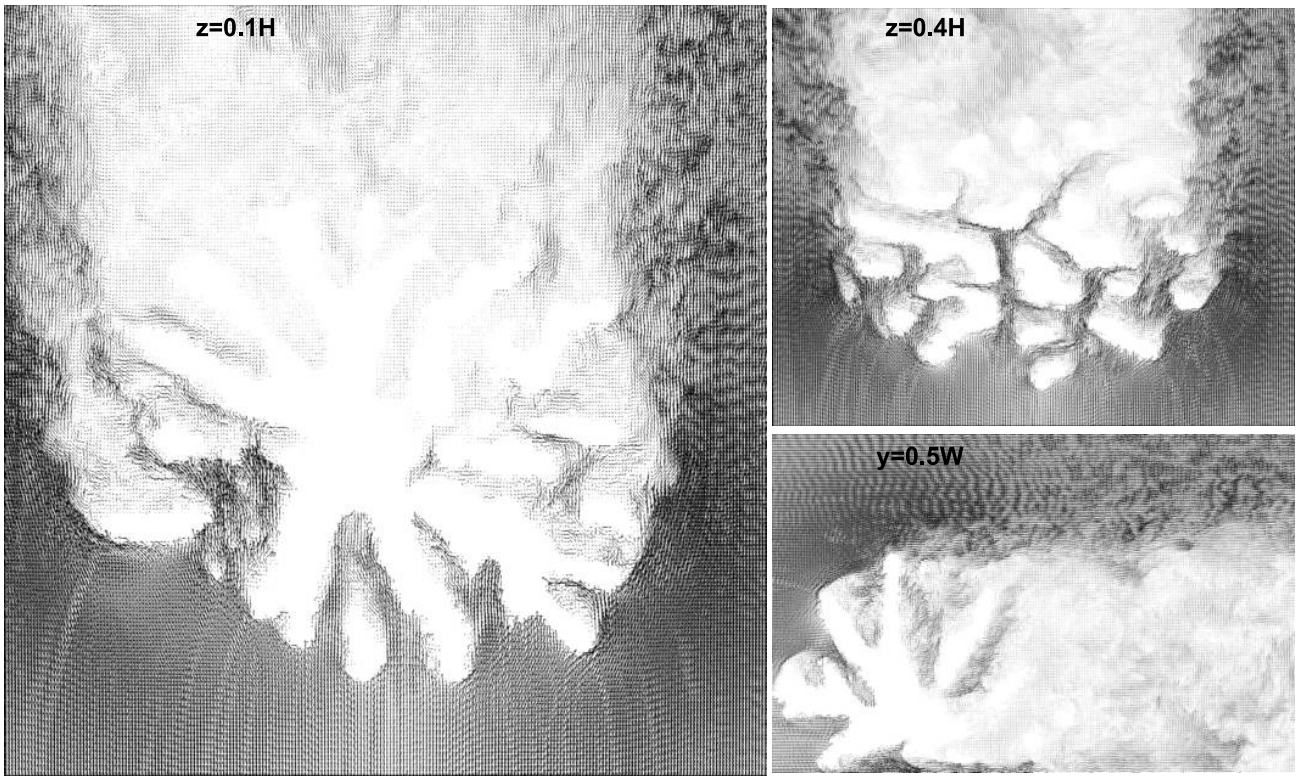


Figure 4.5: (A) Top view of detailed vector profiles at z = 0.1 & 0.4H and (B) side view at y = 0.5W at the different section of *P. menadrina*. Here H and W are the height and width of the colony.

respectively. Now if we consider the control volume around the coral and assume that the mass transfer is limiting (i.e. $c_w$ 0), the transport of the substance will balance the decay in the concentration as described in the equation here:

$$mA = -V\frac{dC_b}{dt} = VkC_b \tag{4.4}$$

Where A is the surface area of the coral, V is the volume of water in the control volume (bounding box formed from the dimensions of the colony) and k is the first order decay rate which is defines as follows:

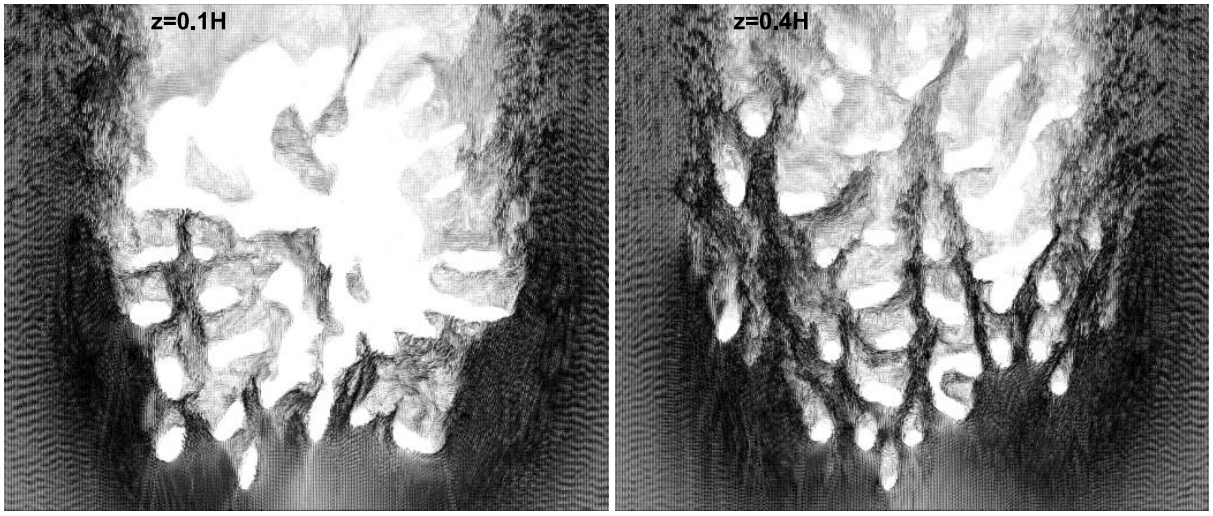


Figure 4.6: Top view of detailed vector profiles at z = 0.1 & 0.4H at the different section of *P. eydouxi*. Here H and W are the height and width of colony.

$$k = -\frac{1}{C_b}\frac{dC_b}{dt} \tag{4.5}$$

Table 4.2: Stanton number calculated along the length of *P. meandrina*.

| Coral | $x'$ | $\overline{u}$ | dia. | tadv | St | increase (%)) |
|---|---|---|---|---|---|---|
| *P. meandrina (branch dia)* | $x'$= 0.2$L$ | 0.142 | 0.013 | 0.091 | 5.92e-5 | |
| *P. meandrina (vortices)* | $x'$= 0.4$L$ | 0.084 | 0.004 | 0.048 | 1.89e-4 | 219% |
| | $x'$= 0.5$L$ | 0.0675 | 0.0045 | 0.066 | 1.70e-4 | 187% |
| | x'= 0.6$L$ | 0.057 | 0.0045 | 0.079 | 1.54e-4 | 160% |
| | $x'$= 0.8$L$ | 0.066 | 0.0050 | 0.075 | 1.71e-4 | 189% |
| *P. eydouxi (branch dia)* | $x'$=0.2$L$ | 0.138 | 0.00585 | 0.0423 | 2.843e-4 | |

To generalize the comparison, the transport of same substance was compared for the calculation of St number for both the geometries. One of the most important physiological process for coral is the calcification, which control the formation of their calcium carbonate skeleton. Generally the concentration of $Ca^{2+}$as approx. $15mol/m^3$ in the water at 16 to 17° [19]. For the decay rate k, $\Delta C_b$, in the order of $mmol/m^3$ was used for the calculation

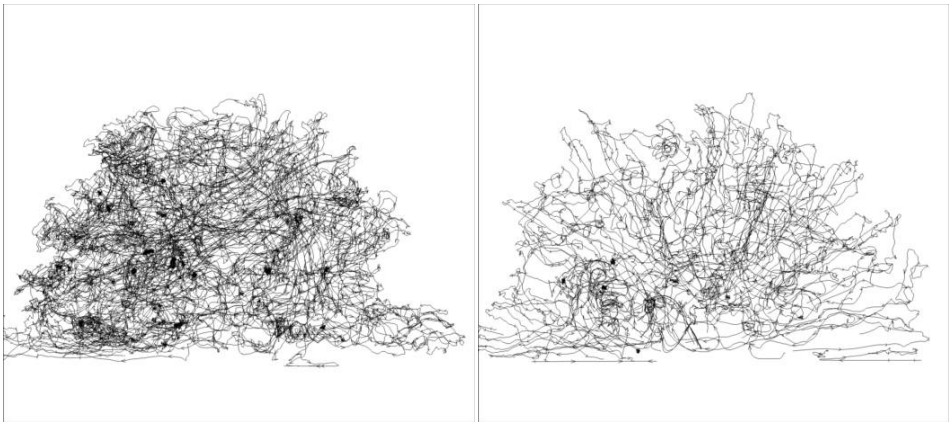


Figure 4.7: Streamlines plotted at x'=0.5 L for both the *Pocillopora* colonies. Formation of vortices in the intra-colonial velocity field of *P. meandrina* whereas relatively small vortices were found at couple of places in *P. eydouxi*. These are the frontal section and the view as if the flow is going perpendicular to the plan.

[44]. The advective time scale inside the colony were used as the $\Delta t$ for the calculation . The mean velocity and the advective time scale for both the colony are shown in table 2. For *P. meandrina* the advective time was calculated from the mean diameter of vortices as mentioned earlier. For *P. eydouxi* the advective time scale is found from the mean diameter of the branches of the colony and the mean velocity magnitude at the colony shown in Fig 4.9. Now if we consider the constant decay of $Ca^{2+}$, the estimation of the Stanton number can be found from equation 3. It should be noted the obtained magnitude are the approximated estimation of the Stanton number. In natural environment, the assumption of constant decay rate for the advective time scale may not hold everywhere in the colony [19]. Besides, if more than one coral were used in the analysis, the result might show significant variation for the Stanton number as the coral in the wake region might have different flow profiles than the frontal coral. Instead, these approximations were used to emphasis the comparative comparison between the transfer rates for the same uniform flow condition rather than the actual calculation. Fig 4.8 shows the values of Stanton number obtained along the length

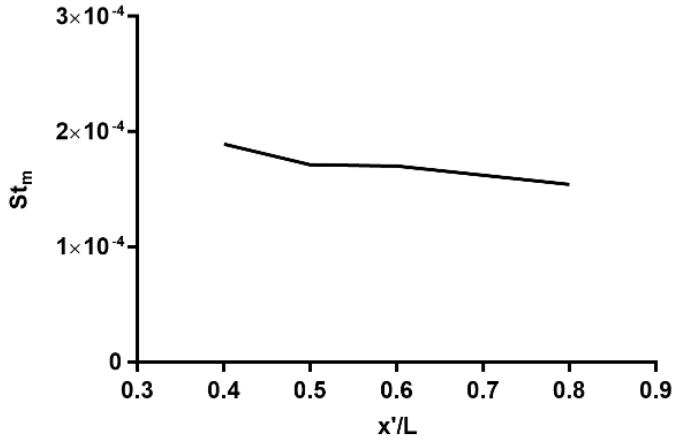


Figure 4.8: Stanton number calculated at the interior of *P. meandrina* at Re 15,000. Here St number was calculated based on internal flow magnitude and advective time scale.

of the *P. meandrina* and Table 2 shows the detail parameters used for the calculation of the St number for both the colonies. Due to the small number of vortices at the frontal section of conlony, calculation of St number were starts from $x' = 0.4L$ at the interior of *P. meandrina*. The result shows up to 216% increase in St number in comparison to magnitude calculated from advective time scale based on branch diameter in *P,meandrina*. However, *P. eydouxi* shows almost the twice the magnitude of St number in comparison to the maximum St number within *P.meandrina*. It is to be noted that the St number calculated in the current study matches well with the St number measured from the flume study by Atkinson and Bilger for the transfer of phosphate within coral colony and the magnitude varies from 13.8 to $106e-5$ studied for the velocity range from 0.0324 to 0.581 m/s.

In addition to the transport mechanism, mean velocity was also calculated along the length of both these geometries for the same incoming velocity. Fig 4.9 shows the variation of the mean velocity (averaged over the y-axis within the coral) with the cross-sectional area inside the coral. From the figure, it can be observed that the cross-sectional area was almost symmetrical for *P. meandrina* along the stream-wise direction. For densely-branched *P.*

*meandrina*, the magnitude of incoming flow reduced significantly in the middle of the coral and recovered up to 60% at the end section. In contrast, the cross-sectional area was not symmetrical for *P. eydouxi* and the flow reduced to approximately 50% of the incoming flow along the length of the coral, which was lower than the flow in *P. meandrina* at the end of coral. But, within the coral, the overall magnitude of velocity was higher in *P. eydouxi* than in *P. meandrina* throughout its length. In terms of food, the interior of the coral has a strong chance of starving if the velocity is not sufficiently high. For *P. eydouxi*, the situation is comparatively better, as the interior of the coral receives a higher flow, which means better mass transport and food availability [7]. However, the conditions for the coral that lives in the wake region are worse, because it takes a comparatively longer distance to recover flow in this area. This means that the nutrient availability for coral in the wake region will be reduced in comparison to the nutrient availability for coral living in the front region.

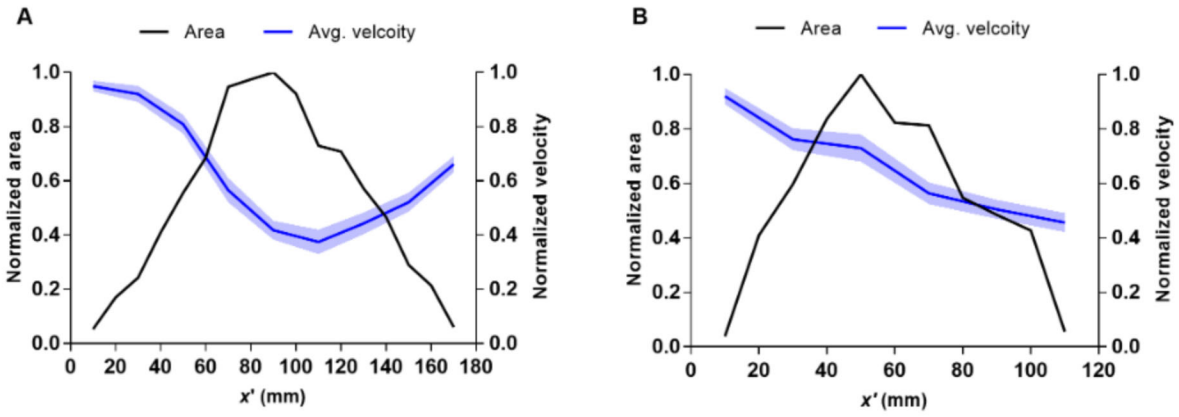


Figure 4.9: Variation of mean cross-sectional area and velocity in *Pocillopora* colonies with different branch densities The normalized colony cross-sectional area and intra-colonial velocity values averaged over two-dimensional planes at eleven locations along the height of the colony for *P. meandrina* (A, relatively densely branched) and *P. eydouxi* (B, relatively loosely branched). Shading in the velocity variable represents one standard deviation from the mean (N=6). While the densely branched colony (A) displays minimum mean velocity values just above the mid-height of the colony, the minimum mean velocity values for the loosely branched colony (B) appear at the top of the colony.

### 4.4.3 Turbulent momentum flux

One of the big challenges for the complex geometry is obtaining the turbulent flow statistics at the interior of the colony. Though numerous turbulent analyses have been performed above the canopy, attaining the fluctuating components and the subsequent calculation of turbulent moments within a single coral structure is not common. In the current study, we were able to obtain this detailed fluctuating flow field around both these structures. Fig 4.10 shows a comparison of the instantaneous and fluctuating vector fields inside and above *P.eydouxi*. Fig 4.10 (left) shows the lateral view of the relatively high concentration of velocity vector at the front and along the top surface of the colony. These velocity fluctuations contribute to the development of turbulent stress on the top of the surface of the coral. This is interesting to notice that velocity fluctuations occurred both at the top and inside the colony, which indicates a significant contribution of the turbulent stress within the coral. This result differs from the general assumption in canopy flow that turbulent stress dampens within the internal flow field.

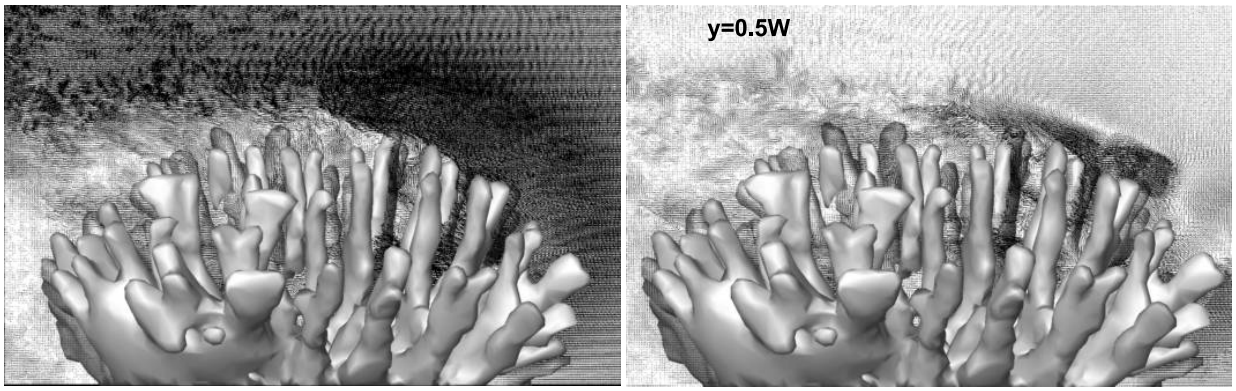


Figure 4.10: Instantaneous (left) and fluctuating (right) velocity components above *P.eydouxi* at y=0.5W. Here W is the width of the colony. The flow is coming from right to left.

From these detailed fluctuating flow field, we were also able to Reynolds stress for these

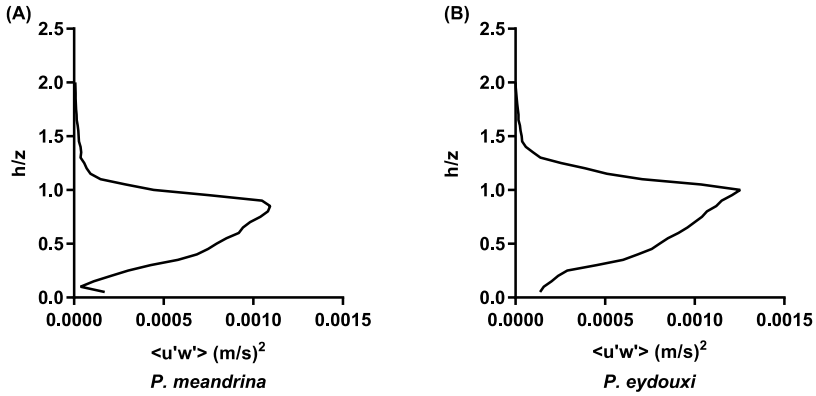


Figure 4.11: Mean Reynolds stress was plotted as a function of normalized height for (A) *P. meandrina* and (B) *P. eydouxi* at Re 15,000. Similar Reynolds stresses were observed in both these colonies despite their difference in branching patterns.

corals. Fig 4.11 shows the formation of the Reynolds stress over both these structures at Re 15000. Here, the Reynolds stress shows almost similar profiles over the geometries, and the maximum magnitude was found at the crest of the colony, which matches the relatively higher fluctuating vector components described earlier over the top of the colonies in Fig 4.10. Even though, there was a slight difference in the magnitude, the internal branching pattern did not alter the general profile of Reynolds stress too much at the interior of the colony. This is a very interesting finding in the sense that the Reynolds stress controls the mixing, transport of nutrients, and scalar from and to the coral colony. Therefore, the contribution of the Reynolds stress on the mass transfer was almost the same for both the *Pocillopora* colonies even with significant difference in their branching pattern. This finding may be tempting to contradict the common assumption that densely branch strictures may dampen the turbulent stress at the interior of the colony. But with only two geometrical structures, it is difficult to come to such a conclusion. The inclusion of more geometries will be suitable for similar studies in the future. Besides, the same magnitude of Reynolds stress at the top of the colony indicates almost similar frictional velocity above both these colonies and the magnitude of the stress reached the zero value almost at the same height over the colony.

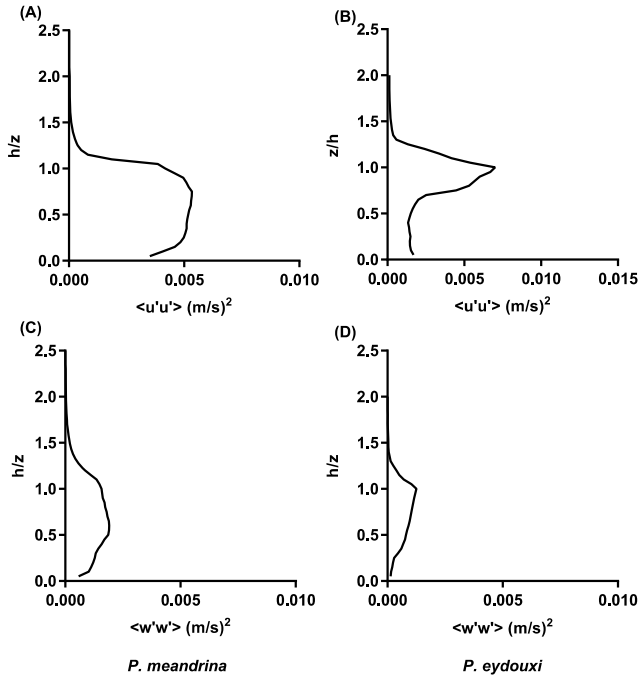


Figure 4.12: (A & B) Stream-wise and (C & D) vertical velocity variance computed over *P. meandrina* and *P. eydouxi* respectively. In both these cases, the magnitude of variance was found relatively higher for *P. meandrina* where the inter-branch distance was smaller than the open branched *P. eydouxi*.

In addition to Reynolds stress, stream-wise and vertical velocity variance were also computed over both these *Pocillopora* structures. Here, the stream-wise velocity variance showed relatively higher magnitude above the top of these heterogeneous structures, which was expected for open branched colony like *P. eydouxi*. But within the canopy, the stream-wise variance did not vary monotonically with the increase or decrease in branch density for both these corals. For densely branched *P.meandrina*, the magnitudes remained constant up to the height of the colony. In contrast, the magnitude of stream-wise variance was relatively small up to the mid-height of the colony in *P. eydouxi* and the variance increased sharply above this height. Similarly, relatively higher vertical velocity variance was observed in the densely branched heterogeneous structure of *P.meandrina*.

## 4.5 Discussion

Mass transport mechanisms were compared between two branching corals and the Stanton number was used to compare the efficacy of mass transfer in two *Pocillopora* branching coral colonies with different branch densities. The advection time scale used to calculate the Stanton number within the colony was found in two different ways.

First, when then were a large number of vortices in the interior flow field, the mean vortex diameter was used as the characteristic length to calculate the advection time scale following [15, 16]. Alternatively, when the number of passive vortices was significantly reduced within the colony and using the mean vortex diameters was not feasible, the branch diameter was used as the characteristic length scale for the advection time scale. The branch diameter was also used by Chang *et al.* [19] for the calculation of the Sherwood (Sh) number from the direct measurement of the dissolution rate of gypsum from the coated coral.

Figure 4.8 and Table 4.2 show the Stanton number calculated along the flow direction in a *P. meandrina* colony based on the mean vortex diameter. These results show a significant increase in the Stanton number compared to the Stanton number calculated using the branch diameter, as tabulated in column 7 of Table 4.2. When the mean branch diameter was used along the length of coral, the results showed a nearly constant Stanton number throughout the colony in the flow direction, which is the upper bound of mass transfer for the complete colony. Meanwhile, experimental results in a similar colony geometry showed a decreasing rend in the interior of the colony [19]).

But even the upper-bound transfer rate does not explain how does coral meet the need for increased mass transport within the densely branched colony due to the increase in the surface area ($\frac{Surface\_Area_{meandrina}}{Surface\_Area_{eydouxi}} \approx 5.65$) to keep the internal polyp healthy. This may fit the transport mechanism for the open-branched colony *P. eydouxi* where the velocity magnitude

is comparatively higher within the larger inter-branch distance and a constant transfer rate might exist but does not fit the mass transfer requirement for the densely branched *P. meandrina*. Therefore, these corals might require an extra mechanism to continue their normal activities. The suggested passive vortices within *P. meandrina* might serve this objective. Recently Shapiro [15] and Pacherres *et al.* [45] visualized the formation of vortices near the coral surface due to the ciliary beating. Stony corals might use passive geometrical features, ciliary beating or both to generate vortical fields inside the colony where fast transport rate is required to reduce the diffusion or concentration boundary layer at the deep interior of the colony.

The detailed vector profiles also explain the requirement for an alternative method to increase the transfer process for a densely branched colony. For example, the vector magnitude at the frontal section (up to $x' \approx 0.5L$) of *P. meandrina* was relatively higher than the downstream side. Therefore, there exists a velocity gradient along with the densely branched colony which also generates a mass transfer gradient within the colony [13, 19]. The blockage of the flow increases with the thickness of the branches and Fig shows mean velocity profile reduced substantially for *P. meandrina*. The situation will be worse for the colony living in the downstream of the other coral and If the colony becomes large enough the transport process should become stagnant within the inner portion of the colony. Coral adapts to the local flow environment to adjust the metabolic process [46] and the local flow information found in the *P. meandrina* might help us understanding such adaptation.

Now if the number of vortices is found in an insignificant number within the thicken branched colony, the branch diameter might be an alternative for the characteristic length scale. The time required for one particle to transport from the diffusion boundary layer from the coral surface to one branch diameter distance within the colony will require approximately $\Delta t \approx \frac{l_{char}}{u_{mean}}$ seconds. For *P. eydouxi* the value of $\Delta t_{peyd}$ was $0.06914s$ for mean branch diameter

$5.85mm$ at $x' = 0.6L$ whereas at same location the magnitude of $\Delta t_{pmean}$ was $0.228s$ based on mean branch diameter. This means *P. meandrina* required almost $\frac{\Delta t_{pmean}}{\Delta t_{peyd}} = 3.28$ more time to reach one branch distance from the surface. To reach the same branch diameter distance as *P. eydouxi*, *P. meandrina* needed almost $1.03s$ which is approximately 1.5 time than the time required for *P. eydouxi*. The extra time required for the transportation inside *P. meandrina* may significantly affect the thickness of diffusive boundary layers as well as the metabolic processes. Therefore, there should exists a mechanism which help the interior of the dense colony remain healthy. Now, from the comparison of St number and advective time scale it is clear that the mass transfer rate is higher within *P. eydouxi* than the densely branched *P. meandrina*. Reidenbach *et al.* measured the mass transfer from coral with different inter-branch spacing and found the similar results showing lowest mass transport for the densely branched colony[20].

The effects of the internal structure of the colony on turbulent stress were also studied for these two geometries. Reynolds stress and variance were calculated for these two *Pocillopora* corals. For Reynolds stress, the general profiles remained the same though the colony though there were substantial differences in their internal geometrical properties. The magnitude of the Reynolds stress has an important impact on parameters such as friction velocity, mass transfer rate, bed shear stress, and drag developed on the corals. For example, the friction velocity directly depends on the maximum magnitude of the Re stress over the colony and the results show the almost similar magnitude of friction velocity developed on both these colonies. Similarly, the coefficient of mass transfer rate is a direct function of shear stress over the colony, which shows an almost similar rate of transfer rate at the top of both these colonies [3].

## 4.6 Conclusions

The mass transport mechanism and the detailed vector profiles were analyzed for two different branching corals. The vector profile shows relatively higher flow penetration for the front half of densely branched *P. meandrina* than the latter half. In contrast, the flow penetrated deep at the interior of *P. eydouxi* due to the openness of the structure. The mean velocity magnitude was computed along the length of coral and used for the calculation of the Stanton number for the estimation of the mass transfer rate. Streamlines were plotted inside the coral to understand the transport mechanism for two different branching patterns. The result showed the formation of passive vortices inside densely branched *P. meandrina*, which stirs the water column and enhances the transfer rate. In contrast, a relatively small number of vortices were found in the open branch colony of P. eydouxi. To quantify the transfer rate, Stanton numbers were calculated and compared along the length of both these corals. The results show a constant mass transfer rate for P.eydouxi from front to back of the colony, which corresponds, to the better flow penetration at the interior. For the densely branched *P. menadrina*, the magnitudes of the Stanton numbers were calculated based on the two different time scales. The results show up to an approximate 200% increase in Stanton number when the mean vortices diameter were used as length instead of mean branch diameter inside *P. menadrina*. However, for both cases, the magnitude of the Stanton number was relatively smaller than the *P. eydouxi* for the same incoming flow. In addition, turbulent statistics were performed around both these *Pocillopra* geometries at Re 15,000. The vector filed displayed a relatively large number of velocity fluctuations near the top of the colony, which has significant contributions in the mixing and momentum transfer from the top of the coral. This flow information was used for the calculation of mean Reynolds stress and velocity variance along with the height of both these colonies. The results exhibit almost the same magnitude of Reynolds stress and variance above the top of the colony with maximum

magnitude at the crest but at the interior these parameters show a significant difference in the magnitude due to the difference in a branching pattern.

# Bibliography

[1] Fabricius KE, Genin A, Benayahu Y. Flow-dependent herbivory and growth in zooxanthellae-free soft corals. Limnology and Oceanography. 1995;40(7):1290–1301.

[2] Mass T, Genin A, Shavit U, Grinstein M, Tchernov D. Flow enhances photosynthesis in marine benthic autotrophs by increasing the efflux of oxygen from the organism to the water. Proceedings of the National Academy of Sciences. 2010;107(6):2527–2531.

[3] Hondzo M. Dissolved oxygen transfer at the sediment-water interface in a turbulent flow. Water resources research. 1998;34(12):3525–3533.

[4] Bruno JF, Edmunds PJ. Metabolic consequences of phenotypic plasticity in the coral Madracis mirabilis (Duchassaing and Michelotti): the effect of morphology and water flow on aggregate respiration. Journal of experimental marine biology and ecology. 1998;229(2):187–195.

[5] Patterson MR, Sebens KP, Olson RR. In situ measurements of flow effects on primary production and dark respiration in reef corals. Limnology and Oceanography. 1991;36(5):936–948.

[6] Kaandorp JA, Kübler JE. The algorithmic beauty of seaweeds, sponges and corals. Springer Science & Business Media; 2001.

[7] Chamberlain Jr JA, Graus RR. Water flow and hydromechanical adaptations of branched reef corals. Bulletin of Marine Science. 1975;25(1):112–125.

[8] Sebens KP, Witting J, Helmuth B. Effects of water flow and branch spacing on particle

capture by the reef coral Madracis mirabilis (Duchassaing and Michelotti). Journal of experimental marine biology and ecology. 1997;211(1):1–28.

[9] Hunter T. Suspension feeding in oscillating flow: the effect of colony morphology and flow regime on plankton capture by the hydroid Obelia longissima. The Biological Bulletin. 1989;176(1):41–49.

[10] Delandmeter P, Lambrechts J, Marmorino GO, Legat V, Wolanski E, Remacle JF, et al. Submesoscale tidal eddies in the wake of coral islands and reefs: satellite data and numerical modelling. Ocean Dynamics. 2017;67(7):897–913.

[11] Storlazzi C, Elias E, Field M, Presto M. Numerical modeling of the impact of sea-level rise on fringing coral reef hydrodynamics and sediment transport. Coral Reefs. 2011;30(1):83–96.

[12] Monismith SG. Hydrodynamics of coral reefs. Annu Rev Fluid Mech. 2007;39:37–55.

[13] Chang S, Elkins C, Alley M, Eaton J, Monismitha S. Flow inside a coral colony measured using magnetic resonance velocimetry. Limnology and Oceanography. 2009;54(5):1819–1827.

[14] Chang S, Iaccarino G, Ham F, Elkins C, Monismith S. Local shear and mass transfer on individual coral colonies: Computations in unidirectional and wave-driven flows. Journal of Geophysical Research: Oceans. 2014;119(4):2599–2619.

[15] Shapiro OH, Fernandez VI, Garren M, Guasto JS, Debaillon-Vesque FP, Kramarsky-Winter E, et al. Vortical ciliary flows actively enhance mass transport in reef corals. Proceedings of the National Academy of Sciences. 2014;111(37):13391–13396.

[16] Hossain MM, Staples AE. Passive vortical flows enhance mass transport in the interior of a coral colony. Physics of Fluids. 2019;31(6):061701.

[17] Atkinson M, Bilger R. Effects of water velocity on phosphate uptake in coral reef-hat communities. Limnology and Oceanography. 1992;37(2):273–279.

[18] Bilger R, Atkinson M. Anomalous mass transfer of phosphate on coral reef flats. Limnology and Oceanography. 1992;37(2):261–272.

[19] Chang S, Elkins C, Eaton JK, Monismith S. Local mass transfer measurements for corals and other complex geometries using gypsum dissolution. Experiments in fluids. 2013;54(7):1563.

[20] Reidenbach MA, Koseff JR, Monismith SG, Steinbuckc JV, Genin A. The effects of waves and morphology on mass transfer within branched reef corals. Limnology and Oceanography. 2006;51(2):1134–1141.

[21] Reidenbach MA, Koseff JR, Monismith SG. Laboratory experiments of fine-scale mixing and mass transport within a coral canopy. Physics of Fluids. 2007;19(7):075107.

[22] Reidenbach MA, Monismith SG, Koseff JR, Yahel G, Genin A. Boundary layer turbulence and flow structure over a fringing coral reef. Limnology and oceanography. 2006;51(5):1956–1968.

[23] Stocking JB, Rippe JP, Reidenbach MA. Structure and dynamics of turbulent boundary layer flow over healthy and algae-covered corals. Coral Reefs. 2016;35(3):1047–1059.

[24] Asher S, Shavit U. The effect of water depth and internal geometry on the turbulent flow inside a coral reef. Journal of Geophysical Research: Oceans. 2019;124(6):3508–3522.

[25] Finnigan J. Turbulence in plant canopies. Annual review of fluid mechanics. 2000;32(1):519–571.

[26] Moltchanov S, Bohbot-Raviv Y, Shavit U. Dispersive stresses at the canopy upstream edge. Boundary-layer meteorology. 2011;139(2):333–351.

[27] Rosman JH, Hench JL. A framework for understanding drag parameterizations for coral reefs. Journal of Geophysical Research: Oceans. 2011;116(C8).

[28] Stocking JB, Laforsch C, Sigl R, Reidenbach MA. The role of turbulent hydrodynamics and surface morphology on heat and mass transfer in corals. Journal of the Royal Society Interface. 2018;15(149):20180448.

[29] Osorio-Cano JD, Osorio AF, Alcérreca-Huerta JC, Oumeraci H. Drag and inertia forces on a branched coral colony of Acropora palmata. Journal of Fluids and Structures. 2019;88:31–47.

[30] Kaandorp JA, Koopman EA, Sloot PM, Bak RP, Vermeij MJ, Lampmann LE. Simulation and analysis of flow patterns around the scleractinian coral Madracis mirabilis (Duchassaing and Michelotti). Philosophical Transactions of the Royal Society of London Series B: Biological Sciences. 2003;358(1437):1551–1557.

[31] Kaandorp JA, Sloot PM, Merks RM, Bak RP, Vermeij MJ, Maier C. Morphogenesis of the branching reef coral Madracis mirabilis. Proceedings of the Royal Society B: Biological Sciences. 2005;272(1559):127–133.

[32] Chindapol N, Kaandorp JA, Cronemberger C, Mass T, Genin A. Modelling growth and form of the scleractinian coral Pocillopora verrucosa and the influence of hydrodynamics. PLoS computational biology. 2013;9(1):e1002849.

[33] Peskin CS. The immersed boundary method. Acta numerica. 2002;11:479–517.

[34] Mohd-Yusof J. methods for complex geometries. Annual Research Briefs-1998. 1998; p. 325.

[35] Fadlun E, Verzicco R, Orlandi P, Mohd-Yusof J. Combined immersed-boundary finite-

difference methods for three-dimensional complex flow simulations. Journal of computational physics. 2000;161(1):35–60.

[36] Balaras E. Modeling complex boundaries using an external force field on fixed Cartesian grids in large-eddy simulations. Computers & Fluids. 2004;33(3):375–404.

[37] Meneveau C, Lund TS, Cabot WH. A Lagrangian dynamic subgrid-scale model of turbulence. Journal of fluid mechanics. 1996;319:353–385.

[38] Yang J, Balaras E. An embedded-boundary formulation for large-eddy simulation of turbulent flows interacting with moving boundaries. Journal of Computational Physics. 2006;215(1):12–40.

[39] Lowe RJ, Koseff JR, Monismith SG, Falter JL. Oscillatory flow through submerged canopies: 2. Canopy mass transfer. Journal of Geophysical Research: Oceans. 2005;110(C10).

[40] Asher S, Niewerth S, Koll K, Shavit U. Vertical variations of coral reef drag forces. Journal of Geophysical Research: Oceans. 2016;121(5):3549–3563.

[41] Hossain MM, Staples AE. Effects of coral colony morphology on turbulent flow dynamics. bioRxiv. 2019; p. 839902.

[42] Lowe RJ, Shavit U, Falter JL, Koseff JR, Monismith SG. Modeling flow in coral communities with and without waves: A synthesis of porous media and canopy flow approaches. Limnology and Oceanography. 2008;53(6):2668–2680.

[43] Pokrajac D, Finnigan J, Manes C, McEwan I, Nikora V. On the definition of the shear velocity in rough bed open channel flows. In: River flow. vol. 1; 2006. p. 89–98.

[44] Langdon C, Takahashi T, Sweeney C, Chipman D, Goddard J, Marubini F, et al. Effect of calcium carbonate saturation state on the calcification rate of an experimental coral reef. Global Biogeochemical Cycles. 2000;14(2):639–654.

[45] Pacherres CO, Ahmerkamp S, Schmidt-Grieb GM, Holtappels M, Richter C. Ciliary vortex flows and oxygen dynamics in the coral boundary layer. Scientific reports. 2020;10(1):1–10.

[46] Mass T, Genin A. Environmental versus intrinsic determination of colony symmetry in the coral Pocillopora verrucosa. Marine Ecology Progress Series. 2008;369:131–137.

# Chapter 5

# Conclusions and future work

## 5.1 Summary and concluding remarks

Due to the variation in geometrical features and lack of experimental data inside the reef, there were no clear concepts of the mass transport mechanism for the branching corals. In addition there was little information on important hydrodynamic parameters such as momentum transport, Reynolds stress, friction velocity, and the drag developed on the single colony, which directly influence the physiological processes of coral. Though porous flow models and canopy flow theory provided a macroscopic overview of the flow dynamics around these reef geometries, the detailed flow information for individual colonies as presented in this dissertation was much needed to obtain the micro-scale flow field and in understanding mass transport mechanisms, and local turbulent statistics within the coral colonies with different branching patterns .

In the first study, an investigation was performed on the densely branched colony of *P. meandrina* and the analysis presents highly vortical internal flows, which enhance the local mass transport inside the coral. The result also showed a 64% reduction in the internal velocity magnitude which was compensated by the constant advection timescale along the length of the colony to keep the internal polyps healthy. To analyze the transport process further, a scalar transport equation was solved in turbulent wavy flow of period T. The concentration of the scalar was computed as a function of radial distance from the center of

the colony at the three different instances of a wave period and the result showed a double-peaked buildup of a passive scalar at the center and outer periphery of the *P. Meandrina* at the end of wave cycle, which should be different for the unidirectional flow where the peak builds only at at the center of the colony. So the transport of the scalar will show two different concentration field near the colony for the wavy and unidirectional flow.

In the second study, the computational analysis was extended further by comparing the internal velocity fields between the *Pocillopora* coral with two different branching patterns. The analysis showed a significant difference in mean velocity profiles between densely- and open-branched colonies. For densely-branched *P. meandrina*, the velocity profiles changed substantially in the colony with three distinctive velocity profiles while similar velocity profiles were found along the length of *P. eydouxi*. In addition, detailed vector profiles were obtained for the first time inside both of these colonies and the comparison shows a significant difference in flow magnitude between frontal and rare half of *P. meandrina* whereas the flow penetration was better for *P. eydouxi* throughout the colony for the same Reynolds number. In the second part of the paper, a hydrodynamic analysis was performed on *M. capitata* with and without verrucae to realize the effect of surface structure on velocity and Reynolds stress. Here, the verrucae changed the location and magnitude of maximum velocity and Reynolds stress above the colony and indicates that the surface structure plays an important role in hydrodynamic adaptation of coral colonies.

As the previous study displayed a significant difference in velocity magnitude and profile between densely and open-branched colony, in the third study, the analysis of the mass transport mechanism was continued to investigate whether the formation of passive vortices inside densely-branched *P. meandrina* also holds for open-branched *P. eydouxi*. In this study, the number of the passive vortices reduced significantly at the interior of *P. eydouxi* indicating that the internal geometry does not require the passive vortices mechanism to

enhance the transport process as the velocity magnitude was relatively high enough within the colony for the same incoming flow. The Stanton number was used to quantify the mass transport rate from both these geometries. The comparison shows a higher St number inside *P. eydouxi* whereas the St number decreased significantly within the densely-branched *P. meandrina*. But if the vortices were used for the calculation of the advection time scale, the St number increased as much as approximately 200% inside *P. meandrina* for the same decay rate of $Ca^{2+}$ from the coral surface at the same Reynolds number. The analysis also highlighted the turbulent flow statistics for the same geometries and showed that Reynolds stress and variance didn't dampen significantly as expected inside the densely-branched *P. meandrina* in comparison to open-branched *P. eydouxi*.

The numerical studies discussed in this dissertation were focused on analyzing the detailed hydrodynamics and mass transport mechanisms for branching corals living in turbulent flow. Understanding these turbulent flow conditions at the interior of natural growing coral is challenging and critical for the survival of reefs in changing flow conditions. Specially, the deteriorating conditions of the reef environment all over the world have created a tremendous challenge for scientists and engineers. The attempt to reveal the interaction of the real coral geometry with the surrounding environment will take us one step further to understand critical parameters such as nutrient transport, diffusion of gas on the coral surface, long-time coral morphology evolution, and thermal micro-environment related to the coral bleaching.

## 5.2 Future research direction

Although local, instantaneous turbulent events are important, detailed flow statistics in and above the coral reefs are rare. The results from the current study may provide a strong platform for the detailed hydrodynamics that can help us to accurately estimate mass transfer

rate, friction velocity, $u_*$ and the coefficient of drag, $C_d$ which are important parameters for shore stability. However, in the current study, the hydrodynamic flow analysis was preformed only on four different coral geometries. The future research may include generation of computational flow data sets for a wide range of coral geometries and spatial distributions at steady or wave flow conditions. These computational data can be used to develop critical parameterizations of subscale flow quantities like Reynolds stresses, dispersive stresses as a function of inter-branch distance, which can create a relationship between colony's internal branch geometry and mean flow characteristics. For example, parametric studies can be used to answer if the normalized mean velocity profiles collapse within the same geometry for the different incoming flow. These parametric studies might also assist us in estimating the variation of mean velocity profile with the change in inter-branch distance inside the coral or can help us in determining the variation of drag with the height and branch density inside the colony. Unfortunately, it is not possible to measure a wide range of ocean conditions experimentally for these arbitrary geometries, and so the proposed future computations are critical to the building a data sets large enough to understand the effect of geometrical variation on coral hydrodynamics.

These computational data sets, along with the ADV and UPIV measurements can help us in the development of precise closure models that bridge the gap between coral and ocean hydrodynamics leading to insights into many critical areas of coral research like growth, bleaching, and nutrient uptake. To achieve this objective, the current analysis may be extended in the future for the direct hydrodynamic analysis of the large-scale reef model at the high spatial resolution with the help of parallel computing. This analysis may have a two-fold advantage. This can be used for the direct computation of solving the momentum equation for Reynolds and dispersive stresses without any closure modeling. This result can also be used to quantify the relative importance of these stated parameters in and above

the the reef and to check the accuracy of the existing closure models by comparing existing canopy flow theories with the directly resolved three-dimensional flow field within the canopy by LES. This knowledge can potentially be translated into designing smarter artificial reefs and more effectively restoring native corals to improve the safety and resilience of coastal regions vulnerable to super storms.